Ida Emilie Malde Jacobsen

Carbon Formation Mechanisms on Co Surfaces: A DFT Study

Master's thesis in Chemical Engineering
Supervisor: Ingeborg-Helene Svenum
Co-supervisor: Mehdi Mahmoodinia

June 2021

Master's thesis

NTNU

Norwegian University of
Science and Technology

Ida Emilie Malde Jacobsen

Carbon Formation Mechanisms on Co Surfaces: A DFT Study

NTNU

Norwegian University of
Science and Technology

Abstract

Fisher-Tropsch synthesis (FTS) is a catalytic process where syngas is converted into water and hydrocarbons such as long-chain alkenes, mono alkanes and oxygenates. Due to the growing concern of carbon emission, the interest of FTS has expanded. The Co-based catalyst use natural gas as a feedstock which is convenient to use because of its high H_2/CO ratio. There are two types of Co crystal structure that can be used in the FTS, where the hcp Co is stable at lower temperatures (<693 K) and gives better results overall than the fcc Co. One of the critical issue with Co-based catalyst in FTS is carbon deposition which can block the active sites on the surface. Co is an expensive material and therefore, to ensure that the process is economical feasible, a long catalytic lifetime is needed.

This thesis is a theoretical study carried out with density functional theory (DFT) implemented in Vienna ab Simulation Package (VASP). Five hcp Co facets were made for the investigation: Co(0001), Co(11-20), Co(10-10), Co(10-11) and Co(10-12). Adsorption of acetylene and the relevant surface intermediates were performed on all surfaces, and vibrational analysis was carried out. The favorable sites was detected for each adsorbate on each surface. All surfaces were compared, it was concluded that Co(10-11) was the most active surface due to the lowest adsorption energy overall. The effect of the van der Walls (vdW) interaction was investigated, and there was a remarkable difference in the adsorption energy calculated with and without vdW interactions, which indicate that the vdW do contribute to the adsorption energy. Also, it was noted that the vdW interactions became greater with higher weight of atom/molecule adsorption on the surface.

The surface free energy was calculated for all five facets together with the corresponding termination of Co(10-10), Co(10-11) and Co(10-12). It was concluded that the flat Co(0001) facet was the most thermodynamical stable surface due to the lowest surface energy of 125 meV/$Å^2$. The more open surfaces, Co(11-20) and Co(10-12), have the highest surface energy of 152 meV/$Å^2$.

Acetylene decomposition was studied on the Co(0001) and Co(11-20) surfaces with climbing nudged elastic band (CI-NEB) method. The transition state was identified with one imaginary frequency for all the decomposition reactions. For both surfaces the C-H bond scission was more advantageous than the C-C bond scission of acetylene and its intermediates due to the lowest activation energy. There was made a potential energy diagram (PED) where three reaction pathways were investigated. It was concluded that the most favorable reaction mechanism was acetylene dehydrogenation to a C_2 specie. This reaction was further investigated with 0 K, 298.15 K, 450 K and 600 K on both surfaces. Which showed that the decomposition reaction became more thermodynamically neutral with increasing temperature.

Deposition of carbon with different coverages was investigated for the flat Co(0001) surface and the corrugated Co(11-20) surface. For the Co(0001) surface carbon deposit in carbon dimer at low coverage and in graphene fragments at high coverage. For Co(11-20) surface the carbon chemisorption was stronger and the carbon deposit general in carbon dimer.

Sammendrag

Fisher-Tropsch syntesen (FTS) er en katalytisk prosess hvor syngas omdannes til vann og hydrokarboner som for eksempel lange kjeder av alkaner, alkener og oksygenater. Interessen for FTS har økt på grunn av den økende bekymringen for karbonutslipp. Co-baserte katalysatorer bruker naturgass som råstoff, dette er gunstig å bruke på grunn av det høye H_2/CO forholdet. Det er to typer Co krystallstrukturer som kan brukes i FTS, hvor hcp Co er stabil ved lave temperaturer (<693 K) og gir generelt bedre resultater enn fcc Co. En av hovedproblemene ved Co katalysatorer i FTS er karbonavsetningen som kan blokkere de aktive setene på overflaten. Co er et kostbart materiale, og for å sikre at prosessen er økonomisk gjennomførbart er det nødvendig med en lang levetid på katalysatoren.

Denne oppgaven er en teoretisk studie utført av tetthetsfunksjonalteorien som var implementert i Vinnea ab simulerings pakken. Fem hcp Co overflater ble laget: Co(0001), Co(11-20), Co(10-10), Co(10-11) og Co(10-12). Adsorpsjon av acetylen og relevante overflate mellomprodukter ble utført på alle overflatene, og vibrasjonsanalyse ble gjort. Hver overlate ble studert og det ble funnet de mest gunstige adsorpsjons setene for hvert adsorbent. Alle overflatene ble sammenlignet med hverandre, og generelt var Co(10-11) overflaten mest reaktiv på grunn av dens lave adsorpsjonsenergi. Effekten av van der Waals (vdW) interaksjoner ble studert og det var en bemerkelsesverdig forskjell mellom adsorpsjonsenergiene beregnet med og uten vdW interaksjonene. Det ble også bemerket at vdW interaksjonene ble større med større vekt av atom/molekyladsorpsjon på overflaten.

Overflateenergien ble beregnet for alle fem overflatene, også den andre termineringen av Co(10-10), Co(10-11) og Co(10-12) ble beregnet. Det ble konkludert at den mest termodynamiske stabile overflaten er Co(0001) overflaten med den laveste overflateenergien på 125 $meV/Å^2$. De mer åpne overflatene, Co(11-20) og Co(10-12), hadde den høyeste overflateenergien på 152 $meV/Å^2$.

Nedbrytning av acetylene på Co(0001) og Co(11-20) overflatene ble studert ved å bruke CI-NEB metoden. Overgangstilstanden ble identifisert med en imaginær frekvens for alle nedbrytningsreaksjonene. For begge overflatene var C-H splittelsen mer fordelaktig enn C-C splittelsen av acetylen og mellomproduktene, dette var på grunn av en lavere aktiveringsenergi ved C-H splittelse. Ut fra tre reaksjonsveier for nedbrytning av acetylen ble det laget et potensielt energidiagram. Det ble konkludert at dehydrogenering av acetylene til C_2 molekyl var den mest gunstige reaksjonsveien. Denne reaksjonen ble også studert ved 0 K, 298.15 K, 400 K og 600 K på begge overflatene. Dette viste at nedbrytnings reaksjonen ble mer termodynamisk nøytral ved høyere temperaturer.

Avsetning av karbon med forskjellig dekningsgrad ble undersøkt på den flate Co(0001) overflaten og den bølgete Co(11-20) overflaten. For Co(0001) overflaten ble det konkludert at karbon opterer i par ved lav dekningsgrad, mens det opptrer i grafen fragmenter ved høy dekningsgrad. For Co(11-20) overflaten binder karbon sterkest og avsettes generelt i par.

Preface

This thesis is submitted to the Norwegian University of Science and Technology (NTNU) for partial fulfilment for the degree of Master of Chemical Engineering. It is a continuation of a project performed in the Fall 2020. The work has been performed at department of Chemical Engineering (IKP), with Adjunct Associate Professor Dr. Ingeborg-Helene Svenum as main supervisor and Dr. Mehdi Mahmoodinia as co-supervisor.

Acknowledgements

I would like to say that this has been a meaningful journey into the world of surface science, and I am grateful for all the knowledge I have received through the work. First, I would like to thank my main supervisor Professor Ingeborg-Helene Svenum for excellent training and support in the theoretical work. This work would not be possible without the guidance from you every single week during the project. I would also like to thank my co-supervisor Dr. Mehdi Mahmoodinia for the cooperation during the project and the computational help. The meeting have been filed with scientific discussion thanks to you.

Many thanks to the Catalysis group for a good working environment, and all the support and tips throughout the project. Finally, I would like to thank my family and friend for supporting me at any time during my five years at NTNU.

Ida Emilie Malde Jacobsen
Trondheim, June, 2021

Table of Content

List of Figures

List of Tables

List of Symbols and Abbreviations

Symbol	Explanation
d	Distance
E_a	Activation energy
E_{ads}	Adsorption energy
E_{surf}	Surface free energy
ΔE	Reaction energy
ΔG	Gibbs Free Energy
h	Planck constant
H	Hamiltonian operator
ΔH	Enthalpy
ΔS	Entropy
T	Temperature
V_{eff}	Effective potential
Ψ	Wave function
E_{XC}	Exchange correlation functional
ν	Vibrational frequency
c	Speed of light

Abbreviation	Explanation
CI-NEB	Climbing image nudged elastic band
DFT	Density functional theory
EXX	Exact-exchange
fcc	faced-centered cubic
FS	Final state
FTS	Fisher-Tropsch synthesis
GGA	Generalized gradient approximation
HA	Harmonic approximation
hcp	Hexagonal closed packed
HK	Hohenberg-Kohn
IS	Initial state
KS	Kohn-Sham
LAPW	Linear augmented-plane-wave
LDA	Local density approximation
MEP	Minimum energy path
ML	Monolayers
PAW	Projector augmented wave
PBE	Perdew-Burke-Ernzerhof functional
PED	Potential energy diagram
SCL	Self-consistent loop
TS	Transition state
TST	Transition state theory
VASP	Vienna ab Simulation Package
vdW	Van der Waals
VESTA	Visualization for Electronic and Structural Analysis
ZPE	Zero-point energy

1. Introduction

1.1. Background

Catalysts accelerate reactions to perform the reaction at the most favorable thermodynamic regime. The key factor in reducing the investment and operational costs of a chemical process is to use an efficiently catalysts, together with an optimized reactor and total plant design [1].

Fisher-Tropsch synthesis (FTS) is a catalytic process where syngas ($CO_{(g)}$ + $H_{2(g)}$) is converted into water and hydrocarbons such as long-chain alkanes, mono alkenes and oxygenates (wax) [2]. FTS is named after the German investors, Franz Fisher and Hans Tropsch in 2920s, and Reaction 1.1 presents the synthesis [3]. Ever since the development, the interest of the FTS has gowned due to the growing concern of the carbon emission. Also due to the limited oil reserves, because the FTS use clean fuel biomass which makes the synthesis renewable [4].

$$(2n + 1)H_2 + nCO \rightarrow C_nH_{(2n+2)} + nH_2O \hspace{3cm} [1.1]$$

There are many catalysts that can be considered for the FTS, which includes iron (Fe), cobalt (Co) or ruthenium (Ru). Generally, Co is preferred over Ru due to the high cost of Ru. Co catalyst are 230 times more expensive than Fe [3], but Co catalyst use natural gas as a feedstock which makes it more convenient to use. Natural gas has a high H_2/CO ratio which obviates the need for shifting CO with steam to yield more hydrogen [5]. Co-based catalyst are promising catalysts for biomass to liquids process like the FTS, because they exhibit high activity, stability and low CO_2 selectivity [4].

The preferred route of FTS, is with use of a metallic Co catalyst which operates right under 500 K with elevated pressure to produce wax [6]. Co-metal particles have different stable phases according to the temperature employed in the preparation and their size. There are three different crystal structure in which cobalt can occur: face centered cubic (fcc), primitive cubic phases (ε) and hexagonal closed-packed (hcp). The hcp structure is more stable at lower temperature than the others in the FTS. Depending on the crystal size, Co hcp are stable below the allotropic transformation temperature around 693–723 K, while Co fcc is thermodynamically stable above this temperature. FTS is a structure sensitive reaction and Co hcp phase presents better results overall [7].

One of the critical issues with Co-based catalyst in the FTS, is deactivations of Co catalysts. Co is an expensive material and therefore, to ensure that the process is economical feasible, a long catalytic lifetime is needed. In low temperature FTS, the main causes of deactivation are sintering, formation of stable compounds between Co and the support, re-oxidation of Co, surface reconstruction, formation of carbon species on Co surface, poisoning and carbiding. The long-term deactivation is often described as two main "schools", one that favoring re-oxidation and one poly-carbon formation on the surface. Both of these are dependent on the catalyst system and the process conditions. Also, if the fresh catalyst contains crystallites in the range of 6-12 nm, an initial sintering stage may appear. A typical lifetime for a catalyst is around 2 years, but with these deactivations mechanisms it could be reduced to 25-30 % of the initial value. This would lead to high operating cost for the FTS [5].

Waxes are products from the low temperature FTS on Co catalysts. The hydrocarbon from the wax product can accumulate on the surface and form carbon or coke that can block the active sites [5]. Carbon and coke can occur on the catalyst metal under decomposition of hydrocarbon [8]. Density functional theory (DFT) is a method that can be used to observe these chemical bonds that appear between the Co and graphene/carbon. It has been found that graphene/carbon on the surface induce Co reconstruction and weakens the CO and H_2 adsorption [5]. Therefore, an understanding of the deactivation mechanism is important in order to maximize the lifetime of the Co catalyst.

Besides the hydrogenation of CO in reaction 1.1, to produce long chain hydrocarbons, shorter hydrocarbons can also be formed [9]. To gain a more complex picture of the reaction, insight into adsorption and decomposition of hydrocarbons together with carbon deposition will be beneficial.

1.2. Previous Work

This thesis is a continuation of the specialization project performed in the fall 2020. In that project, two hcp Co model system were made: Co(0001) and Co(11-20). The atom/molecule C, H, CH, C_2, C_2H and C_2H_2 were adsorbed above high symmetry sites on both surfaces to investigate the most stable adsorptions sites by DFT calculations. The results that was obtained are presented in Table 1.1.

It was concluded that the hollow sites were the most stable adsorption sites for Co(0001). For Co(11-20) it was the tB-offsite site, where the adsorbate was between the zigzag rows in the B layer, that was the most favorable. Except for the hydrogen that preferred to be in a bA site on Co(11-20). Overall, all the adsorption containing carbon was stronger on the Co(11-20) surface than the Co(0001) surface. Acetylene chemisorbed on both surfaces with its C-C bond parallel to the Co surface.

Table 1.1: Favorable site for the adsorbate on Co(0001) and Co(11-20) surfaces and the adsorption energy (E_{ads}).

Adsorbate	Adsorption site Co(0001)	E_{ads} [eV] Co(0001)	Adsorption site Co(11-20)	E_{ads} [eV] Co(11-20)
C	hcp	-6.90	tB (offsite)	-7.32
	fcc	-6.65	bB	-7.09
	top	-4.80		
H	hcp	-2.77	tB (offsite)	-2.60
	fcc	-2.81	bB	-2.57
	top	-2.17	bA	-2.67
			bAB_2	-2.42
CH	hcp	-6.97	tB (offsite)	-7.22
	fcc	-6.85	bB	-6.97
	top	-5.29		
C_2	fcc-hcp	-7.34	tB-tB (offsite)	-7.93
	top	-4.06	tB-tB (offsite)2	-7.58
			tB-bB	-7.94
			bA-tB	-6.78
C_2H	fcc-hcp	-5.50	tB-tB (offsite)	-5.66
	hcp	-4.49	tB-tB (offsite)2	-5.48
	fcc	-4.51	tB-bB	-5.55
	top	-3.82	tB-bB2	-5.50
			bA-tB	-5.53
C_2H_2	fcc-hcp	-2.66	tB-tB (offsite)	-2.30
			tB-tB (offsite)2	-2.19
			hAAB-hAAB	-2.17

1.3. Objectives

The objective of this study is to investigate the carbon formation mechanisms by performing first principle spin-polarized DFT calculations. It is also important to gain a better understanding of the process occurring at the catalyst surfaces. The two hcp Co model system, Co(0001) and Co(11-20), that was made in the specialization project will be further investigated by applying different carbon monolayers (ML) on the surfaces. The surfaces hcp Co(10-10), Co(10-11) and Co(10-12) will also be investigated. For all the five surfaces, the zero-point energy (ZPE) contribution and the van der Waals (vdW) interactions will also be included in the adsorption energy. The decomposition reaction of acetylene using climbing nudged elastic band (CI-NEB) calculation will also be performed which is a step in graphene growing. All the C-H bond and C-C bond scission will be presented, and all intermediate will be considered during the decomposition of acetylene on Co(0001) and Co(11-20) surfaces. Gibbs free energy will be calculated in order to see how the decomposition of acetylene changes with increasing temperature.

2. Theory

2.1. Heterogeneous Catalysis

Catalysts comes in various forms, they can either be atoms, molecules, large zeolites or enzymes. Homogeneous catalysis, heterogeneous catalysis and bio catalysis are the three main subtitles for catalysis. In homogeneous catalysis, the catalyst and the reactants are in the same phase, in heterogeneous catalysis on the other hand, they are not. The heterogeneous catalyst is in solid material, while the reactants are in gas phase or in a solution. Catalysts are important, and many of the processes in chemical industry would not be able to do without a catalyst, or they would not be economical to implement. The catalyst cause reactions to proceed at much milder conditions of temperatures and pressures. Catalytical routes often optimize the process by using raw materials efficiently and minimize the waste production. Therefore, roughly 85-90 % of the chemical industry are made in a catalytic process. In every catalytic reaction the reactants bind to the catalyst where they react, and after the products detaches from the surface, the catalyst can react again. This cycle is illustrated in Figure 2.1 [1].
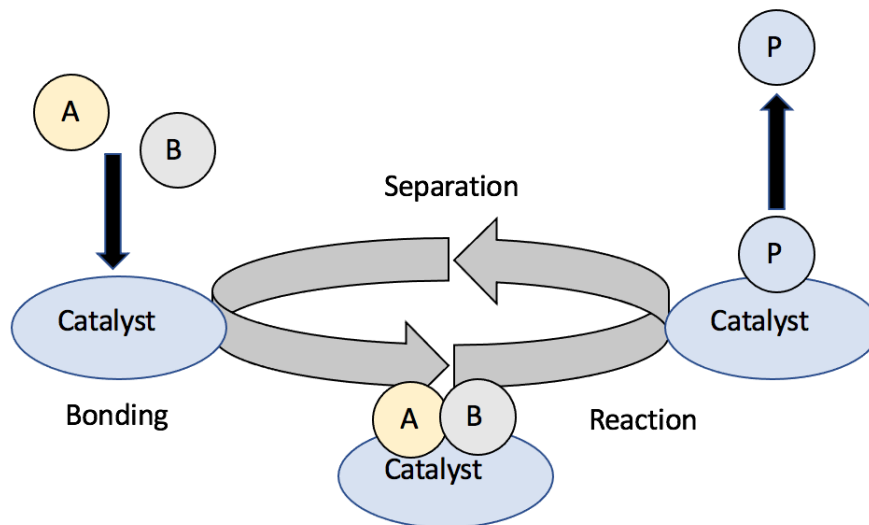
Figure 2.1: Elementary steps of a catalyst cycle [1].

Heterogeneous catalyst is easier separated from the reactants and products due to the different phases. Therefore, the heterogeneous catalysis is often preferred in industry. The chemical reaction takes place at the surface of the material, that is why the surface area is important for a heterogeneous catalyst. To understand how a heterogeneous catalyst works, the surface processes must be investigated [10].

2.1.1. Surface Processes

The different elementary steps on a catalytic surface reaction are illustrated in Figure 2.2. The Figure shows how a diatomic molecule adsorbate to the surface where it react and form a new molecule [10, 11].
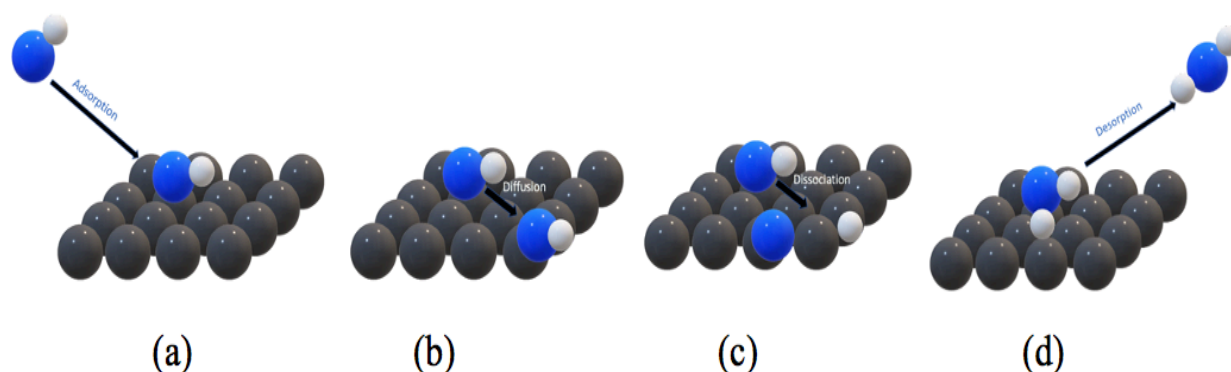
Figure 2.2: Sketch of a diatomic molecule adsorbed to the surface (a), diffusion of the molecule (b), dissociation of the molecule (c) and desorption of the new molecule (d) [10, 11].

Adsorption

When an atom or a molecule approaches the surface, it interacts with the metal atom in the surface by feeling its potential energy (Fig. 2.2, a). The interaction is described as physisorption and chemisorption. Physisorption is a weak interaction between the adsorbate and the surface, and no electrons are shared. Van der Waals (vdW) interactions is a type of physisorption interaction and take place at medium distance. It occurs when the electron in a particle set up a dipole, and then induce an image dipole in the polarizable solid which leads to attractive [1]. Figure 2.3 illustrates the polarization between two atoms which causes vdW interaction [12].
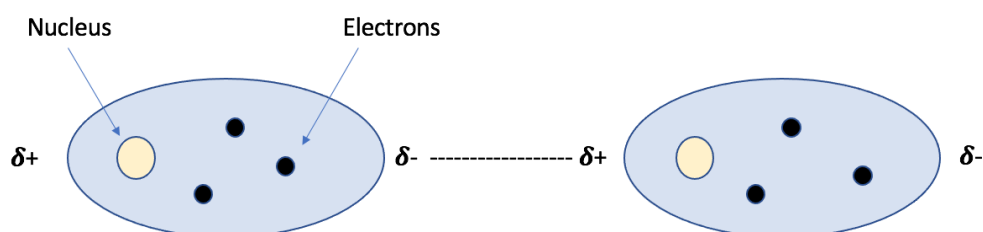
Figure 2.3: Illustration of a vdW forces [12].

Adsorption of an atom/molecule can also form stronger bond with the surface by chemisorption. A chemical bond is formed when the electron cloud in the surface and the adsorbate overlap each other [10]. Then, the adsorbate will choose a site on the surface which maximize the chemical bond [11]. A chemical bond includes both strong intramolecular interaction and

weaker intermolecular forces like vdW forces [13]. Attractive and repulsive forces act simultaneous between atoms when forming a chemical bond. The atoms is placed in a equilibrium point by making the atoms move closer and further apart continuously [14]. To get an overview of the significant information about an adsorption system, a potential energy diagram (PED) can be made. The adsorption energy is then the minimum energy in the PED [10].

Diffusion, Dissociation and Desorption

When the adsorbate is adsorbed to the surface in a site, they often do not stay long in that site. If the temperature is high enough, they will start jumping to other sites which is called diffusion (Fig. 2.2, b). The intramolecular bond in a molecule is weakened due to the chemical bond that the molecule has made with the surface. Therefore, the molecule may end up dissociated into its constituents on the surface (Fig. 2.2, c). These atoms form strong bonds with the surface, but they are also mobile on the surface and can form a new molecule with other atoms on the surface. The new molecule may leave the surface in a desorption process (Fig. 2.2, d) [11].

Density functional theory (DFT) is an established method to investigate surface processes and the electronic structure in molecules and solids. DFT has played an important role in the science behind applied heterogeneous catalysis for the past 20 years [15].

2.2. Background for Density Functional Theory (DFT)

DFT is one of the most successful theories in chemistry and physics the last half century. It is essentially used to predict the properties and the structures of the atoms, molecules and solids. In material design, DFT is a key ingredient in making a new material with specific properties. It can also be an important tool in biology for investigation of, for example, proteins and DNA. After its birth, DFT is growing at an exponential rate [16]. It is based on finding a solution of the many-body Schrödinger equation which describes the quantum behavior of atoms and molecules in setting of a practical value. DFT uses the electron density when solving the Schrödinger equation in place of the many-body wave function. The fundamental principle of DFT is that the total energy is a unique functional of the electron density. Therefore, it is not essential to complete the full many-body wave function for the system [17]. In order to understand DFT, it is important to explain the background for the method by explaining essential theory like the Schrödinger equation.

2.2.1. The Time-Independent Schrödinger Equation

The time independent, nonrelativistic Schrödinger equation is shown in Equation 2.1 [17].

$$H \Psi = E \Psi \qquad\qquad [2.1]$$

H is the Hamiltonian operator which is described by the sum of the kinetic and potential energy [18]. Hamiltonian operator together with the wavefunction, Ψ, is a set of solutions of the Hamiltonian [17]. E is the eigenvalue for the system [18], and each of the solutions, Ψ_n, has an associated eigenvalue, E_n. A more advanced description of the Schrödinger equation is shown in Equation 2.2 where multiple electrons are interacting with multiple nuclei. This Equation contains the ground state energy, E, which is independent of time [17].

$$\left[-\frac{h^2}{2m} \sum_{i=1}^{N} \nabla_i^2 + \sum_{i=1}^{N} V(r_i) + \sum_{i=1}^{N} \sum_{j<i} U(r_i, r_j) \right] \Psi = E\Psi \qquad\qquad [2.2]$$

Where m is the electron mass and h is the Planck constant in Equation 2.2. The first term describes kinetic energy of each electron, the second term describes the interaction energy between each electron and the collection of atomic nuclei, and the third term describes the interaction energy between different electrons. The Schrödinger equation is a many-body problem, and the third term is the most critical one for solving the equation. Only the probability that the N electrons are at a particular set of coordinates is the quantity that can be measured. The density of a particular position in space, n(r), is a closely related quantity and can be expressed as in Equation 2.3 [17].

$$n(r) = 2 \sum_i \Psi_i^*(r) \Psi_i(r) \qquad\qquad [2.3]$$

The equation describes the sum of the probability that an electron in individual wave function, $\Psi_i(r)$ is located at position r. Pauli exclusions principle state that each individual electron wave function can be occupied by two separate electrons on condition that they have different spins, therefore the equation contains a factor of two. The electron density, n(r), contains a portion of information that is observed from the full wave function solution to the Schrödinger equation. To further understand the entire field of DFT, two fundamental mathematical theorems by Kohn and Hohenberg are essential to know [17].

2.2.2. Hohenberg-Kohn (HK) Theorems

Hohenberg-Kohn (HK) theorem is the starting point in any discussion of DFT. It ensures that stationary many-particle system can be characterized by the ground state density [19]. In the mid of 1960s, Hohenberg and Kohn provided two fundamental mathematical theorems [17].

1. "The ground-state energy from Schrödinger's equation is a unique functional of the electron density" [17, p. 11]
2. "The electron density that minimizes the energy of the overall functional is the true electron density corresponding to the full solution of the Schrödinger equation" [17, p.11]

The first theorem establishes that there exists a one-to-one mapping between the ground-state electron density and the ground-state wave function. The ground-state electron density uniquely determines all properties of the ground state, and this can be used in approximately solving the Schrödinger equation. Unfortunately, the first theorem says nothing about what the functional actually is. Therefore, a second theorem was provided by HK. It says that it is possible to vary the electron density until the energy from the functional is reduced if the "true" functional form were known. Equation 2.4 is a useful way to write down the functional described by the HK theorems [17].

$$E[\Psi_i] = E_{known}[\Psi_i] + E_{XC}[\Psi_i] \qquad [2.4]$$

The equation is split into two terms, where $E_{known}[\Psi_i]$ is the known term that can be written down in an analytical form. The known terms include the Coulomb interaction between the electrons and the nuclei, the Coulomb interaction between pairs of electrons, the Coulomb interaction between pairs of nuclei and the kinetic energies [17]. Coulomb interaction tells that the magnitude of the electrostatic force between two point is proportional to the scalar multiplication of the magnitudes electrical charge. The force is also inversely proportional to the square of the distance between them. It can either be repulsive or attractive, depending on if the charge has the same sign or not [20]. The second term in Equation 2.4, $E_{XC}[\Psi_i]$, is the exchange-correlation functional, and it includes everything else that is not included in the known term. Nevertheless, solving the Schrödinger equation for the wave function need further calculations, which Kohn and Sham (KS) extended [17].

2.2.3. Kohn-Sham (KS) Equation

KS showed that solving a set of equations, in which each equation only involves a single electron, can be used to find the correct electron density. The KS equation is expressed in Equation 2.5 [17].

$$\left[-\frac{h^2}{2m}\nabla^2 + V(r) + V_H(r) + V_{XC}(r)\right]\psi(r) = \varepsilon_i\,\Psi_i(r) \qquad [2.5]$$

This equation describes the solution of a single-electron wave functions that depend on only spatial variables, $\Psi_i(r)$. In the KS equation there are three potentials: V, V_H and V_{XC}. Where V describes the interaction between an electron and the collection of atomic nuclei. The second term, V_H, is the Hartree potential which describes the Coulomb repulsion between the electron and the total electron density. The last term, V_{XC}, defines exchange and correlation contribution to the single-electron equations. This term can be defined in Equation 2.6, which shows how the V_{XC} can be defined as a functional derivative of the exchange-correlation energy, E_{XC}. Therefore, to solve this equation and thereby solve the KS equation E_{XC} needs to be solved [17].

$$V_{XC}(r) = \frac{\delta E_{XC}(r)}{\delta n(r)} \qquad [2.6]$$

2.2.4. Exchange-Correlation Functional Approximation

The Exchange-Correlation function, E_{XC}, is demanding to define and it must be specified to solve the KS equation. HK theorems guaranteed the existence of the true form of the E_{XC}, but this existence is not known except for one case. E_{XC} is known for the uniform electron gas where the electron density is constant in all points in space. Unfortunately, it is the variation in electron density that define chemical bonds and generally make materials interesting, and the uniform electron gas is a limited value [17].

There are some approximations for the E_{XC} term, where the simplest one is the local density approximation (LDA). By using the LDA, it is possible to solve the KS equation. Although, it does not solve the true Schrödinger equation, because it is not using the true E_{XC} functional [17]. There are hundreds of different forms apparated to approximation of E_{XC}, Figure 2.4 shows a schematically illustration for some of them [16].
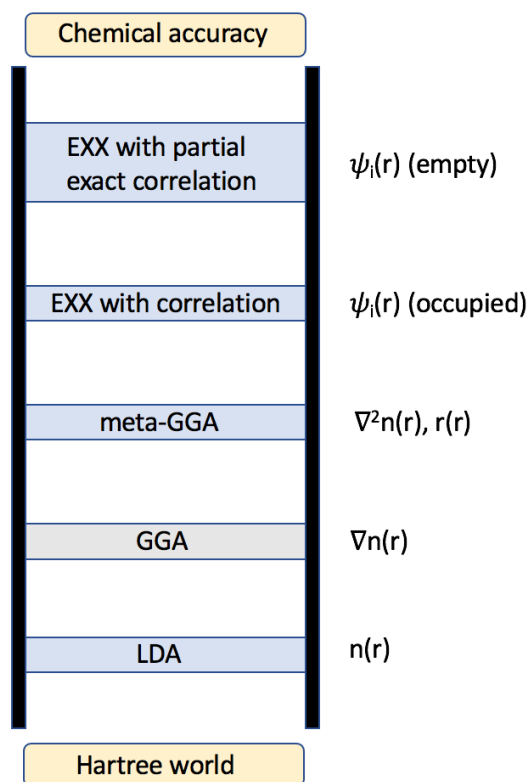
Figure 2.4: Jacob's ladder [16].

In 2001, John Perdew made an illustration of methods to solve the approximated solution of the E_{XC} according to its chemical accuracy, named Jacob's ladder (Fig. 2.4). Each step in the figure adds a dependency on another quantity. The Jacob's ladder thereby describes that increase the precision of the functional is related to the numerical complexity and computational time [16].

At the bottom of the ladder (Fig. 2.4), is the LDA which only depends on the density. The second step is the generalized gradient approximation (GGA), where the gradient of the density is added as a parameter to the energy density [16]. Heterogeneous catalysis is investigated particularly at GGA level. There is a large number of districts GGA functionals, and one of them is the Perdew-Burke-Ernzerhof (PBE) functional. PBE functionals are often used for isolated molecules. In general, GGA functional provides better predictions for total energy, structural properties and atomization energies in comparison with LDA. On the downside, GGA fails to reproduce vdW forces and it gives a low barrier height [21].

After the GGA, the next approximation in the figure are meta-GGA, exact-exchange (EXX) with correlation and EXX with partial exact correlation. These approximations include more detailed physical information according to the rise in the figure. In common, all methods in

the figure are used to find an approximate solution of E_{XC}, so it become possible to solve the Schrödinger equation. This is the whole principle of doing DFT calculations [16]. In order to do DFT calculation it is significantly to define the atomic structure of the bare surfaces [17].

2.3. DFT for Surface Solids

Understanding the geometry and electronic structure of a catalyst surface is important, because there is a relation between the surface and its catalytic activity. To perform DFT calculation for surface solids, it is important to understand how the slab model is built [17].

2.3.1. The Slab Model

A supercell is defined as a material of a solid surface with a periodic boundary conditions in all three dimensions. x and y directions are filled with atoms in the lower portion of the supercell and the top position is filled with empty space above the atoms. When the supercell is repeated in all three dimensions, it is called the slab model. Figure 2.5 illustrated the slab model, where it defines a series of stacked slabs of solid material separated by empty space. The empty space along the z direction of the figure is called vacuum. When performing DFT calculation, it is important to have enough vacuum, so the top of the supercell does not affect the bottom of the next supercell [17]. When the slab model is made, surface relaxation and reconstruction is two phenomena that are relevant to look at.
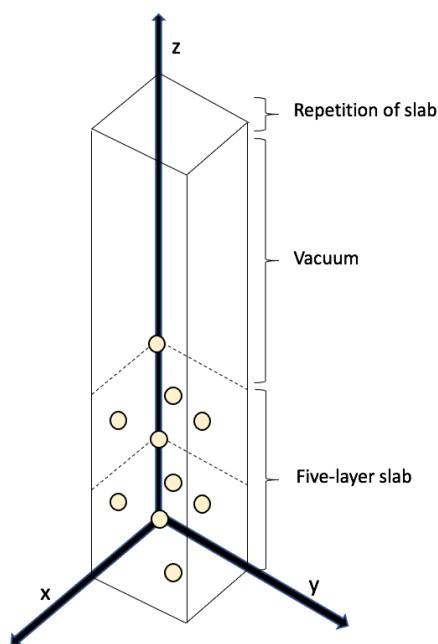
Figure 2.5: The slab model in x, y and z directions [17].

2.3.2. Surface Relaxation and Reconstruction

Relaxation and reconstruction of a surface involves rearrangements of surface atoms and this process is driven of the energetic of the system [22]. Surface relaxation is a phenomena that describes that the layers near the surface might be somewhat different from those in the bulk [17]. This will give no changes in the periodicity parallel to the surface or to the symmetry of the surface [22]. The surfaces can also undergo a surface reconstruction where atoms in the surface forms new bonds [17]. This would lead to a change in the periodicity of the surface, and in some cases changes to the surface symmetry. Minimization of the surface free energy is the driving force for the reconstruction [22].

2.4. DFT Calculations

DFT is a good established method for performing different calculations. It helps to understand the experimental observations, but approximations are needed in order to do the DFT calculations. Before using DFT, it is useful to know about the advantages and limitations of the method [17].

2.4.1. Advantages and Limitation of DFT

The first advantage, is that there are no experimental input when performing DFT, because it is a theoretical method. Another advantage, is that the adsorption energies can be calculated by using DFT with high accuracy and compared to experimental results it is often a little derivation. Bond length and angles can be calculated with high correctness by using DFT [17].

On the other hand, the limitations of DFT calculation is that the solution is not the exact solution of the Schrödinger equation. Every time someone performs a DFT calculation there will be an intrinsic uncertainty that exists between the energies calculated and the true ground-state energies of the Schrödinger equation. The only way to estimate the magnitude of this uncertainty is to make comparisons with experimental measurements. There are also some cases where DFT calculation cannot be expected to be physically accurate. In calculation of electronic exited states, the DFT calculation have limited accuracy. This is due to the statement of HK theorems, because they only apply to the ground-state energy. The calculation of the band gabs in semiconducting and isolating materials using DFT is also inaccuracy. The errors can be larger than 1 eV comparing with the experimental data, which will not be beneficial. Weak vdW attractions exist between atoms and molecules, and this is also something that leads to

inaccurate results. Describing these interactions with DFT is challenging. It is vital to use high-level wave-function-based method to calculate the strength of the interactions with DFT [17].

DFT has limited system size, which means that calculations involving thousands of atoms or more are possible but needs the world's largest computers. Therefore, using DFT on a daily basis is limited to fewer atoms. It is important to understand how information from calculation with extremely small numbers of atoms can be connected with information that is physically relevant to real materials. It is also important to keep in mind that DFT is performed at 0 K, which is not realistic to the material down on earth. Although, there are some limitation DFT, it is also a well method to understand experimental results. The DFT calculations are self-consisted and use loop to find the right output from the input [17].

2.4.2. Self-Consistent Loop (SCL)

As mention above, the exchange and correlation function are the complicated part of solving DFT. However, this could be solved by using an interactive method, namely the self-consistent loop (SCL) which is schematically showed in Figure 2.6 [23].
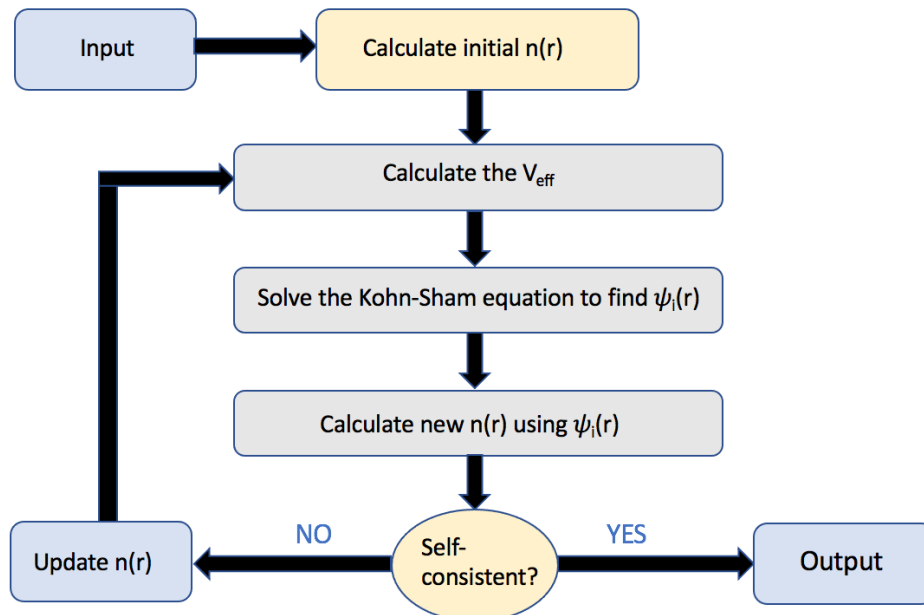
Figure 2 6: Flow chart of the SCL for solving KS equations [23].

KS equations are sets of Schrödinger-like independent-particle equations which must be solved. Figure 2.6 illustrates that the effective potential (V_{eff}), which are the sum of V, V_H and V_{XC} in Equation 2.6, and the density ($n(r)$) must be consistent in order to solve the KS equations. The

V_{eff} and n is assumed to designate both space and spine dependence. SCL will change V_{eff} and n during the calculation through a numerical procedure. It will solve the KS equation with a given input to determine the output. If the input and output potentials and densities do not agree, the SCL defines a new potential which can starts a new cycle [24]. This loop is used in DFT when calculating for example adsorption energies. To make a more realistic calculations of the material adsorption energy, the zero point energy (ZPE) can be added.

2.4.3. Zero Point Energy (ZPE)

The atoms in a material that has a temperature above 0 K will start to vibrate about their equilibrium positions. It is also a fact that the vibrations contribute to the material energy via ZPE. By using spectroscopy, these vibrations can be measured experimentally, but it can also be calculated theoretically with DFT [17].

A harmonic oscillator can be defined by each vibrational mode. For a harmonic oscillator the lowest quantum mechanical energy that can exist is presented in Equation 2.7. Where E_0 is the energy with zero kinetic energy and potential energy, h is Plank constant and v are the classical vibrational frequency of the oscillator [17].

$$E = E_0 + \frac{hv}{2}$$
[2.7]

The ZPE is the second term in the equation , and it is the difference between the energy in and the classical minimum energy, E_0. It is possible to determine the ZPE of each mode independently, thus calculate the energy that can be achieved by the set of atoms from Equation 2.8. Where E_0 is the energy that is obtained from a DFT calculation, v_i are the normal mode frequencies [17].

$$E = E_0 + \sum_i \frac{hv_i}{2}$$
[2.8]

The frequency is correlated with the bond strength, because it requires more energy to stretch a stronger bond. Frequency is a function of bond length and atom types, but motions of atoms can also affect the frequencies. Imaginary frequencies are negative vibrational frequencies and it do not exist in reality. The imaginary frequencies are useful in the transition state theory (TST) [25].

2.4.4. Transition State Theory (TST)

In 1935, Erying and Polyanyi formulated the theory in order to explain the relationship between kinetics and thermodynamics. TST explains that there can be formed an unstable, high energy complex when atoms and molecules collide [26]. The transition state (TS) is located at the top of the energy barrier between reactants and products. Crossing this barrier is only possible in the forward direction, and the situation is presented in Reaction 2.9 [1]. Existence of a chemical equilibrium between the reactants and activated state is an important assumption for the TST [26].

$$R \leftrightarrow R^{\#} \rightarrow P \qquad\qquad\qquad [2.9]$$

In the reaction, it is assumed that R (reactants) is in fully equilibrium with the $R^{\#}$, which is the reactants at TS [1]. When the molecules fall out of this high energy state, they may form another molecule or their original state. If the molecules are charged into something new, they must reach the energy for the activation state. The existence of an activation state which is formed by the reactants, is the basic assumption for the TST [26].

However, there are some limitations with the TST. The intermediate can in some cases have a short lifetime which causes that the Boltzmann distribution of energy is not reached before the reaction continues to the next step. If the reaction is occurring at high temperature or at very low temperature the TST will in some cases fail. The TST can also fail if it is applied to each elementary step of a multiple reaction [26]. To identify the TS, nudged elastic band (NEB) method can be used.

2.4.5. Nudged Elastic Band (NEB) Method

The saddle point and minimum energy path (MEP) between reactants and products can be found using the NEB method. Along the reaction path, NEB method optimize a number of intermediate images. The images are spacing to the neighbors by adding spring forces and each of them tries to find the lowest energy [27]. It is possible to use DFT to compute the force acting on the system. The aim of the NEB calculation is to find the MEP connecting two minima on the energy surface, this is done by defining a series of atomic coordinates (images) [17]. Figure 2.7 illustrates the reaction path computed with NEB [28].
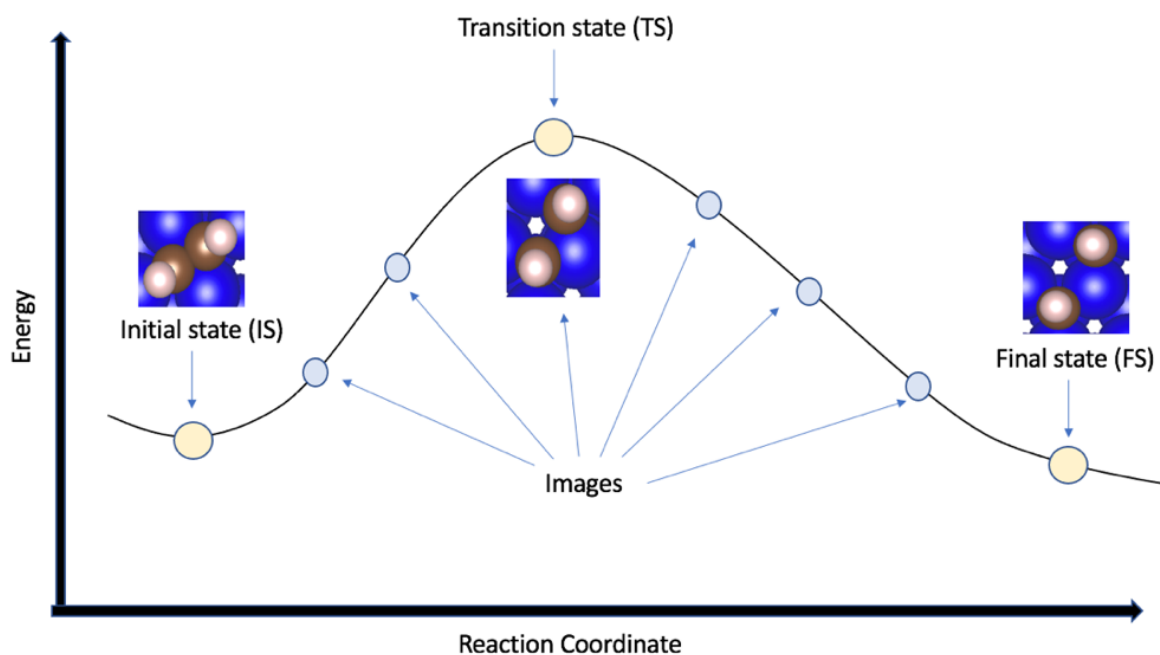
Figure 2.7: Energy profile of the reaction path computed with NEB [28].

A small modification to the NEB method is the climbing image NEB (CI-NEB), which the highest energy image is driven up to the saddle point. This image has inverted the true force at this image instead of the spring forces along the band. The highest energy image tries to maximize its energy along the band and minimize in all other directions. The exact saddle point will be found when this image converts [27].

By using CI-NEB method, it is possible to find the TS located in along the MEP between two state. The TST describes the rates of elementary reaction on molecular scale [17]. The TS is characterized with one imaginary frequency, this could be verified by doing a vibrational analysis [29]. To describe the overall reaction, thermodynamics quantities is important to take into consideration.

2.5. Thermodynamics

Thermodynamics is the study of thermal, mechanical, electrical and chemical energy. In chemistry the most important thermodynamics is the study of how energy changes during a chemical reaction. A favorable reaction occurs at the lowest overall energy [30].

During the chemical reaction, enthalpy (ΔH) is the measure of the flow of energy. The entropy (ΔS) measures the energy that is unavailable for use in the chemical reaction. ΔS is always

positive but is generally larger for gases than solids. Gibbs free energy (ΔG) is a function of enthalpy, entropy and temperature and is shown in Equation 2.10. If ΔG is negative, the reaction is thermodynamic favorable [30].

$$\Delta G = \Delta H - T \Delta S \qquad [2.10]$$

2.5.1. Ideal Gas Limit

Energy comes in various forms, and the sum of contributions from different modes of motion is the energy of a molecule. Equation 2.11 shows how to calculate the energy of a molecule, where the letters T, R, E and V indicates translation, rotation, electronic and vibrational contribution respectively [31].

$$\varepsilon_i = \varepsilon_i^T + \varepsilon_i^R + \varepsilon_i^E + \varepsilon_i^V \qquad [2.11]$$

The only term in Equation 2.11 that are not a mode of motion is the electronic contribution, but it is convenient to include. Assuming that the energy is a sum of independent contribution, it is possible to write the partition function as a factorizes into a product of contribution. This is shown in Equation 2.12 and means that it is possible to investigate the contribution separately [31].

$$q = q^T + q^R + q^E + q^V \qquad [2.12]$$

Translational Contribution

Equation 2.13 shows the translational contribution which is a function of the molecule mass (m) in a container of volume (V) [31]

$$q^T = \frac{V}{\Lambda^3} \qquad [2.13]$$

Where de Brolige thermal wavelength, Λ, is expressed in Equation 2.14 [31].

$$\Lambda = \frac{h}{(2\pi m k_B T)^{1/2}} \qquad [2.14]$$

Where h is Planck constant and k_B is the Boltzmann constant. The approximation is only valid if Λ is large compared to the many dimensions of the container [31]. Exceptions only occur at very low temperatures or at extremely high pressure [1].

Rotational Contribution

The rotational contribution may be approximated to linear rotors (Eq. 2.15) and non-linear rotors (Eq. 2.16), where A, B and C are the rotational constants [31].

$$q^R = \frac{kT}{hcB} \tag{2.15}$$

$$q^R = \left(\frac{kT}{hc}\right)^{\frac{3}{2}} \left(\frac{\pi}{ABC}\right)^{\frac{1}{2}} \tag{2.16}$$

Electronic Contribution

The electronic contribution is in most cases equal to one. Exceptions is where an atom/molecule have electronically degenerate ground state, like for example alkali metal. Equation 2.17 shows the electronic contribution assuming that the first excited state is energetically inaccessible [31].

$$q^E = v_o e^{-\frac{E_0}{k_B T}} \tag{2.17}$$

Vibrational Contribution

The vibrational contribution comes from partition function of a molecule calculated by substituting the measured vibrational energy levels. A diatomic molecule in the gas phase has only one vibration, but when it adsorbs to the surface it receives several mode. The total partition of vibrational contribution can be calculated in equation 2.18 [1].

$$q^V = \prod_i \frac{e^{-\frac{1}{2}hv_i/k_B T}}{1 - e^{-hv_i/K_B T}} \tag{2.18}$$

In the Harmonic approximation (HA), only the translational and rotational contribution is taken into consideration.

2.5.2. The Harmonic Approximation (HA)

The HA often describes the entropies of the immobile species. It is the simplest reasonable method for vibrational mode [32, 33]. There are also more complex methods like hindered translation, free translation and the most complex one complete potential energy sampling. The adsorbate in the HA is treated as a quantum harmonic oscillator, where the translations and rotations are treated as frustrated vibrations. The potential energy is assumed to be parabolic [32]. The lack of anharmonicity and lack of bond dissociation are two of the most serious limitation of the HA [33].

3. Methodology

3.1. Vienna ab Simulation Packages (VASP)

Vienna ab Simulation Packages (VASP) together with Python version 3.6 was used here to perform all the quantum chemical calculations. The computer program VASP is used for atomic scale modelling materials, and it computes an approximated solution to the many-body Schrödinger equation [34]. To run VASP, four different input files are required: INCAR, POSCAR, KPOINTS and POTCAR. A short description of these is found in Table 3.1, and an example of an INCAR, POSCAR and KPOINTS file can be seen in Appendix A [35].

Table 3 1: Short description of the four input files [35].

Input files	Description
INCAR	The central input file of VASP which determines what to do and how to do it
POSCAR	Used to specify the k-points in the Brillouin zone in the calculation
KPOINTS	Contains the lattice geometry and the ionic position
POTCAR	Contain the pseudopotential for each atomic species in the calculation

There are generated different output files from the parameters in the input files, where the main output file is the OUTCAR. A CONTCAR file is also generated, and both output files are described in Table 3.2 [35].

Table 3.2: Short description of the two output files [35].

Output files	Description
OUTCAR	The central output file of VASP which contains a summary of the input parameters, information about the electronic steps, stress tensors, forces of the atoms, local charges, magnetic moments and dielectric properties
CONTCAR	Has the same format as a POSCAR-file, and is written after each ionic step and the end of the job

3.2. Co as a Hexagonal Closed Packed (hcp) Structure

The main goal in heterogeneous catalysis is to identifying the structure sensitivity of chemical reaction. Co can exist in two crystallographic structures in the FTS, the hcp Co and the fcc Co. hcp Co is reported to have higher activity than the fcc Co [36], and overall, the hcp Co presents better results [7]. Therefore, hcp Co facets are used in this study. For heterogeneous catalysis, the effect of morphologies and crystal planes of nanostructured catalyst on the catalyst

performance plays an important role [37]. It is beneficial to specify the structures that are used in the study. A general rule of thumb says that the more open the surface is, the more reactive it is [1]. hcp material has four miller indexes, because they have a sixfold axis normal to the basal plane. In this study, it was investigated five different hcp Co structure planes: Co(0001), Co(11-20), Co(10-10), Co(10-11), and Co(10-12). The hcp Co structure planes are illustrated in Figure 3.1 [17, 38].
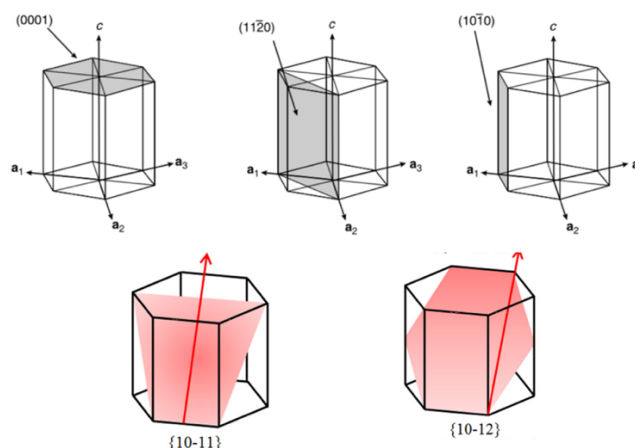
Figure 3.1: Illustration of the structure planes for the hcp miller index (0001), (11-20), (10-10), (10-11) and (10-12) [17, 38].

3.2.1. hcp Co Bulk

During the specialization project, hcp Co bulk was made by placing two Co atoms in a box. This was created by the main supervisor Ingeborg-Helene Svenum. There were also performed different convergence test on the hcp Co bulk to determine different parameters for the continuing DFT calculations. The convergence test was performed in the specialization project and are listed in Appendix B. The parameter that was found to be the optimal values was a cutoff energy of 500 eV and a sigma value of 0.1. The lattice parameter for the Co bulk was found to be a=2.492 and c=4.025.

3.2.2. Surface Models

Five hcp Co surface models were made: Co(0001), Co(11-20), Co(10-10), Co(10-11) and Co(10-12). This was performed with close cooperation with the main supervisor Ingeborg-Helene Svenum, and some of the scripts were made by her. It is important to study each surface, to gain an intrinsic into how the adsorbate will behave in contact with the Co catalyst. All the structures illustrations presented here are made in Visualization for Electronic and Structural Analysis (VESTA), which is a 3D visualization program for structure models [39].

Co(0001) Surface

A periodic p(3x3) supercell containing six layers Co atoms has been employed to model hcp Co(0001) surface. The surface model was made up by 54 Co atoms, and a 16 Å vacuum (8 Å on each side) was inserted between the periodically repeated slab model. This was done to avoid interaction between the Co atoms [17]. The two bottom layer in the slab model were kept fixed, and the remaining four layers were allowed to relax. There are four possible high symmetry adsorption sites on the flat hcp Co(0001) surface: top, bridge and two hollow site (fcc and hcp), as presented in Figure 3.2 [40]. The Python script of the surface is attached in Appendix C, Figure C.1.
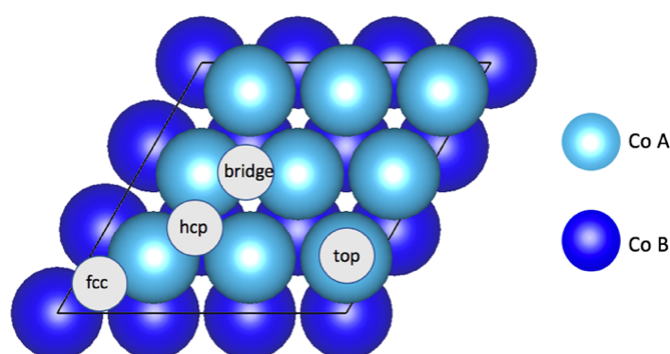
Figure 3.2: Illustration of the adsorption sites on Co(0001) surface [40].

Co(11-20) Surface

The second surface model used in this study was the corrugated hcp Co(11-20) surface. This was made with a periodic p(3x4) supercell containing six layers of Co atoms. hcp Co(11-20) surface consist of 72 Co atoms with a 16 Å vacuum inserted between the repeated slab model. The two bottom layer in the slab model were kept fixed, and the remaining layers were allowed to relax. This surface contains zigzag rows along the [0001] direction in altering layers of Co A and Co B. There are seven possible high symmetry adsorption sites on Co(11-20) surface. Where two of them are top sites, one top site on Co A layer (tA) and one top site on Co B layer (tB). There are four bridge sites, one between the Co A layer (bA), one between the Co B layer (bB) and two bridge sites between Co A and Co B (bAB$_1$ and bAB$_2$). Also, there are one hollow site located between two Co A and one Co B (hAAB). All of the sites are illustrated in Figure 3.3 [41]. The python script of the surface is attached in Appendix C, Figure C.2, which was created by Ingeborg-Helene Svenum.
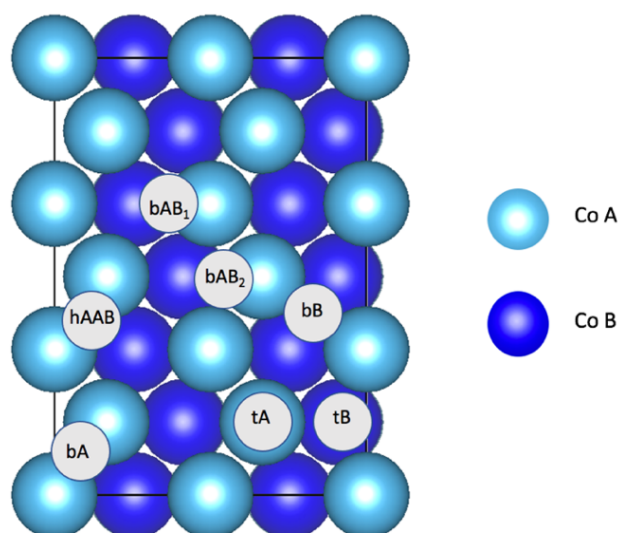
Figure 3.3: Illustration of the adsorption sites on Co(11-20) surface [41].

Co(10-10) Surface

The hcp Co(10-10) was the third surface made in this study. This was created from a periodic p(3x2) supercell with six layers of Co atoms. The supercell contains 72 Co atoms, where the two bottom layers were kept fixed and the other four layers were allowed to relax. It was inserted 16 Å vacuum between the repeated slab model. hcp Co(10-10) are slightly rippled, and it has several different adsorption sites. The six possible adsorption sites are top sites (t_1 and t_2), two bridge sites (b_1 and b_2) and two 3-fold hollow sites ($3f_1$ and $3f_2$). The numbers indicate whether the Co atom are in the front or in the back. Co atoms in the front are indicated with 1 and Co atoms in the back are indicated with 2. All of the adsorption sites on Co(10-10) surface are indicated in Figure 3.4 [4]. The python script of the surface is attached in Appendix C, Figure C.3. It is also an important point to note that the Co(10-10) surface has two different surface terminations: termination A and B. Co(10-10) A has a short interlayer spacing outermost, and Co(10-10) B has a long interlayer spacing outermost. However, the equilibrium configuration of the clean annealed Co(10-10) surface is with a short interlayer spacing outermost [42]. The Co(10-10) A termination is the one used in this study. Both terminations can be seen in Appendix D, Figure D.3 (Co(10-10) A) and Figure D.4 (Co(10-10) B).
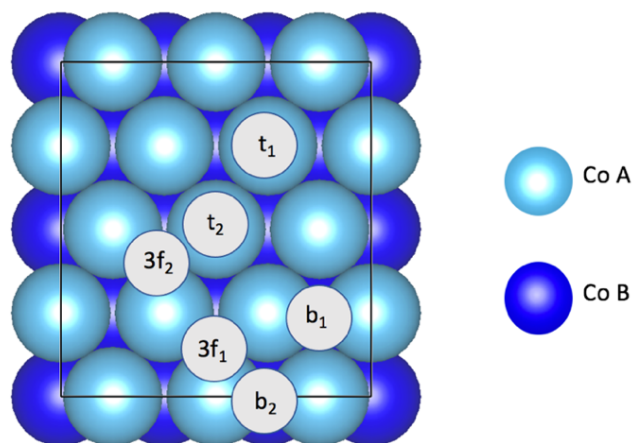
Figure 3.4: Illustration of the adsorption sites on Co(10-10) surface [4].

Co(10-11) Surface

The fourth surface made in this study was the slightly rippled hcp Co(10-11) surface. It contains 72 Co atoms with a periodic p(2x3) supercell with six layers. The two bottom layers were fixed, and the others were allowed to relax. It was inserted 16 Å vacuum between the repeated slab model. There are five possible high symmetry sites on the surface. Where three of them are hollow sites, the fcc and hcp are surrounded by three Co A atoms and the 4-fold hollow site (4fh) is surrounded by four Co A atoms. There is also one bridge site and one top site as illustrated in Figure 3.5 [43]. The python script of the surface is attached in Appendix C, Figure C.4, and was created by Ingeborg-Helene Svenum. There exist two termination of Co(10-11) surface: termination A and B, which can be seen in Appendix D, Figure D.5 (Co(10-11) A) and Figure D.6 (Co(10-11) B).
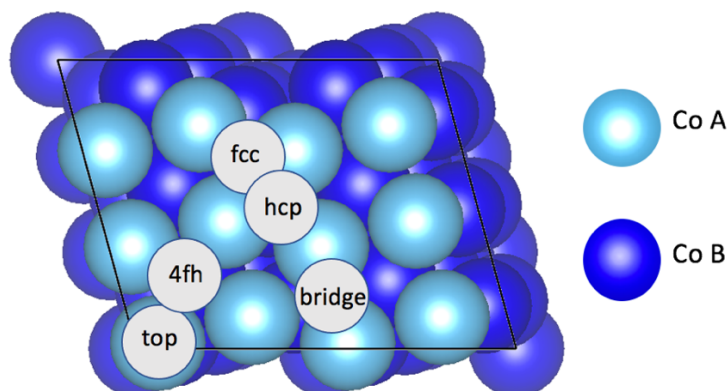
Figure 3.5: Illustration of the adsorption sites on Co(10-11) surface [43].

Co(10-12) Surface

The last surface was the stepped hcp Co(10-12) surface. The surface consists of 72 Co atoms in a periodic p(4x1) supercell with six layers. It has three different Co layers and several possible high symmetry sites. Where three of them are top sites, one above Co A (tA), one above Co B (tB) and one above Co C (tC). There are four bridge sites, one between two Co atoms in the A layer (bA), one between two Co atoms in the B layer (bB), one between two Co atoms in the C layer (bC) and one between Co A and Co B (bAB). Also, there are three hollow sites, one 3-fold hollow site between two Co A and one Co C (3hAAC), one 3-fold hollow site between two Co B and one Co C (3hBBC) and one 4-fold hollow site between two Co A and two Co B (4fh). The sites are illustrated in Figure 3.6, and may regard as a stepped surface [44]. The python script of the surface is attached in Appendix C, Figure C.5, and was created by Ingeborg-Helene Svenum. It is worth mention that there are two terminations: termination A and B. In previous studies there are concluded that the A-termination consist predominantly [45], therefore it is also used in this study. Appendix D, Figure D.7 (Co(10-12) A) and Figure D.8 (Co(10-12) B) shows the geometric illustrations of the two terminations.
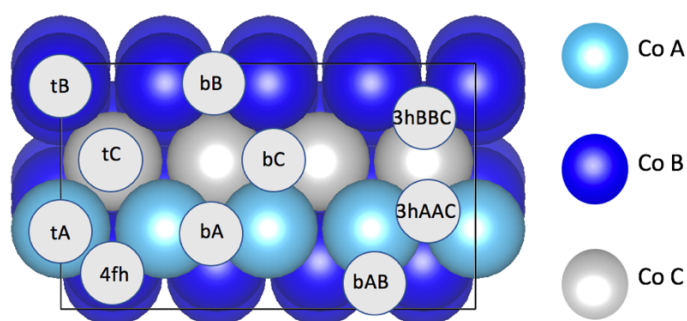
Figure 3.6: Illustration of the adsorption sites on Co(10-12) surface [44].

3.3. Calculation Method

All calculation reported here were carried out using spin-polarized DFT with the projector augmented wave (PAW) method implemented in VASP. In a natural way, PAW generalizes both the pseudopotential method and the linear augmented-plane-wave (LAPW) method. Simulations of high quality first principle molecular dynamics are possible using this method [46]. The GGA with PBE functional has been used to describe the exchange correlation energy of electrons. PBE functionals are often used for isolated molecules [21], which is also the case in this study. All calculations were performed with a cutoff energy of 500 eV to describe the

interactions between ion cores and valence electrons [44]. A K-point sampling of 5x5x1 was used via the Monkhorst-Pack Procedure in the Brillioin Zone [47].

3.3.1. Adsorption Energy (E_{ads})

Energy is a fundamental quantity that can describe adsorption [17]. The energy for all of the five clean surfaces were calculated by using the submission script (Appendix E, Figure E.1) in VASP. The adsorbates, C, H, CH, C_2, C_2H and C_2H_2, were placed above high symmetry sites on Co(0001) surface (Fig. 3.2), Co(11-20) surface (Fig. 3.3), Co(10-10) surface (Fig. 3.4), Co(10-11) surface (Fig. 3.5) and Co(10-12) surface (Fig. 3.6). This was performed in order to calculate the adsorption energy which only occur at one side of the slab model.

The dispersion correction was taken into consideration by implying the vdW interaction (IVDW=11) in the INCAR-file. It was selected the zero damping DFT-D3 method proposed of Grimme [48]. The convergence criteria was set to an EDIFFG=-0.01 and EDIFF=10^{-6} eV. Vibrational frequencies analysis was also performed in order to identify the stationary points [29]. All of the Co atoms were fixed while the adsorbate on the surface was allowed to relax. The convergence criteria was set to EDIFF=10^{-8} eV and the frequencies were used to calculate the ZPE value with equation 2.8. Adsorption energy (E_{ads}) with ZPE correction was calculated with Equation 3.1 [43]. The Co atoms were assumed to be unchanged upon the adsorption, while the adsorbate was allowed to displace in each direction by +-0.015Å. The ZPE correction was also included when the dispersion correction was taken into consideration. Negative adsorption energy indicates that the site is favorable [44].

$$E_{ads} = (E_{\frac{n}{surface}} + ZPE) - (E_{n(g)} + ZPE) - E_{surface} \quad\quad\quad [3.1]$$

Where $E_{n/surface}$ is the calculated energy of the surface with the adsorbate, and the ZPE value is added on that term. The $E_{n(g)}$ is the calculated energy of the gas phase, and the ZPE value is also added on this term. $E_{n(g)}$ is calculated by placing atoms inside a simple cubic unit cell with 10 Å, this was performed by Ingeborg-Helene Svenum. The $E_{surface}$ in Equation 3.1 is the calculated energy for the clean surface [43].

3.3.2. Surface Free Energy (E_{surf})

The surface free energy was calculated for all the five facets, and the other termination for the Co(10-10), Co(10-11) and Co(10-12) surfaces. The slab model was repeated with two from the

ordinary surfaces. The Co(0001) surface consist of 108 Co atoms while the remaining facets consist of 144 Co atoms. The geometric picture made in VESTA can be seen for all the slabs (top view and side view) in Appendix D, this was made by Ingeborg-Helene Svenum. A vacuum of 16 Å was used between the repeating slab. For the surface energy calculations all the atoms were fully relaxed. Equation 3.2 shows how the surface free energy (E_{surf}) was calculated [4].

$$E_{surf} = \frac{(E_{slab} - NE_{bulk})}{2A} \hspace{4cm} [3.2]$$

Where E_{slab} and E_{bulk} is the total energy for the slab and one bulk unit respectively. N in the equation is the number of slab in the bulk unit, and A is the surface area of the slab [4].

3.3.3. CI-NEB Calculation and Thermodynamics

CI-NEB calculation was performed to investigate acetylene decomposition on the surfaces at atomic level. There were used 11 intermediate states along the initial reaction path connecting the initial state (IS) and final state (FS). CI-NEB calculations were performed for all reactants and products configuration in the acetylene decomposition pathway on Co(0001) and Co(11-20) surfaces. There was performed a normal mode harmonic frequencies analysis on the TS geometry to confirm the nature of transition state with one imaginary frequency [41]. To minimize the barrier for the reaction, the atoms were placed in the most favorable site for that specific adsorbate on the surface. There was also performed a vibrational frequencies analysis on the IS and the FS in order to calculate the activation energy (E_a) and reaction energy (ΔE) with Equation 3.3 and Equation 3.4 [43].

$$E_a = (E_{TS} - E_{IS}) - \Delta ZPE_{barrier} \hspace{4cm} [3.3]$$
$$\Delta E = (E_{FS} - E_{IS}) - \Delta ZPE_{reaction\,energy} \hspace{3cm} [3.4]$$

Where E_{IS}, E_{TS} and E_{FS} are the total energies of the IS, TS and FS from the DFT calculation. The $\Delta ZPE_{barrier}$ and $\Delta ZPE_{reaction\,energy}$ are the ZPE correction for the E_a and ΔE, and are respectively calculated with Equation 3.5 and Equation 3.6 [43].

$$\Delta ZPE_{barrier} = \left(\sum_{i=1}^{vibrations} \frac{h\nu_i}{2}\right)_{TS} - \left(\sum_{i=1}^{vibrations} \frac{h\nu_i}{2}\right)_{IS} \hspace{2cm} [3.5]$$

$$\Delta ZPE_{reaction\,energy} = \left(\sum_{i=1}^{vibrations} \frac{h\nu_i}{2}\right)_{FS} - \left(\sum_{i=1}^{vibrations} \frac{h\nu_i}{2}\right)_{IS} \hspace{1.5cm} [3.6]$$

Gibbs free energy were calculated for the gas species H_2 and C_2H_2 taking into consideration the translational, rotational and vibrational contribution. The python script is shown in Appendix F, Figure F.1, this was created by Ingeborg-Helene Svenum. It computes ΔH and ΔS in order to calculate ΔG with Equation 2.10. The HA were used when calculating the Gibbs free energy for all of the adsorbate, the python script can be seen in Appendix F, Figure F.2. A potential energy diagram (PED) was made from the E_{ads} and activation barrier with different temperatures calculated with Gibbs free energy.

3.3.4. Increasing Carbon Coverage

Carbon were placed above Co(0001) surface and Co(11-20) surface with different monolayers (ML). A coverage of one ML is used when there is one adsorbate per surface atom [17]. The carbon adsorption energy was calculated with different coverage on both surfaces. The average E_{ads} was calculated with Equation 3.7. Where n is the number of carbon atoms placed on the surface [49].

$$E_{ads(\theta)} = \frac{E_{Surf/nC} - E_{Surf} - \left(\frac{n}{2}E_{C2H2}\right) + \left(\frac{n}{2}E_{H2}\right)}{n} \qquad [3.7]$$

In Equation 3.7, the energy calculated for the gas phases for acetylene (E_{C2H2}) and hydrogen (E_{H2}) were used as a reference. This was done to get an realistic insight into the adsorption energy, because acetylene and hydrogen can occur in gas phase in the realistic world.

4. Results & Discussion

4.1. Adsorption of Acetylene and Relevant Surface Intermediates

The stable adsorption sites found in the specialization project on the surfaces Co(0001) and Co(11-20) were further investigated (Table 1.1). Also, three new facets were made, Co(10-10), Co(10-11) and Co(10-12), where C, H, CH, C_2, C_2H and C_2H_2 were placed above high symmetry sites. In this section, there was placed one atom/molecule on each surface. The molecules C_2, C_2H and C_2H_2 are placed perpendicular to the surface in one adsorption site and they are also laid down on the surface in two adsorption sites. The CH molecule is only placed perpendicular to the surface in one site, because a study performed by Zhang *et al.* [50] showed that CH adsorbs perpendicular to the surface with C-Co binding [50].

Vibrational frequency analysis was performed to find the stationary points and include ZPE correction to the calculated E_{ads} (Eq. 3.1). The adsorption energies for "unstable" sites are obtaining by fixing the position of the adsorbate along x- and y-axes, and relaxing the distance along z-axis. If the surface was completely relaxed, then the adsorbates would be moved to the nearby stable sites [44]. It was also performed vibrational frequencies analysis for the gas phases with ideal gas limit in VASP, and the ZPE value was calculated with Equation 2.8. The frequencies and the calculated ZPE values for the gas phases CH, C_2, H_2, C_2H and C_2H_2 is attached in Appendix G, Table G.1. It was assumed that there were no changes in the energy of the clean surface with vibrational analysis.

The chemical bonding between the adsorbate and the Co surface occurs due to strong intramolecular bonding and weaker intermolecular bonding like vdW interactions [13]. Based on this, vdW interaction was implemented in DFT calculation, since the PBE functional fails to reproduce vdW [21]. This was done by carry out DFT-D3 functional, and the E_{ads} was calculated with the ZPE corrections (Eq. 3.1). All the E_{ads} calculated in this section is calculated with respect to the corresponding atom/molecule in the gas phase.

Further, the adsorption energy for the adsorbate in its most stable site was compared with each other on the different surfaces. The surface free energy was also computed for all five facets together with the corresponding terminations.

4.1.1. Low Coverage on Co(0001) Surface

The flat hcp Co(0001) surface have four possible high symmetry sites (Fig. 3.2). Table 4.1 shows the calculated E_{ads} with ZPE correction for Co(0001) surface with PBE and DFT-D3 functional. The energy for the clean surface was computed to be -367.03 eV and the energy for the clean surface with vdW interaction was computed to be -381.50 eV. The distance (d) was found in VASP, and it is measured from where the atom in the adsorbate (n) was closest to the Co atom in the surface. The frequencies and ZPE values for all of the sites are listed in Appendix H, Table H.1. An example for the calculation of ZPE value is shown in Appendix I.

All the possible sites were investigated for the adsorbates on the Co(0001) surface. By performing a vibrational frequency analysis, it is possible to see that the sites presented of imaginary nodes in the calculation is not at the local minima [25]. Therefore, the sites illustrated with "-" under the E_{ads} are unstable for that specific adsorbate on Co(0001) surface.

Table 4.1: ZPE corrected E_{ads} with PBE functional and DFT-D3 functional together with the distance and ΔE_{ads} on Co(0001) surface at 0 K.

Ads.	Sites	E_{ads} [eV] with ZPE (PBE)	d_{n-Co} [Å] (PBE)	E_{ads} [eV] with ZPE (DFT-D3)	d_{n-Co} [Å] (DFT-D3)	ΔE_{ads} [eV]	Ref. E_{ads} [eV]
C	hcp	-6.81	1.777	-6.98	1.777	0.17	-6.38[51], -6.83[52]
	fcc	-6.56	1.786	-6.73	1.785	0.17	
	top	-	-	-	-	-	
H	hcp	-2.60	1.746	-2.73	1.738	0.13	
	fcc	-2.63	1.738	-2.76	1.731	0.13	-2.88[53], -2.78[52]
	top	-	-	-	-	-	
CH	hcp	-6.80	1.861	-7.04	1.859	0.24	-6.72[54],-6.30[52]
	fcc	-6.69	1.866	-6.91	1.866	0.22	
	top	-	-	-	-	-	
C_2	fcc-hcp	-7.23	1.873	-7.50	1.873	0.26	
	top	-	-	-	-	-	
C_2H	fcc-hcp	-5.35	1.836	-5.70	1.833	0.35	
	hcp	-	-	-	-	-	
	fcc	-	-	-	-	-	
	top	-3.70	1.830	-3.97	1.824	0.27	
C_2H_2	fcc-hcp	-2.60	1.993	-3.04	1.990	0.44	

The top site for the closed packed Co(0001) surface were not stable for any of the adsorbates except for C_2H molecule. There are also listed some E_{ads} found in other study [51-54] listed in the table to verify the accuracy of the E_{ads} found in this study. Although there is a slight difference between the reference [51-54] and the numbers reported here, but this can be due to the difference in the input parameters and the slab model. The other studied listed here uses different slab model, therefore, the comparison might not be directly, but it is an indication that

the results here are reliable. Also the adsorption of C, H and CH in the reference [51-54] was found to have the same favorable site as found here. The acetylene chemisorbed to the surface with an energy of -3.04 eV at fcc-hcp site with its C-C bond parallel to the surface.

To evaluate the effect of vdW interaction, DFT calculations performed with PBE functional is compared with those using DFT-D3 functional. As shown in Table 4.1, the distance between the adsorbate and the nearest Co atom on the surface is slightly lower or similar with DFT-D3 functional than the PBE functional. This is probably due to the repulsive interaction caused by the vdW forces [14, 47]. It is found that the E_{ads} are 0.13–0.44 eV higher with the PBE functional than with DFT-D3 functional. Based on this, it is noted that the vdW interactions do contribute to the E_{ads}. The difference between the E_{ads} is also increasing with the increasing weight of the atom/molecule. This indicates that the vdW interaction is increasing with the increasing weight of the adsorbate.

Since the E_{ads} with vdW interaction and ZPE correction were calculated separately, it was appropriate to perform a test to find the bare relation between the ZPE with and without vdW correction. The ZPE with vdW correction became 0.7708 eV while the ZPE without vdW correction became 0.7689 eV. The difference in the ZPE values is 0.0019 eV, but the difference is too small to affect the E_{ads}. The calculated E_{ads} for both was 2.60 eV, which was calculated with the same E_{clean} as a reference for comparison. Although, this means that it is possible to ignore this error and use the ZPE correction when calculated the E_{ads} with vdW interaction.

Nevertheless, the most stable site for the adsorbate and where it prefers to be, will be the lowest E_{ads} calculated for all the adsorbates [44]. Therefore, the sites marked in yellow in the table are the most preferred site for the adsorbate. Figure 4.1 shows the most stable configurations for the different adsorbates on Co(0001) surface made in VESTA.
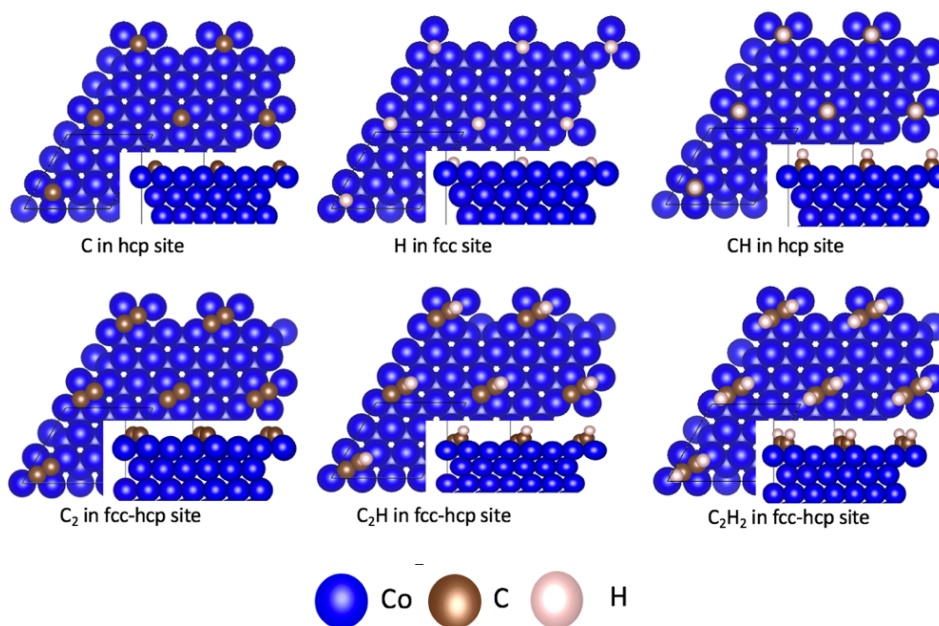
Figure 4.1: Pictures of the most stable sites on Co(0001) with different adsorbates in front and side views (inserted).

4.1.2. Low Coverage on Co(11-20) Surface

Table 4.2 shows the resulting E_{ads} calculated on Co(11-20) surface with PBE and DFT-D3 functional. The energy of the clean surface was computed to -473.36 eV and the energy of the clean surface with vdW interactions was computed to -489.55 eV. The distance (d) from the adsorbate (n) to the nearest Co atom on the surface found in VASP is also listed for both. Vibrational frequencies and the calculated ZPE values for all of the adsorbates are listed in Appendix H, Table H.2.

The corrugated hcp Co(11-20) surface have seven possible high symmetry sites (Fig. 3.3) where the adsorbates were placed on. C_2 adsorption at tB-tB (offsite) lies horizontal to the surface, while C_2 adsorption at tB-tB (offsite)2 lies vertical to the surface. The difference of C_2H adsorption at tB-tB (offsite) and at tB-tB (offsite)2 was the orientation of hydrogen on Co(11-20) surface. Where tB-tB (offsite) has the hydrogen atom in C_2H on its left side (front view), while tB-tB (offsite)2 has its hydrogen atom in C_2H on its right side (front view). For the C_2H adsorption in tB-bB the CH was placed in bB site, while in the tB-bB2 site the CH was placed in tB site. There was also two tB-tB (offsite) for the C_2H_2 adsorption where the tB-tB (offsite) lies horizontal to the surface and the tB-tB (offsite)2 lies obliquely on the surface.

Table 4.2: ZPE corrected E_{ads} with PBE functional and DFT-D3 functional together with the distance and ΔE_{ads} on Co(11-20) surface at 0 K.

Ads.	Sites	E_{ads} [eV] with ZPE (PBE)	d_{n-Co} [Å] (PBE)	E_{ads} [eV] with ZPE (DFT-D3)	d_{n-Co} [Å] (DFT-D3)	ΔE_{ads} [eV]	Ref. E_{ads} [eV]
C	tB (offsite)	-7.24	1.945	-7.33	1.943	0.09	-7.22[52]
	bB	-7.00	1.825	-7.13	1.827	0.13	
H	tB (offsite)	-	-	-	-	-	
	bB	-2.41	1.778	-2.54	1.765	0.13	
	bA	-2.50	1.673	-2.62	1.668	0.12	-2.66[52]
	bAB$_2$	-2.40	1.618	-2.54	1.615	0.14	
CH	tB (offsite)	-7.22	1.901	-7.30	1.897	0.08	-6.47[52]
	bB	-6.97	1.914	-7.07	1.917	0.10	
C$_2$	tB-tB (offsite)	-7.83	1.823	-8.09	1.823	0.26	
	tB-tB (offsite)2	-7.50	1.840	-7.75	1.841	0.25	
	tB-bB	-7.84	1.885	-8.10	1.886	0.26	
	bA-tB	-6.68	1.912	-6.89	1.914	0.21	
C$_2$H	tB-tB (offsite)	-5.53	1.864	-5.81	1.863	0.28	
	tB-tB (offsite)2	-5.37	1.897	-5.67	1.893	0.30	
	tB-bB	-5.43	1.928	-5.76	1.938	0.33	
	tB-bB2	-5.35	1.891	-5.70	1.892	0.35	
	bA-tB	-5.40	1.864	-5.68	1.863	0.28	
C$_2$H$_2$	tB-tB (offsite)	-2.28	1.910	-2.68	1.906	0.40	
	tB-tB (offsite)2	-2.15	1.986	-2.61	1.980	0.46	
	hAAB-hAAB	-2.14	1.908	-2.52	1.908	0.38	

The sites shown in the Table 4.2 were denoted as stable due to the same configuration during the calculation in VASP. By performing the vibrational frequency analysis, it is possible to see that the sites presented of imaginary nodes in the calculation is not at the local minima [25]. The results in Table 4.2 shows that only the H adsorption in tB (offsite) site was not stable after the vibrational analysis, and is therefore denoted with "-".

The carbon atom prefers to bind in an tB (offsite) site, and the hydrogen prefers to bind in an bA site, which agrees with the results done in a previous study [52]. The favorable site for the CH adsorption is in tB (offsite) site, which is also in agreement with the previous study [52]. Although there is a slight difference in the E_{ads} calculated here and the E_{ads} calculated in the reference [52], the results here are in good agreement. The derivation in E_{ads} could appear because the study performed by Liu *et al.* [52] used a periodic unit cell of p(2x2) with 56 Co atoms, while in this study it was used a periodic unit cell of p(3x4) with 72 Co atoms. Also, they have not included the ZPE-value and vDW interaction, which will also lead to a discrepancy [52].

By analyzing the distance listed in Table 4.2 it can be noted that there is no specific trend. Some have closer distance from the adsorbate to the surface with PBE functional, and some have

closer distance from the adsorbate to the surface with DFT-D3 functional. This is due to the attractive and repulsive forces occurring to the vdW interactions [14]. It is found that the E_{ads} were 0.09–0.46 eV higher with the PBE functional than with DFT-D3 functional. Based on this, it is noted that the vdW interactions do contribute to the E_{ads} also on Co(11-20) surface.

The lowest E_{ads} for each adsorbate indicates the most favorable site for that specific adsorbate [44], and these are marked in yellow in Table 4.2. Figure 4.2 shows the gematric information of the most stable sites for the different adsorbates on Co(11-20) surface made in VESTA.
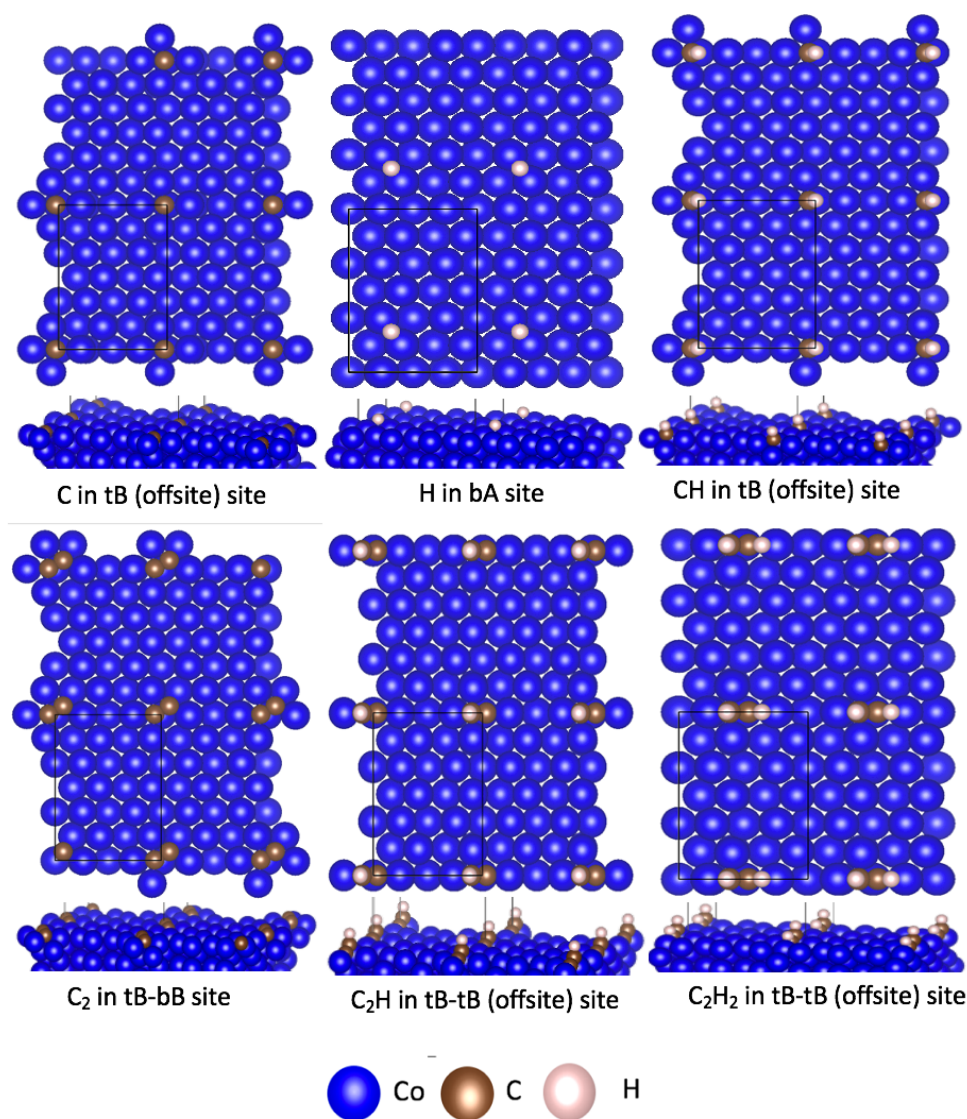
Figure 4 2: Pictures of the most stable sites on Co(11-20) with different adsorbates in front and side views (under).

4.1.3. Low Coverage on Co(10-10) Surface

The adsorbates C, H, CH, C_2, C_2H and C_2H_2 were placed above the slightly rippled Co(10-10) surface in all possible sites (Fig. 3.4) and the E_{ads} was calculated. This was performed with both PBE and DFT-D3 functional to note the difference, shown in Table 4.3. The energy of the clean surface was computed to -489.35 eV and the energy of the clean surface with vdW interactions was computed to -509.07 eV. The distance (d) from the adsorbate (n) to the nearest Co atom on the surface found in VASP is also listed for both. Appendix H, Table H.3 shows the vibrational frequencies and the calculated ZPE values for all of the adsorbates. The presents of imaginary frequencies tells that the site is not stable [25]. All the E_{ads} calculated in the table are ZPE corrected.

Table 4.3: ZPE corrected E_{ads} with PBE functional and DFT-D3 functional together with the distance and ΔE_{ads} on Co(10-10) surface at 0 K.

Ads.	Sites	E_{ads} [eV] with ZPE (PBE)	d_{n-Co} [Å] (PBE)	E_{ads} [eV] with ZPE (DFT-D3)	d_{n-Co} [Å] (DFT-D3)	ΔE_{ads} [eV]	Ref. E_{ads} [eV]
C	$3f_1$	-6.65	1.785	-6.81	1.785	0.16	
	b_2	-7.05	1.819	-7.17	1.817	0.12	
H	$3f_1$	-2.62	1.729	-2.73	1.726	0.11	-2.72[55]
	b_2	-2.57	1.728	-2.69	1.726	0.12	
CH	$3f_1$	-6.79	1.860	-7.01	1.858	0.22	
	b_2	-7.07	1.888	-7.30	1.885	0.23	-6.53[55]
C_2	b_1-$3f_1$	-6.27	1.808	-6.52	1.806	0.25	
	b_2-$3f_1$	-7.55	1.927	-7.80	1.929	0.25	
	$3f_1$-$3f_1$	-7.54	1.950	-7.77	1.943	0.23	
	$3f_2$-$3f_2$	-7.43	1.807	-7.69	1.807	0.26	
C_2H	b_1-$3f_1$	-4.99	1.804	-5.28	1.805	0.29	
	b_2-$3f_1$	-5.55	1.913	-5.88	1.907	0.33	
	b_2-$3f_1$ 2	-5.27	1.836	-5.63	1.835	0.36	
	b_1	-	-	-	-	-	
	b_1-t_1	-4.66	1.830	-4.97	1.826	0.31	
C_2H_2	b_2-$3f_1$	-2.45	1.975	-2.89	1.974	0.44	-2.18[55]
	t_1	-	-	-	-	-	
	t_2	-	-	-	-	-	
	b_1-t_1	-1.52	1.859	-1.87	1.857	0.35	
	$3f_1$-$3f_1$	-2.19	1.966	-2.64	1.964	0.45	

From Table 4.3 it is noted that the carbon prefers to adsorb in the b_2 site, while the hydrogen prefers to adsorb in the $3f_1$ site due to its lowest E_{ads} [44]. An E_{ads} of -2.72 eV for hydrogen at $3f_1$ site was found in a present study [55], which is just a slight difference from the E_{ads} of -2.73 eV found here. In an experimental study performed by Ernst *et al.* [56], they have investigated hydrogen on Co(10-10) surface with ultrahigh vacuum using Video-LEED. The LEED structure showed that hydrogen deposits in the same site which was found favorable here [56]. All of the adsorbates found in the reference listed in the table [55] preferred to adsorb in the

same site as found here, which indicates that the results obtained here are credible. Acetylene preferred to chemisorbed at b_2-$3f_1$ site (E_{ads}=2.89 eV) with its C-C bond parallel to the surface and the hydrogen pointing out from the surface.

The distance (d) between the surface and the nearest atom in the adsorbate was decreasing with DFT-D3 functional, which indicates that the repulsive forces are dominating between the surface and the adsorbate [14, 47]. There was also found a difference (0.11-0.45 eV) in the E_{ads} when calculating with both functional, this indicates that the vdW interaction do contribute to the E_{ads}.

The sites marked in yellow in the table were the favorable site for each of the adsorbent due to its lowest E_{ads} [44]. Figure 4.3 shows the configuration of all the adsorbent in its most favorable site.
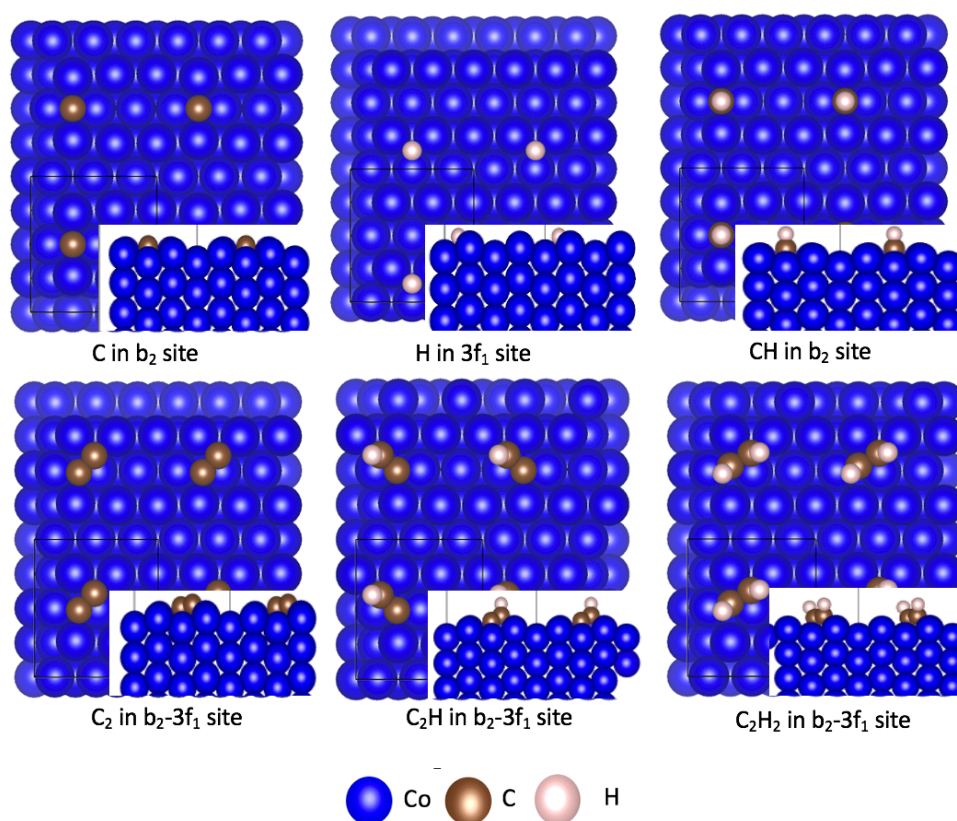
Figure 4.3: Pictures of the most stable sites on Co(10-10) with different adsorbates in front and side views (inserted).

4.1.4. Low Coverage on Co(10-11) Surface

All possible adsorbed sites with acetylene and its intermediates have been investigated on Co(10-11) surface (Fig. 3.5). Table 4.4 presents the stable adsorption sites for all of the different adsorbates. The energy of the clean surface was calculated to -485.86 eV, while the energy of the clean surface with vdW interaction was calculated to -504.86 eV. All the E_{ads} are ZPE corrected, and the frequencies together with the calculated ZPE value can be seen in Appendix H, Table H.4.

Table 4.4: ZPE corrected E_{ads} with PBE functional and DFT-D3 functional together with the distance and ΔE_{ads} on Co(10-11) surface at 0 K.

Ads.	Site	E_{ads} [eV] with ZPE (PBE)	d_{n-Co} [Å] (PBE)	E_{ads} [eV] with ZPE (DFT-D3)	d_{n-Co} [Å] (DFT-D3)	ΔE_{ads} [eV]	Ref. E_{ads} [eV]
C	4fh	-8.07	1.855	-8.23	1.857	0.16	-8.29[43]
	fcc	-6.83	1.779	-6.98	1.779	0.15	
	hcp	-6.83	1.775	-6.99	1.774	0.16	
H	4f	-2.64	1.859	-2.75	1.854	0.11	
	fcc	-2.68	1.731	-2.79	1.724	0.11	-2.68[43]
	hcp	-2.65	1.743	-2.77	1.738	0.12	
CH	4fh	-7.53	1.940	-7.77	1.940	0.24	-6.93[43]
	fcc	-6.93	1.857	-7.14	1.856	0.21	
	hcp	-6.90	1.856	-7.12	1.855	0.22	
C$_2$	4fh-fcc	-7.47	1.839	-7.75	1.836	0.28	
	4fh-hcp	-7.91	1.933	-8.19	1.931	0.28	
	bridge	-	-	-	-	-	
	fcc-hcp	-7.48	1.873	-7.73	1.872	0.25	
	4fh-4fh	-7.43	1.806	-7.68	1.804	0.25	-7.55[43]
C$_2$H	4fh-fcc	-5.12	1.867	-5.47	1.857	0.35	
	4fh-bridge	-5.85	1.927	-6.18	1.925	0.33	
	4fh-bridge 2	-5.80	1.922	-6.14	1.920	0.34	
	fcc-bridge	-5.25	1.818	-5.56	1.819	0.31	
	4fh-hcp	-5.50	1.864	-5.84	1.862	0.34	
	fcc-hcp	-5.56	1.830	-5.89	1.827	0.33	
	top	-	-	-	-	-	
C$_2$H$_2$	4fh-fcc	-2.51	1.925	-2.94	1.921	0.43	
	4fh-hcp	-2.71	1.969	-3.14	1.964	0.43	
	4fh-4fh	-2.65	1.884	-3.05	1.879	0.40	-2.73[43]
	fcc-hcp	-2.77	1.982	-3.18	1.972	0.41	

The ones marked in yellow in the table was the most favorable site for that specific adsorbent due to the lowest calculated E_{ads} [44] which is shown in Figure 4.4. The C atom prefers to adsorb in an 4fh site on Co(10-11) surface, and the H atom prefers to adsorb in an fcc site. These results are consistent with the results done by Liu *et al.* [43]. It is noted that the E_{ads} in the reference [43] has a slight discrepancy from the results found here, except for the hydrogen which is similar to the one reported here without vdW interaction. The difference could be due to different parameters in the input files. Although there is a slight difference, it was the same

favorable site for the adsorbates that were concluded except for the C_2 and C_2H_2 adsorptions. C_2 has the most stable configuration in 4fh-hcp site, while in the reference the 4fh-4fh was reported as the favorable site. Acetylene chemisorb to the surface with -3.18 eV in an fcc-hcp site with its C-C bond, while in the reference acetylene adsorbs in the 4fh-4fh site was the most favorable. The reason for this is unknown. In the study performed by Liu *et al.* [43], they did not report the E_{ads} for C_2 and C_2H_2 in the 4fh-hcp and fcc-hcp sites [43]. Therefore, it may be due to absence from these adsorptions.

The difference in E_{ads} for the ones calculated with PBE functional and the ones calculated with DFT-D3 functional varies from 0.11-0.43 eV. Which can indicate that the vdW do contribute to the E_{ads}.

| C in 4fh site | H in fcc site | CH in 4fh site |
| C_2 in 4fh-hcp site | C_2H in 4fh-bridge site | C_2H_2 in fcc-hcp site |

Co   C   H

Figure 4.4: Pictures of the most stable sites on Co(10-11) with different adsorbates in front and side views (under).

4.1.5. Low Coverage on Co(10-12) Surface

Adsorption of acetylene and the relevant intermediates were also investigated on the stepped surface Co(10-12) with ten adsorption sites (Fig. 3.6). Table 4.5 shows the sites that had the same configuration after the calculation in VASP. The E_{ads} were calculated with both PBE functional and DFT-D3 functional, and they are ZPE corrected. The energy of the clean surface was computed to -487.72 eV and the energy of the clean surface with vdW interaction was computed to -507.46 eV. Distance (d) from the nearest atom in the adsorbate (n) and the Co

surface is also shown in the table. All the frequencies and the ZPE values can be seen in Appendix H, Table H.5.
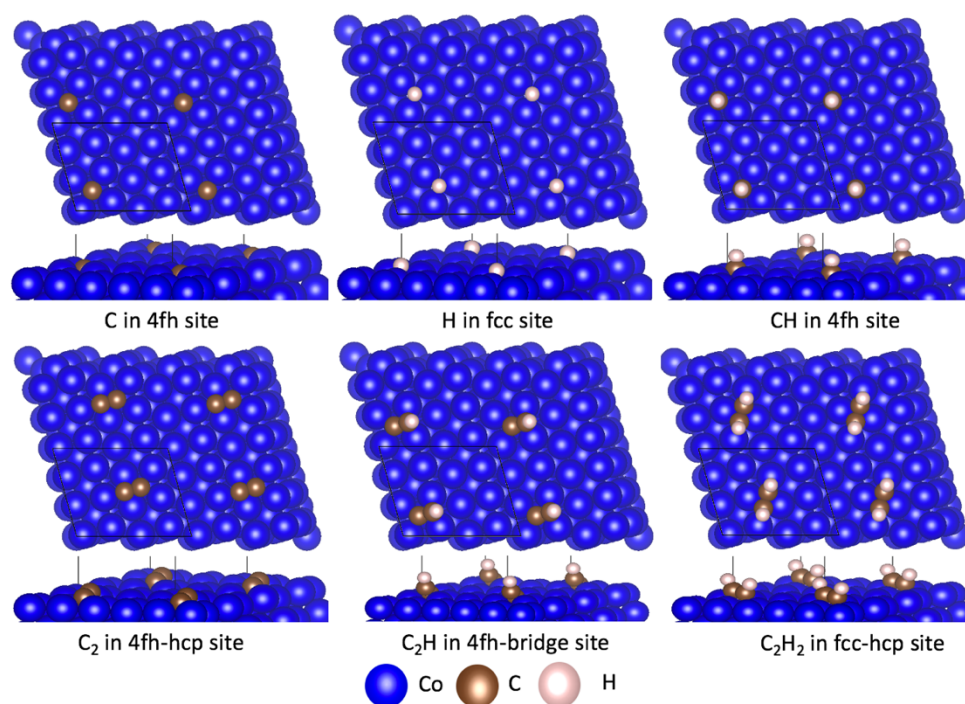
Table 4.5: ZPE corrected E_{ads} with PBE functional and DFT-D3 functional together with the distance and ΔE_{ads} on. Co(10-12) surface at 0 K.

Ads.	Site	E_{ads} [eV] with ZPE (PBE)	d_{n-Co} [Å] (PBE)	E_{ads} [eV] with ZPE (DFT-D3)	d_{n-Co} [Å] (DFT-D3)	ΔE_{ads}	E_{ads} [eV] ref.
C	tC	-7.10	1.850	-7.24	1.844	0.14	
	bC	-7.17	1.787	-7.31	1.787	0.14	
	4fh	-7.78	1.864	-7.93	1.866	0.15	-7.85[52]
H	tC	-2.48	1.748	-2.61	1.748	0.13	
	bA	-2.52	1.663	-2.62	1.657	0.10	
	bC	-2.48	1.781	-2.61	1.771	0.13	
	3hBBC	-2.50	1.718	-2.64	1.710	0.14	
	4fh	-2.61	1.866	-2.70	1.874	0.09	-2.73[52]
	bAB	-2.46	1.667	-2.57	1.658	0.11	
CH	tC	-6.71	1.870	-6.96	1.867	0.25	
	bC	-6.89	1.861	-7.14	1.862	0.25	
	3hBBC	-6.71	1.872	-6.96	1.868	0.25	
	4fh	-7.33	1.958	-7.55	1.958	0.22	-6.84[52]
C_2	tA-bAB	-	-	-	-	-	
	tC-tC	-7.80	1.886	-8.07	1.885	0.27	
	bA-4fh	-7.30	1.923	-7.56	1.919	0.26	
	4fh-4fh	-7.36	1.823	-7.60	1.824	0.24	
	3hBBC-4fh	-7.02	1.874	-7.30	1.865	0.28	
C_2H	tA	-	-	-	-	-	
	tC-bC	-5.30	1.914	-5.67	1.910	0.37	
	tC-tC	-5.65	1.938	-5.96	1.934	0.31	
	bA-4fh	-5.78	1.945	-6.08	1.940	0.30	
	bB	-	-	-	-	-	
	bB-4fh	-5.60	1.921	-5.93	1.922	0.33	
	4fh-4fh	-5.54	1.791	-5.85	1.792	0.31	
	bAB-4fh	-	-	-	-	-	
C_2H_2	tA	-	-	-	-	-	
	tB	-	-	-	-	-	
	tA-bA	-1.59	1.869	-1.93	1.865	0.34	
	tC-bA	-1.83	1.919	-2.25	1.917	0.42	
	tC-bC	-2.41	1.991	-2.91	1.984	0.50	
	tC-3hBBC	-2.06	1.904	-2.50	1.908	0.44	
	4fh-4fh	-2.60	1.890	-2.98	1.887	0.38	

Those marked in yellow in the table was the most favorable for that specific adsorbate due to its lowest E_{ads} [44]. For the Co(10-12) surface, hydrogen and carbon preferers to adsorb in the same site, 4-fold hollow site. This is consistent with the C and H adsorption done in previous study [44, 52]. The E_{ads} found in the reference [52] has a little derivation from the ones found here. The reason for this may be that the slab in the reference was p(2x2) and contained 48 Co atoms [52], while the one used here was p(4x1) and contained 72 Co atoms. However, the discrepancy is so small, that the results found here are reliable. Acetylene molecule prefer to

chemisorb at 4fh-4fh site with -2.98 eV with its carbon atoms parallel to the surface, while the hydrogen atoms are pointing out from the surface.

It is possible to see a remarkable difference in the E_{ads} calculated with both functionals, and it varies from 0.09 eV in hydrogen adsorption all the way up to 0.50 eV for acetylene adsorption. This indicates that the vdW interaction have an impact on the E_{ads}, and it is a higher difference for the more heavier components. However, the most favorable site for each adsorbates can be seen in Figure 4.5.
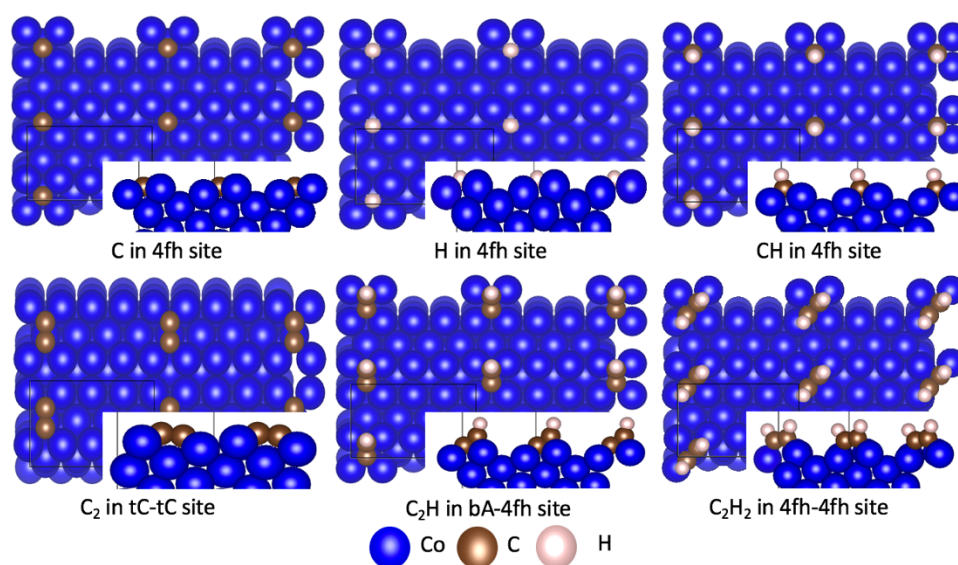
Figure 4.5: Pictures of the most stable sites on Co(10-12) with different adsorbates in front and side views (inserted).

4.1.6. Surface Free Energy and Comparison of E_{ads} on all Facets

The surface free energy was calculated with Equation 3.2 for all five facets and the corresponding termination of the surfaces Co(10-10), Co(10-11) and Co(10-12). Table 4.6 presents all the calculated surface free energies. Among the facets studied, the closed-packed Co(0001) facet has the lowest surface free energy, therefore, this facet is the most thermodynamically stable. In an study performed by Chen *et al.* [4] it was also concluded that the Co(0001) surface was the most thermodynamically stable facet among 15 facets [4].

Table 4.6: Calculated surface free energy for the five facets and its other termination.

Facet	Slab	A [Å^2]	E_{surf} [meV/Å^2]	Ref. E_{surf} [meV/Å^2]
Co(0001)	p(3x3)	48	125	134[4], 131[36], 133[37]
Co(11-20)	p(3x4)	104	152	157[4], 155[36], 155[37]
Co(10-10) A	p(3x2)	60	134	143[4], 140[36], 144[37]
Co(10-10) B	p(3x2)	60	173	
Co(10-11) A	p(2x3)	91	147	152[4], 149[36], 152[37]
Co(10-11) B	p(2x3)	91	175	
Co(10-12) A	p(4x1)	59	152	159[4], 156[36], 160[37]
Co(10-12) B	p(4x1)	59	153	

In Table 4.6 it was noted a large difference between the two terminations of Co(10-10) and Co(10-11). The B termination for both of the surfaces has higher E_{surf} than the A termination. Therefore, the A termination will consist predominantly in the Co-particle, because the it tries to minimize the surface free energy [22]. There was just a slight difference in the A and B termination of Co(10-12) surface, this could be a result of the fully relaxed surface which makes the surfaces more similar. Nevertheless, also for this surface the A termination is more stable than the B termination.

In an study performed by Liu *et al.* [37], said that relaxed surface stability increases in the following order: Co(10-12)<Co(11-20)<Co(10-11)<Co(10-10)<Co(0001) [37]. Which is in agreement with the results shown in the table, except that Co(10-12) and Co(11-20) have the same calculated surface free energy, which means that they are equal thermodynamically stable. It is noted that the E_{sur} in the three reference [4, 36, 37] listed in the table have some variations. It is also a derivation to the results found here, but this could be due to the difference in slab models like the lattice parameters or the k-point mech. However, E_{surf} calculated here are in good agreement with the literature findings [4, 36, 37]. It can be noted than in general the E_{surf} increases by increasing Miller index [4].

To get an insight in how all of the adsorbates adsorbs to the different facets, a diagram was made to compare all of the E_{ads} (with vdW interaction and ZPE correction) in their most stable configuration, shown in Figure 4.6. The numbers under each column represents the E_{ads} calculated.
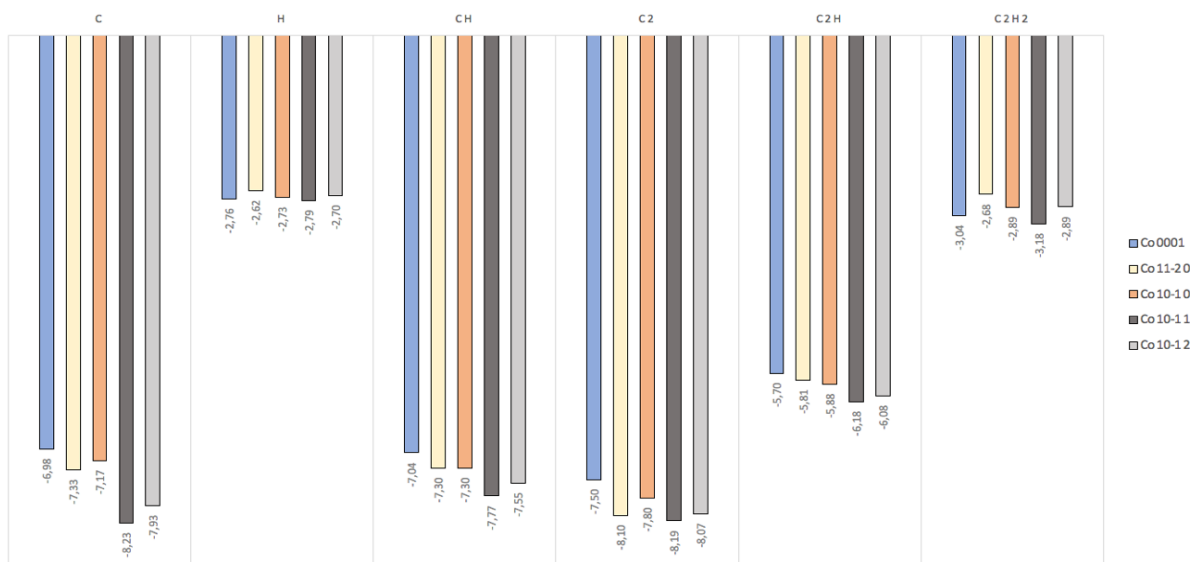
Figure 4.6: C, H, CH, C$_2$, C$_2$H and C$_2$H$_2$ adsorption in its most favorable sites on the five different facets calculated with vdW interactions and ZPE correction.

It is important to note that the Co(0001) facet only consist of 54 Co atoms and has 9 Co atoms in the top layer of the surface, while the other four facets consist of 72 Co atoms with 12 Co atoms in the top layer of the surface. Therefore, the coverage will be a bit different on the Co(0001) surface compared with the others. However, this is just a small inaccuracy and will be disregarded in the further discussion.

From Figure 4.6, it was possible to note that the carbon atom adsorb strongest on the Co(10-11) surface. In an study performed by Liu *et al.* [52] they investigated three Co surfaces, and concluded that the carbon adsorbed strongest in the order Co(10-12)>Co(11-20)>Co(0001) [52]. This is in agreement with results here performed at those three surfaces.

The hydrogen atom binds strongest to the Co(10-11) surface which was noted from the diagram in Figure 4.6. In an study performed by Weststrate *et al.* [44], they concluded that the E$_{ads}$ for hydrogen decreases from Co(0001) to Co(10-12) to Co(11-20) which was the trend in the desorption temperatures observed in thermal-programed desorption (TPD) spectra. This was also verified with DFT calculations in the same study [44]. From Figure 4.6, the hydrogen binds strongest in the order Co(10-11)>Co(0001)>Co(10-10)>Co(10-12)>Co(11-20), where the three surfaces is consistent with the Weststrate *et al.* study [44]. This indicates that the hydrogen adsorbs weaker on the more open surfaces, except for the Co(10-11) surface.

The CH molecule adsorbs strongest on the Co(10-11) surface, then the order was Co(10-12) to Co(11-20) and Co(10-10) to Co(0001) surface. The study performed by Liu *et al.* [52] showed that the CH molecule binds strongest Co(10-12), then Co(11-20) and then Co(0001) surface [52]. This is in accordance with the results obtained here.

The strongest E_{ads} for the C_2 molecule was in the order Co(10-11)>Co(11-20)>Co(10-12)>Co(10-10)>Co(0001), while the C_2H molecule binds strongest in the order Co(10-11)>Co(10-12)>Co(10-10)>Co(11-20)>Co(0001). For all facets, the acetylene molecule binds parallel to the surface with its C-C bond, while the hydrogen atoms are pointing out form the surface. This is also verified in another study [57]. The acetylene chemisorbed strongest on the Co(10-11) surface, then the order is Co(0001)>Co(10-12)>Co(10-10)>Co(11-20).

In general, the more open the surface is, the more reactive it is [1]. From this statement it is expected that the surfaces Co(11-20) and Co(10-12) with high miller index adsorbs the strongest. Those surfaces also have the highest surface energy (E_{surf}=152 meV/Å^2) which makes them reactive. However, the results from Figure 4.6 shows that the Co(10-11) (E_{surf}=147 meV/Å^2) binds all the six adsorbate 0.03-1.25 eV stronger to the surface than the other four facets. Therefore, the results are not consistent with the statement that more open surface is most reactive [1]. There are not many previous studies on the Co(10-11) surface which makes it difficult to state a reason for this. Although, it may be due to the present of undercoordinated surface atoms and the favorable hollow sites. This could also be a results from the high surface energy calculated for Co(11-20) and Co(10-12) surfaces, which makes the surfaces to reactive to stabilize the binding of the adsorbate. While the Co(10-11) is an open surface but lies more in the plane, and it has just 5 meV/Å^2 difference in the surface energy.

In general, the weakest binding was on the Co(0001) surface. This could be due to the low surface energy calculated (E_{surf} = 125 meV/Å^2) together with the fact that the Co(0001) is flat and has higher coordination number than the other facets. The only exception here is hydrogen and acetylene which binds the second strongest on Co(0001) surface. This indicates that hydrogen and acetylene prefer to bind on more open surfaces with higher coordination number.

Figure 4.7 shows the same diagram as figure 4.6, but here are all the E_{ads} calculated without the vdW interactions. By comparing Figure 4.6 (calculated with vdW interactions and ZPE

correction) and Figure 4.7 (calculated with ZPE corrections) it is noted that both have the same trends. Therefore, in further results and discussion the E_{ads} is used with only ZPE corrections.
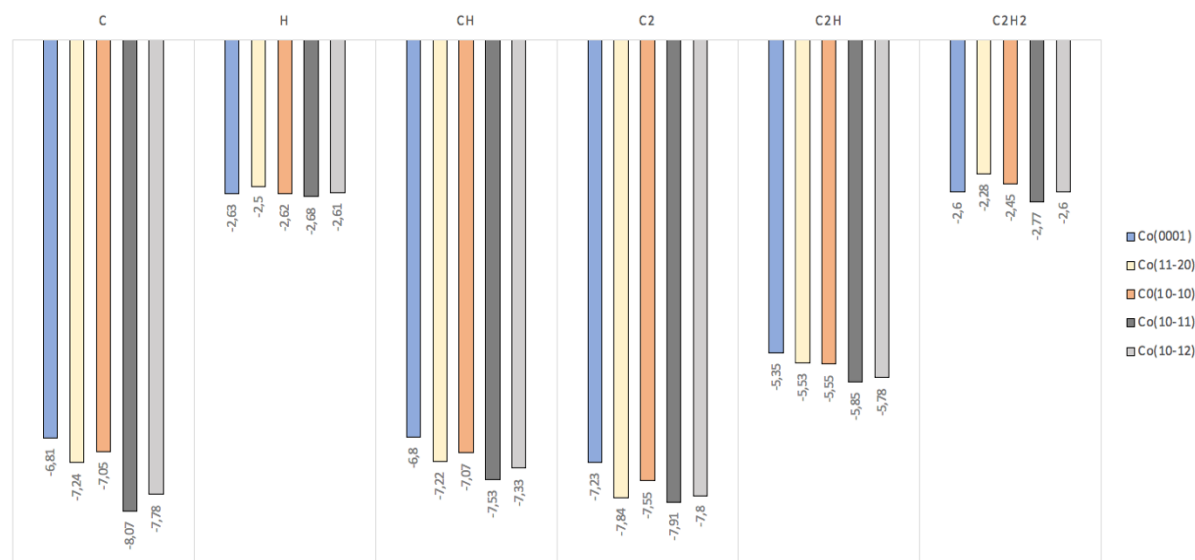
Figure 4.7: C, H, CH, C2, C2H and C2H2 adsorption in its most favorable sites on the five different facets calculated with ZPE correction.

4.2. Acetylene Decomposition

Acetylene decomposition over Co(0001) and Co(11-20) surfaces have been systematically studied by DFT calculation to investigate the detail mechanism at atomic level. This was done by CI-NEB calculations, where the intermediates were placed in their most favorable site for the specific surface in order to minimize the reaction barrier. C-H bond scission and C-C bond scission will be discussed for both of the surfaces. There were performed a vibrational analysis on the IS, TS and FS in order to calculate the E_a (Eq. 3.3) and ΔE (Eq. 3.4) with ZPE correction. Gibbs free energy was also calculated with the python script shown in Appendix F, in order to calculate the E_a and ΔE with different temperatures. The TS was identified by one imaginary frequency [29].

4.2.1. Co(0001) Surface

Acetylene decomposition over Co(0001) surface was performed with CI-NEB. Three dehydrogenation reactions of acetylene and its intermediates was investigated over the surface. Table 4.7 shows the imaginary frequency in TS, together with the calculated E_a and the calculated ΔE at different temperatures. The IS, TS and FS geometry for all the three reactions are illustrated in Figure 4.8.

Table 4.7: Imaginary frequency in TS, and the calculated E_a and ΔE for the C-H bond scission on Co(0001) surface at different temperatures.

Reaction	IS site	ν_i [cm^{-1}]	Temp. [K]	E_a [eV] with ZPE	ΔE [eV] with ZPE	Ref. E_a [eV], ΔE [eV]
C$_2$H$_2$ → C$_2$H+H	fcc-hcp	881	0	0.92	0.35	0.99[50], 0.22[50]
			298.15	0.90	0.34	
			450	0.89	0.33	
			600	0.87	0.31	
C$_2$H → C$_2$+H	fcc-hcp	929	0	1.02	0.48	1.33[50], 0.36[50]
			298.15	1.00	0.49	
			450	0.98	0.49	
			600	0.97	0.49	
CH → C + H	hcp	831	0	0.90	0.24	1.15[50], 0.33[50]
			273.15	0.90	0.25	
			450	0.89	0.25	
			600	0.89	0.25	

C$_2$H$_2$ → C$_2$H + H

a(IS)   b(TS)   c(FS)

C$_2$H → C$_2$ + H

d(IS)   e(TS)   f(FS)

CH → C + H

g(IS)   h(TS)   i(FS)
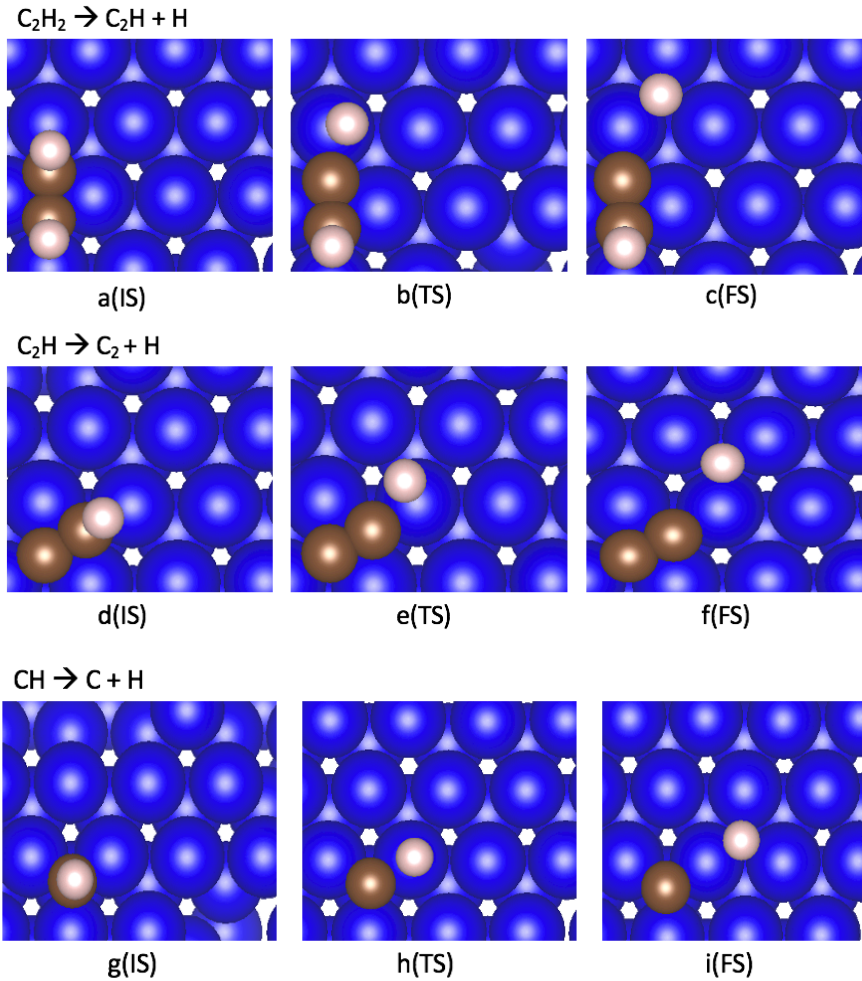
Figure 4.8: Geometric structure of the IS, TS and FS for C-H bond scission over Co(0001) surface.

C₂H₂ → C₂H + H

Acetylene dehydrogenation is shown in Figure 4.8 (a-c). In IS, the acetylene molecule lies parallel to the surface with C atom located in the fcc and hcp site. The reaction proceeds with one H atom dissociating to a fcc site, because the results above showed that hydrogen prefers to be in a fcc site (Table 4.1). The reaction barrier was 0.92 eV, and the reaction energy was calculated to 0.35 eV at 0 K, which tells that the reaction is endothermic. The CI-NEB graph for this reaction is attached in Appendix J, Figure J.1.

C₂H → C₂ + H

Configuration of dehydrogenation to carbon dimer is shown in Figure 4.8 (d-f). In IS, the C_2H was placed in its favorable fcc-hcp site. The H atom diffuses over the top site in TS to its favorable fcc site in the FS. The computed barrier for the reaction was 1.02 eV, and the reaction energy was calculated to 0.48 eV at 0 K. The CI-NEB graph for the reaction can be seen in Appendix J, Figure J.2.

CH → C+H

CH dehydrogenation is illustrated in Figure 4.8 (g-i). The IS shows the most stable adsorption configuration of CH in hcp site. In TS, the H atom was above the top site on the Co(0001) surface. Further, the hydrogen was adsorbed in a fcc site in FS, while the C atom was still in the hcp site. The computed barrier was 0.90 eV, and the reaction energy was 0.24 eV at 0 K. Since the reaction energy is positive, the reaction is endothermic. The CI-NEB graph is shown in Appendix J, Figure J.3.

All the three dehydrogenation reactions carried out on this surface is consistent with the ones observed in a study performed by Zhang *et al.* [50]. Where the IS, TS and FS have the same geometrical information as shown here. However there is a slightly derivation in the E_a and ΔE calculated, shown in Table 4.7. The reason of this derivation may be that the E_a and ΔE in the reference are calculated without ZPE correction, also the slab consistent of four layer with p(4x4) supercell [50]. It was also investigated three C-C bond dissociation reaction of acetylene and its intermediates on Co(0001) surface. Table 4.8 list all the reaction with the calculated Ea and ΔE at different temperatures together with the imaginary frequency in the TS. Figure 4.9 shows the geometry for all the IS, TS and FS in the reactions.

Table 4.8: Imaginary frequency in TS, and the calculated E_a and ΔE for the C-C bond scission on Co(0001) surface at different temperatures.

Reaction	IS site	ν_i [cm^{-1}]	Temp. [K]	E_a [eV] with ZPE	ΔE [eV] with ZPE	Ref. E_a [eV], ΔE [eV]
C$_2$H$_2$ → CH + CH	fcc-hcp	531	0	1.19	0.60	1.69[50], 0.73[50]
			273.15	1.19	0.61	
			410	1.20	0.61	
			600	1.20	0.61	
C$_2$H → CH + C	fcc-hcp	416	0	1.43	0.95	1.69[50], 0.73[50]
			273.15	1.43	0.96	
			410	1.44	0.96	
			600	1.45	0.96	
CC → C+ C	fcc-hcp	354	0	1.60	1.07	1.81[50], 0.70[50]
			273.15	1.60	1.08	
			410	1.61	1.08	
			600	1.62	1.09	

C$_2$H$_2$ → CH + CH

a(IS)   b(TS)   c(FS)

C$_2$H → CH + C

d(IS)   e(TS)   f(FS)

C$_2$ → C + C

g(IS)   h(TS)   i(FS)
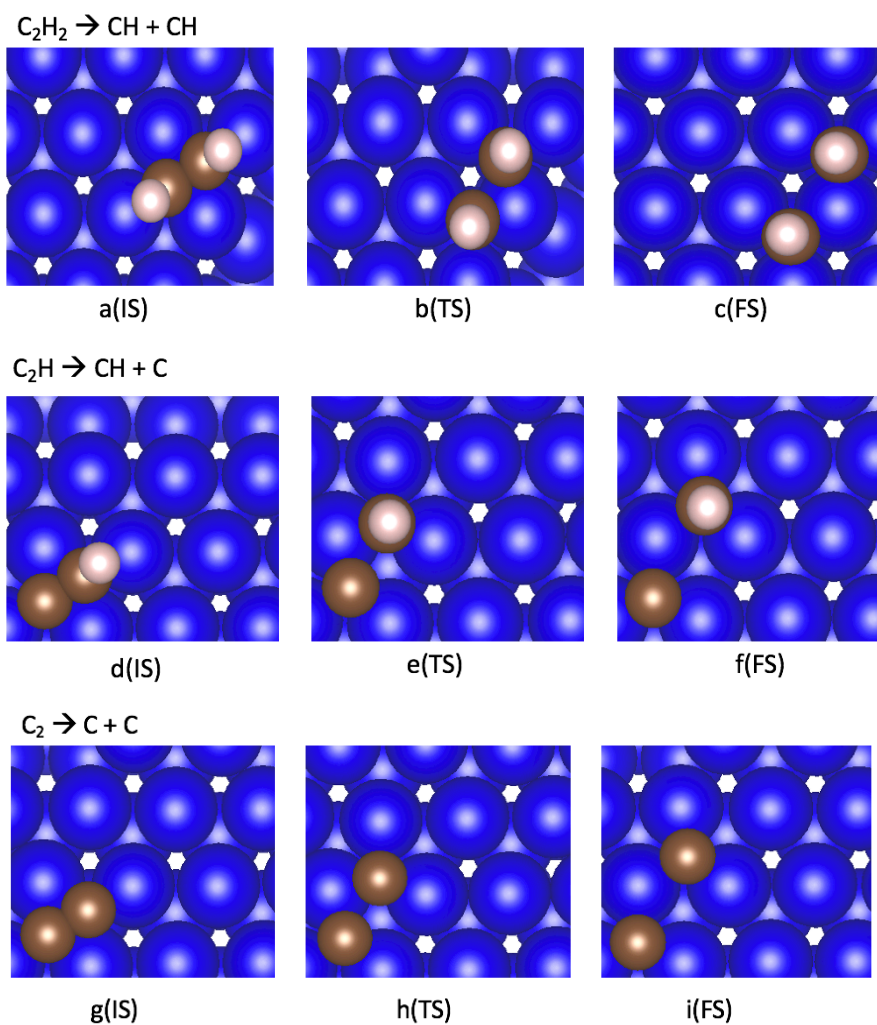
Figure 4.9: Geometric structure of the IS, TS and FS for C-C bond scission over Co(0001) surface.

C₂H₂ → CH + CH

The most stable adsorption configuration of acetylene on Co(0001) surface was in a fcc-hcp site with the C-C axis parallel to the surface (Fig. 4.9, a). In TS (Fig. 4.9. b), the CH in the fcc site diffuses to its most stable hcp site, where it ends up in the FS (Fig. 4.9, c). The activation barrier was calculated to 1.19 eV, and the reaction energy was calculated to 0.69 eV at 0 K which indicates that the reaction is endothermic. The CI-NEB graph for this reaction is shown in Appendix J, Figure J.4.

C₂H → CH + C

The C-C bond scission process of C_2H is shown in Figure 4.9 (d-f). The C_2H molecule was in its most stable site (fcc-hcp site) in the IS. In TS, the CH molecule migrates to the hcp site where it ends up in FS. This is the most favorable site for the CH molecule. Appendix J, Figure J.5 shows the CI-NEB graph for this reaction, and the calculated activation energy was 1.43 eV, and the reaction energy was 0.95 eV at 0 K.

C₂ → C + C

The C-C bond scission of C_2 is illustrated in Figure 4.9 (g-i). In Is, the C_2 was adsorbed parallel with its bond in a fcc-hcp site. The C migrates to another hcp site because this was the favorable site for the C adsorption. The barrier was calculated to 1.60 eV, and the reaction energy was calculated to 1.07 eV at 0 K which indicates that the reaction is endothermic. The CI-NEB graph for the reaction can be seen in Appendix J, Figure J.6.

All three C-C bond scission of acetylene on Co(0001) surface have the same geometric information as the C-C bond scission study carried out by Zhang *et al.* [50]. There is a slight derivation in the Ea and ΔE calculated, shown in Table 4.8. This may be due to the lack of ZPE value and the difference in the slab model [50]. Although, since it is only a slight derivation, it indicates that the decomposition reactions done her are credible.

4.2.2. Co(11-20) Surface

The decomposition of acetylene has also been studied over the corrugated Co(11-20) surface. There were three dehydrogenation reactions of acetylene and its intermediates over Co(11-20) surface. Table 4.9 shows the calculated Ea and ΔE together with the imaginary frequency found in the TS. The geometry of the IS, TS and FS for all reaction are illustrated in Figure 4.10.

Table 4 9: Imaginary frequency in TS, and the calculated E_a and ΔE for the C-H bond scission on Co(11-20) surface at different temperatures.

Reaction	IS site	ν_i [cm^{-1}]	Temp. [K]	E_a [eV] with ZPE	ΔE [eV] with ZPE
C$_2$H$_2$ → C$_2$H+H	tB-tB (offsite)	700	0	0.22	-0.20
			298.15	0.21	-0.20
			450	0.20	-0.20
			600	0.20	-0.20
C$_2$H → C$_2$+H	tB-tB (offsite)	751	0	0.88	0.10
			298.15	0.88	0.08
			450	0.89	0.06
			600	0.90	0.04
CH → C + H	tB (offsite)	803	0	0.78	0.17
			298.15	0.78	0.13
			450	0.79	0.10
			600	0.80	0.07

C$_2$H$_2$ → C$_2$H + H

a(IS)   b(TS)   c(FS)

C$_2$H → C$_2$ + H

d(IS)   e(TS)   f(FS)

CH → C + H

g(IS)   h(TS)   i(FS)
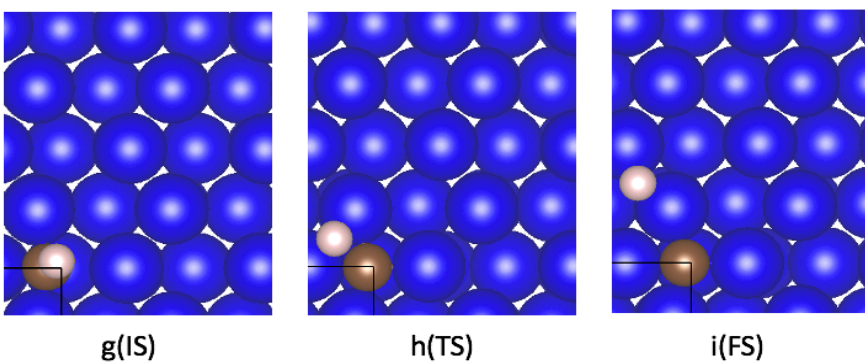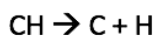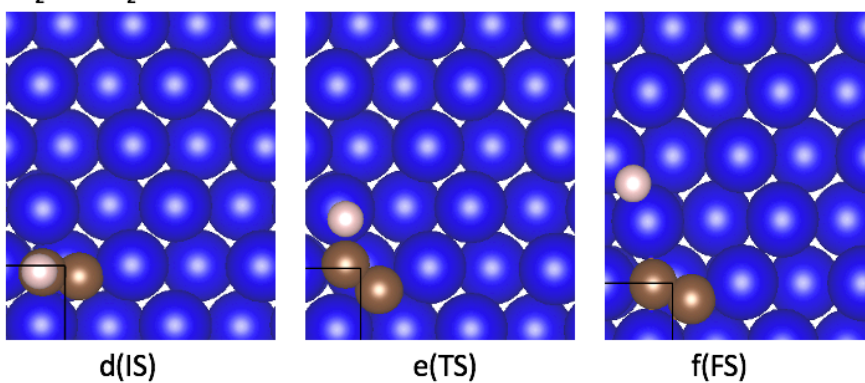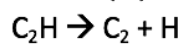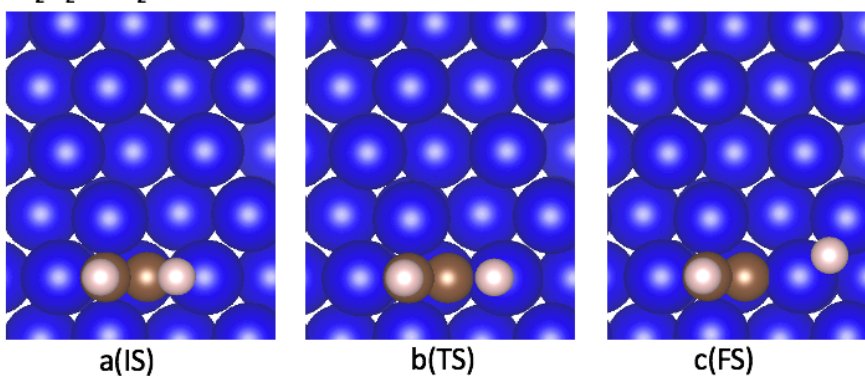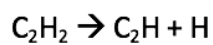
Figure 4.10: Geometric structure of the IS, TS and FS for C-H bond scission over Co(11-20) surface.

C₂H₂ → C₂H + H

Acetylene was placed in its most favorable site, tB-tB (offsite) site, in IS (Fig. 4.10, a). The hydrogen start to diffuse over the tA site in TS (Fig. 4.10, b), and ends up in its most stable site, bA site, in FS (Fig. 4.10, c). The reaction barrier was calculated to 0.22 eV, and the reaction energy was calculated to -0.20 eV at 0 K which indicates that the reaction is exothermic. The CI-NEB graph of the dehydrogenation of acetylene can be seen in Appendix K, Figure K.1.

C₂H → C₂ + H

Dehydrogenation reaction of C_2H is illustrated in Figure 4.10 (d-f). C_2H was placed in its most favorable site, tB (offsite) site, in IS. The H atom migrates to its most favorable bA site in FS. The reaction energy was calculated to 0.10 eV at 0 K which indicates that the reaction is endothermic. The activation energy was calculated to 0.88 eV at 0 K, and the CI-NEB graph for the reaction is shown in Appendix K, Figure K.2.

CH → C + H

Dehydrogenation process of CH is shown in Figure 4.10 (g-i). In IS, the CH molecule is placed in the most favorable tB (offsite) site. The reaction pathway was equal to the C_2H dehydrogenation reaction where H migrates to the bA site in FS. The activation energy was calculated to 0.78 eV, and the reaction energy was calculated to 0.17 eV at 0 K. The CI-NEB graph for the reaction is attached in Appendix K, Figure K.3.

There were investigated three C-C bond scission reactions of acetylene and its intermediates on Co(11-20) surface. The calculated E_a and ΔE at different temperatures is shown in Table 4.10, and the imaginary frequency for the TS of each reaction. Figure 4.11 shows the IS, TS and FS geometry for all the C-C bond breaking reactions.

Table 4.10: Imaginary frequency in TS, and the calculated E_a and ΔE for the C-C bond scission on Co(11-20) surface at different temperatures.

Reaction	IS site	ν_i [cm^{-1}]	Temp. [K]	E_a [eV] with ZPE	ΔE [eV] with ZPE
$C_2H_2 \rightarrow CH + CH$	tB-tB (offsite)	367	0	0.73	-0.17
			298.15	0.74	-0.16
			450	0.75	-0.15
			600	0.76	-0.15
$C_2H \rightarrow CH + C$	tB-tB (offsite)	260	0	1.06	0.19
			298.15	1.07	0.21
			450	1.09	0.21
			600	1.11	0.22
$CC \rightarrow C + C$	tB-bB	219	0	2.02	0.30
			298.15	2.04	0.31
			450	2.05	0.31
			600	2.07	0.31

$C_2H_2 \rightarrow CH + CH$

a(IS)   b(TS)   c(FS)

$C_2H \rightarrow CH + C$

d(IS)   e(TS)   f(FS)

$CC \rightarrow C + C$

g(IS)   h(TS)   i(FS)
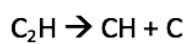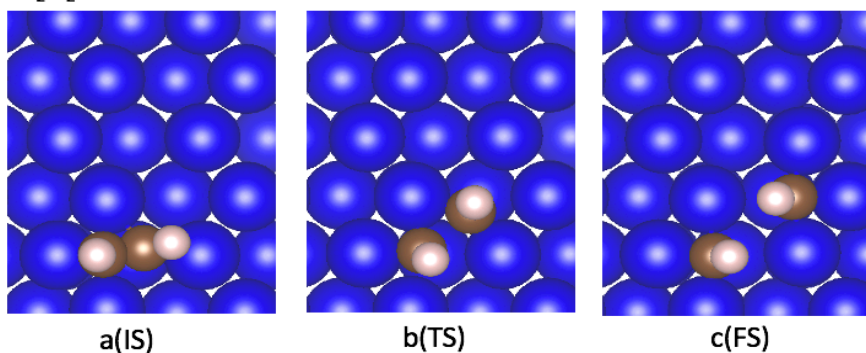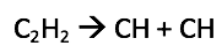
Figure 4.11: Geometric structure of the IS, TS and FS for C-C bond scission over Co(11-20) surface.

C₂H₂ → CH + CH

Acetylene was placed in a tB-tB (offsite) site in IS (Fig. 4.11, a), which was the most favorable site. The CH molecule in acetylene migrates to its most stable site, tB (offsite) site, where it ends up in FS (Fig. 4.11, c). The CI-NEB graph for the C-C scission of acetylene can be seen in Appendix K, Figure K.4. At 0 K, the activation energy was calculated to 0.73 eV, and the reaction energy was calculated to -0.17 eV, which tells that the reaction is exothermic.

C₂H → CH + C

The C-C bond scission of C_2H can be seen in Figure 4.11 (d-f). The C_2H molecule was in its most stable site, tB (offsite) site in IS. The carbon atom migrates to its most favorable tB (offsite) site, where it ends up in FS. The reaction energy was computed to 0.19 eV, which tells that the reaction is endothermic. The activation energy was calculated to 1.06 eV, and the CI-NEB graph can be seen in Appendix K, Figure K5.

C₂ → C + C

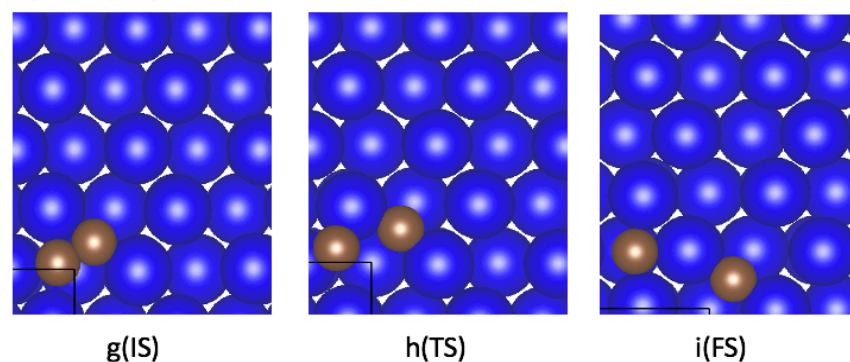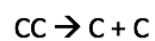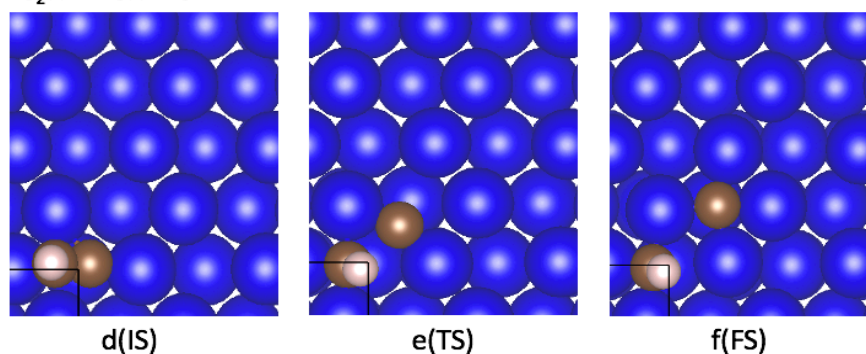Figure 4.11 (g-i) illustrate the C-C bond splitting of the C_2 molecule. In IS, the C_2 molecule was placed in the tB-bB site, which was the most stable site for this molecule. The C atom diffuses over the tB site in the TS. In FS, the carbon atom ends up in a bB site. This is not the most stable site of the C atom, and could be further optimized by placing the C atom in a tB (offsite) site to lower the $E_a/\Delta E$. However, the activation energy was calculated to 2.02 eV and the reaction energy was calculated to 0.30 eV. The CI-NEB graph for the reaction is attached in Appendix K, Figure K.6.

4.3. Analysis of Acetylene Decomposition and Reaction Pathway

Carbon can occur on the Co catalyst under decomposition of hydrocarbon in FTS [8]. In this study, acetylene which can be formed by decomposing of ethylene (or larger hydrocarbon) or directly by 2CH coupling in FTS [58] is studied. Acetylene is the most energetic favorable adsorbate compared with other C_2H_x and C_3H_x molecule [9], which means that acetylene have a strong binding to the Co surface. There are three decomposition reaction where acetylene decompose to atomic carbon. The "*" notation tells that the atom/molecule is adsorbed in an active site on the surface. It is assumed that the hydrogen atom desorbs from the surface in gas phase.

The elementary steps of the first decomposition mechanism is shown in Reaction 4.1, 4.2, 4.3 and 4.4.

$$C_2H_2 + * \rightarrow C_2H_2* \quad\quad\quad\quad\quad\quad\quad\quad\quad\quad\quad [4.1]$$

$$C_2H_2* + * \rightarrow CH* + CH* \quad\quad\quad\quad\quad\quad\quad\quad\quad [4.2]$$

$$CH* + CH* + * \rightarrow C* + H* + CH* \quad\quad\quad\quad\quad [4.3]$$

$$C* + CH* + * \rightarrow C* + C* + H* \quad\quad\quad\quad\quad\quad [4.4]$$

The second decomposition mechanism is shown in Reaction 4.5, 4.6, 4.7 and 4.8.

$$C_2H_2 + * \rightarrow C_2H_2* \quad\quad\quad\quad\quad\quad\quad\quad\quad\quad\quad [4.5]$$

$$C_2H_2* + * \rightarrow C_2H* + H* \quad\quad\quad\quad\quad\quad\quad\quad\quad [4.6]$$

$$C_2H* + * \rightarrow C_2* + H* \quad\quad\quad\quad\quad\quad\quad\quad\quad\quad [4.7]$$

$$C_2* + * \rightarrow C* + C* \quad\quad\quad\quad\quad\quad\quad\quad\quad\quad\quad [4.8]$$

The third decomposition mechanism is shown in Reaction 4.9, 4.10, 4.11 and 4.12

$$C_2H_2 + * \rightarrow C_2H_2* \quad\quad\quad\quad\quad\quad\quad\quad\quad\quad\quad [4.9]$$

$$C_2H_2* + * \rightarrow C_2H* + H* \quad\quad\quad\quad\quad\quad\quad\quad [4.10]$$

$$C_2H* + * \rightarrow CH* + C* \quad\quad\quad\quad\quad\quad\quad\quad\quad [4.11]$$

$$CH* + C* + * \rightarrow C* + H* + C* \quad\quad\quad\quad\quad\quad [4.12]$$

4.3.1. Potential Energy Diagram (PED)

All three decomposition mechanism presented in reaction 4.1-4.12 were investigated on Co(0001) and Co(11-20) in order to identify the reaction mechanism that is most likely to happen. The favorable reaction pathway would be the one with the lowest overall energy [30]. It was made a PED for the three reaction mechanism where the E_{ads} with ZPE correction (Eq. 3.1) for all species are included as well as the reaction barriers (Eq. 3.3). All the E_{ads} in this section is calculated with respect to acetylene and hydrogen gas phases to get a realistic picture.

Co(0001)

Figure 4.12 shows the PED for the three reaction pathways of acetylene decomposition over Co(0001) surface where energy is plotted against the reaction coordinate. The numbers on top of the barriers are the calculated activation energy (Table 4.7 and Table 4.8).
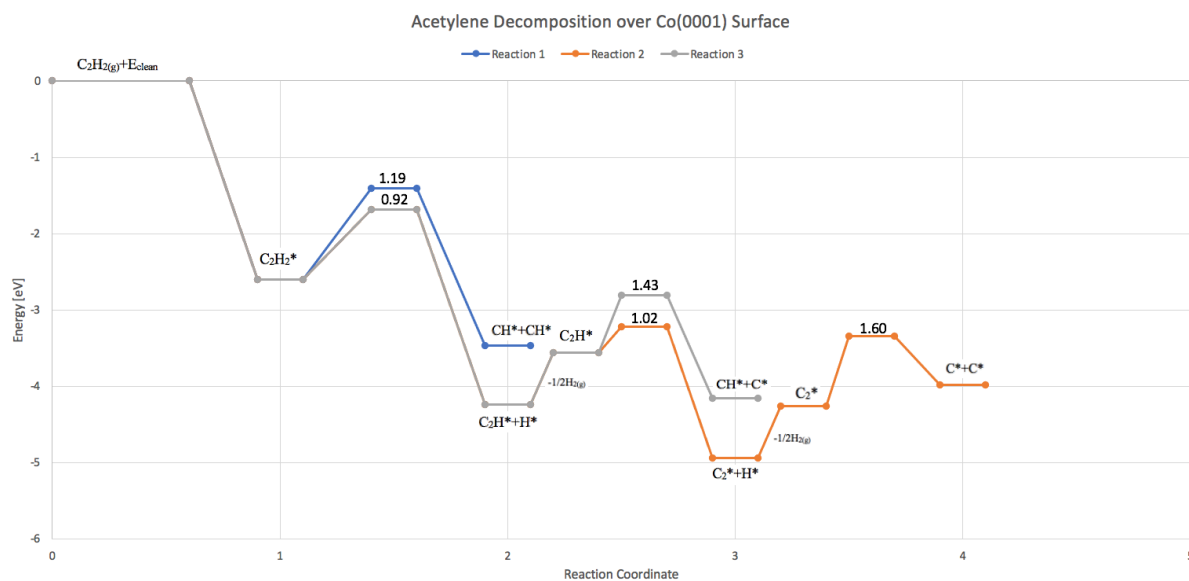
Figure 4.12: Three reaction mechanism of acetylene decomposition over Co(0001) surface at 0 K. Energy [eV] is plotted against the reaction coordinate in the PED.

First in the figure, the C_2H_2 is adsorbed to the surface. This is an exothermic reaction with an E_{ads} of -2.60 eV. Then, the acetylene may dehydrogenate to the C_2H which is the case in reaction mechanism 1 (Rx. 4.1-4.4) and reaction mechanism 2 (Rx. 4.5-4.8). Both the dehydrogenation fragments in reaction mechanism 2 (C_2H and H) will adsorb to the surface, but the hydrogen may desorb in the gas phase which requires energy. The activation barrier for C-H cleaving reaction was 0.92 eV. This is lower than for the C-C bond scission process in reaction mechanism 3 (Rx. 4.9-4.12), which was 1.19 eV. This indicates that the C-H bond breaking reactions is thermodynamically favorable. In reaction mechanism 2 the C_2H dehydrogenates with an activation barrier of 1.02 eV, which was lower than in reaction mechanism 3 where C_2H breaks its C-C bond (E_a=1.43 eV). It is therefore thermodynamically favorable to break the C-H bond of C_2H to C_2 and H than to break the C-C bond. The last reaction barrier is C-C breaking of the C_2 molecule, which has a high reaction barrier of 1.56 eV. The high reaction barrier together with the fact that the single carbon is less stable than the carbon in dimer indicates that this is not favorable. The dehydrogenation reaction was also favorable in a study performed by Zhang *et al.* [50].

54

Co(11-20)

Figure 4.13 shows the three acetylene decomposition mechanism (Rx. 4.1-4.12) on the corrugated Co(11-20) surface where energy is plotted against the reaction coordinate. The numbers on top of the barriers are the calculated activation energy (Table 4.9 and Table 4.10).
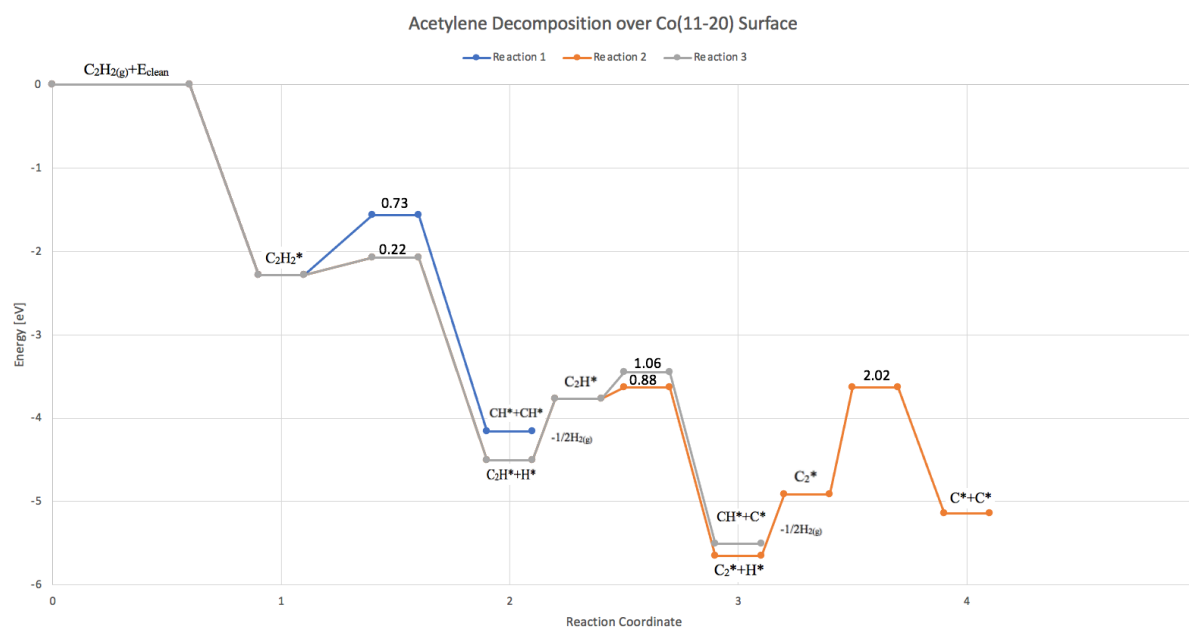

Figure 4.13: Three reaction mechanism of acetylene decomposition over Co(11-20) surface at 0 K. Energy [eV] is plotted against the reaction coordinate in the PED.

First in Figure 4.13, acetylene adsorbs to the surface with an E_{ads} of -2.28 eV. Then, acetylene can either break the C-C bond (Rx. 4.1-4.4) or the C-H bond (Rx. 4.4-4.8 and Rx. 4.8-4.12) in the start of the decomposition. In reaction mechanism 1, acetylene breaks its C-C bond (E_a=0.73 eV), which is a remarkable higher barrier than the C-H bond breaking (E_a=0.22 eV). Therefore, it is most likely that the acetylene dehydrogenates to C_2H and H. The hydrogen atom was first adsorbed to the surface in the dehydrogenation reaction, but then it can desorb from the surface which requires energy. Further, the orange graph shows the dehydrogenation of C_2H (E_a=0.88 eV), while the grey graph shows the C-C bond scission of the C_2H (E_a=1.06 eV). The dehydrogenation has lower barrier than the C-C bond scission, and is thus most likely to happen. The hydrogen atom formed by the dehydrogenation reaction of C_2H can desorb from the surface. In the last step, the C_2 molecule can break its bond into two atomic carbons. The barrier of C-C bond breaking is as high as 2.02 eV, which can indicate that the last stage in Figure 4.13 will be excluded.

By looking at the PED for both surfaces (Fig. 4.12 and 4.13), the most advantages reaction mechanism is the dehydrogenation which happens in reaction mechanism 2 due to the lowest overall energy [30]. In an experimental study performed by Ramsvik *et al.* [57], they concluded that the acetylene may decompose to C_2H or C_2 where its C-C bond is maintained [57]. Based on this, and the fact that the C-C bond breaking has a high barrier, it is concluded that the dehydrogenation may stop after forming C_2 on both surfaces.

4.3.2. PED with Different Temperatures

The Gibbs free energy for all adsorbates were also calculated with the python scripts shown in appendix F, Figure F.2. This was used to construct a PED of acetylene decomposition with different temperatures for both surfaces. In an experimental study performed by Ramsvik *et al.* [57], acetylene decomposition was investigated with photoemission spectroscopy and near-edge X-ray adsorption fine structure (NECAFS). They found out that acetylene decomposition start at low temperature around 200 K on the Co(11-20) surface, which is significantly lower than for the Co(0001) surface. The fragments below 300 K are suggested to involve C_2 and C_2H [57]. Another experimental study performed by Vaari *et al.* [59] looked at decomposition of acetylene over Co(0001) surface, and concluded that the decomposition started at 410 K and continues with smaller rate up to 550 K [59]. Therefore, the favorable decomposition reaction of acetylene has been investigated with a wide range of temperatures from 0 K up to 600 K in this study. Figure 4.14 shows the PED of reaction mechanism 2 over Co(0001), and Figure 4.15 shows the PED of reaction mechanism 2 over Co(11-20) surface.
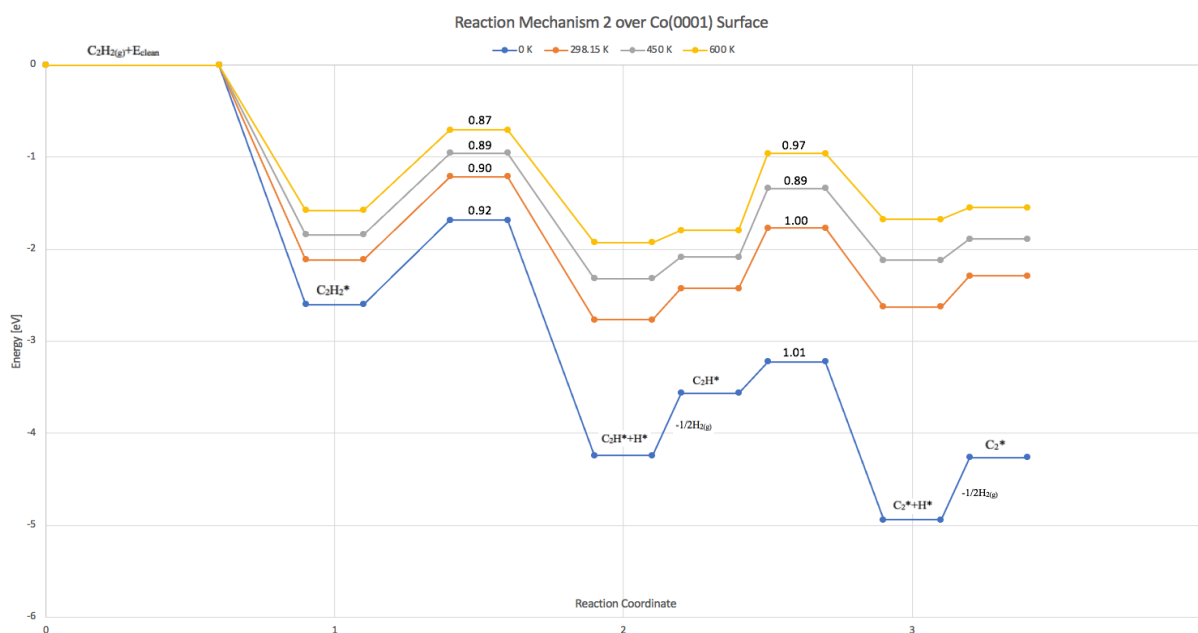
Figure 4.14: Reaction mechanism 2 over Co(0001) surface with temperatures at 0 K, 298.15 K, 450 K and 600 K.
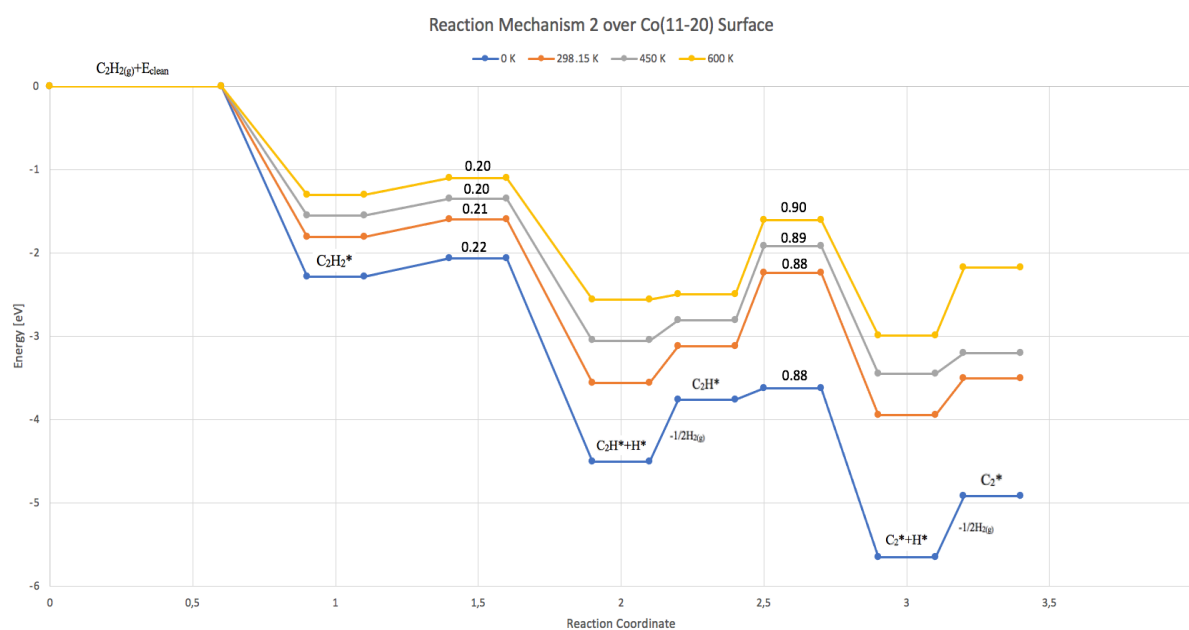
Figure 4.15: Reaction mechanism 2 over Co(11-20) surface with temperatures at 0 K, 298.15 K, 450 K and 600 K.

For both surfaces (Fig. 4.14 and 4.15) the blue graph at 0 K is strongly exothermic, but by increasing the temperature the reaction becomes more thermodynamically neutral. The FTS synthesis with Co as a catalyst operates with temperature below 500 K [44]. Thus, the reaction mechanism with 450 K will be relatively close to the temperature that FTS operates with. By looking at the grey curve in Figure 4.14, it is possible to see that C_2H was more thermodynamical stable than the C_2H_2 and C_2 on Co(0001) surface. It is also most stable at room temperature and 600 K. Therefore, it may be that the dehydrogenation stops after forming

C$_2$H on this surface. In a study performed by Weststrate *et al.* [9] they said that acetylenic (C$_2$H) adsorbates can react with other acetylenic adsorbate and can in this way form polymeric carbon [9]. This could then lead to deactivation of the catalyst by carbon deposition. However, in Figure 4.15 the C$_2$ molecule is the most thermodynamical stable at 450 K (and the other temperatures). Therefore, the dehydrogenation may go all the way to the C$_2$ molecule on Co(11-20) surface. But, since both C$_2$ and C$_2$H are more stable than acetylene on both surfaces, both molecules can be formed by dehydrogenation, which is in line with the study carried out by Ramsvik *et al.* [57].

As seen in Figure 4.15, the overall energy was lower on Co(11-20) surface than the overall energy for reaction mechanism 2 on the Co(0001) surface (Fig. 4.14). Also, the reaction barrier was lower for the dehydrogenation reaction on Co(11-20) surface. This tells that the decomposition of acetylene is structure sensitive, and it is favorable on the more open surface. In the study performed by Ramsvik *et al.* [57] they found that the decomposition of acetylene over Co(11-20) surface started at a lower temperature than over Co(0001) surface [57]. Which indicates that the acetylene decomposition over Co(11-20) surface requires less temperatures (energy), and may be the reason why the overall energy is lower on this surface.

In the study performed by Vaari *et al.* [59] it was found that the final product of decomposition was carbon overlayer in graphitic carbon and a small amount of carbide carbon, which will be further investigated in adsorption of carbon with higher coverage [59].

4.4. Effect of Carbon Coverage on Co(0001) and Co(11-20) Surfaces

If acetylene do dehydrogenate to carbon it is interesting to look at the distribution and localization of carbon atoms. In this section carbon has been placed at Co(0001) surface and Co(11-20) surface at different carbon ML.

Co(0001) Surface

Co(0001) surface was covered with carbon form 0.11–1.33 ML on the p(3x3) unit cell, and the average E$_{ads}$ was calculated with Equation 3.7. All of the E$_{ads}$ was calculated with H$_2$ and C$_2$H$_2$ in gas phase as a reference. The carbon atoms was placed separately at hcp sites, in carbon dimer and graphene fragments on surface Co(0001), Figure 4.16 shows examples of the carbon

deposition. The results are presented in Figure 4.17, which shows the calculated average E_{ads} at different carbon ML on Co(0001) surface.

(a, θ=0.33 ML)   (b, θ=0.88 ML)   (c, θ=1.33 ML)
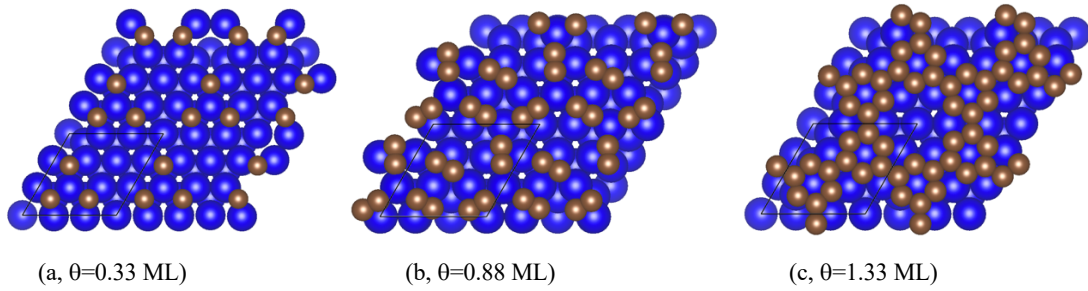
Figure 4.16: Examples of C deposit at hcp site (a), carbon dimer (b) and graphene fragments (c).
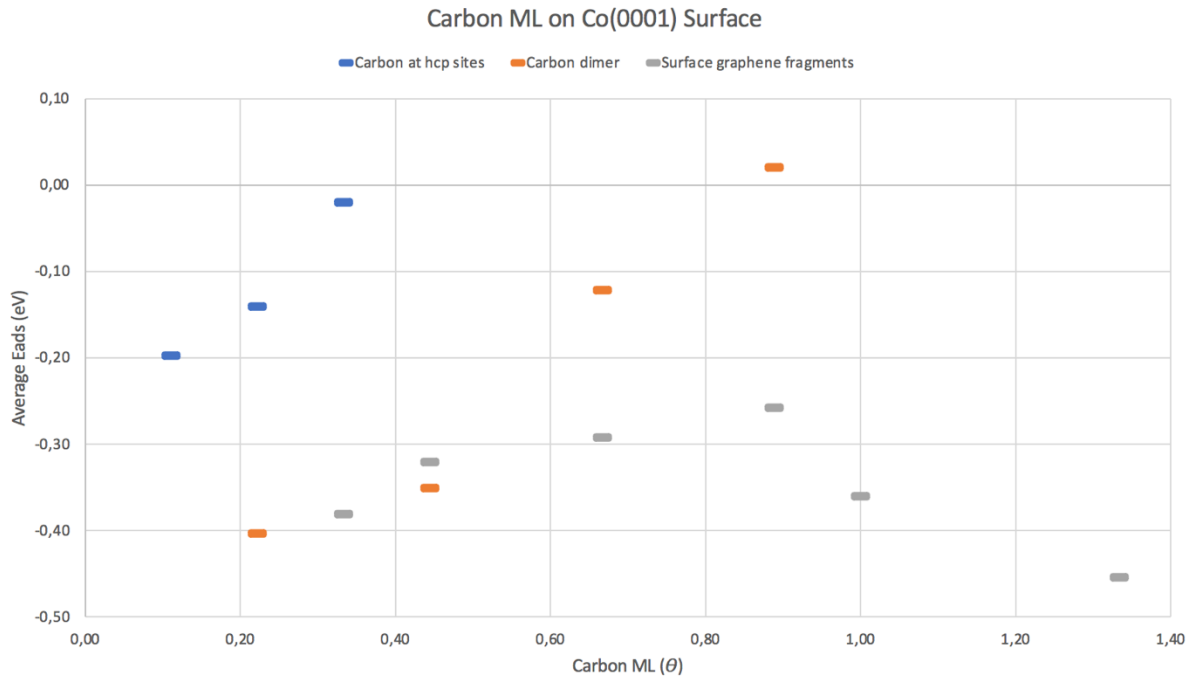
Figure 4.17: Average E_{ads} [eV] as a function of carbon ML with three different types of carbon deposition. Surface carbon at hcp sites (blue), surface carbon forming dimer (orange) and surface carbon forming graphene fragments (grey).

Since the carbon atom preferred to be in a hcp site on Co(0001) surface, all the separate carbon were placed in hcp site at low coverage (θ=0.11-0.33 ML). An attempt was also made at 0.44 ML and higher, but then the carbon atoms were pulled together in a C-C coupling during the calculation. This was also the founding in the study performed by Zhang *et al.* [51], where they concluded that at 0.5 ML the most stable configuration was the C_2 species [51]. According to the results in the figure, separately carbon at hcp sites becomes less stable when increasing the coverage. The carbon dimer was placed at hcp-fcc site, since the results above showed that this was the most stable sites for C_2 (Table 4.1). By comparing the 2C placed in two separate hcp

site (second mark, blue) and the C_2 bonded together in a hcp-fcc site (first mark, orange), it can be concluded that the carbon atoms like to be in pair when the carbon ML was low (θ=0.22-0.44). At 0.66 ML the graphene fragments of carbon was the most favorable on Co(0001) surface due to the figure. This is in agreement with experimental finding [6]. In a previous theoretical study, it was concluded that as the carbon concentration increases, the adsorbed carbon turns into graphene [51]. This is consistent with the results in Figure 4.17. Therefore, it is concluded that the graphene fragments is most favorable on Co(0001) with high carbon coverage. All of the three types of carbon depositions is consistent with the trends in the study performed by Jansen *et al.* [49].

Co(11-20) Surface

hcp Co(11-20) surface was covered with carbon from 0.08 – 1.00 ML on the p(3x4) unit cell, and the average E_{ads} was calculated with equation 3.7 with H_2 and C_2H_2 in gas phase as the reference. The carbon atoms where placed at tB (offsite) site, in carbon dimer and in carbon rows at the surface, some examples is illustrated in Figure 4.18. Figure 4.19 presents the results of the average E_{ads} with different carbon ML on Co(11-20) surface.

(a, θ=0.83 ML)   (b, θ=1.00 ML)   (c, θ=1.00 ML)

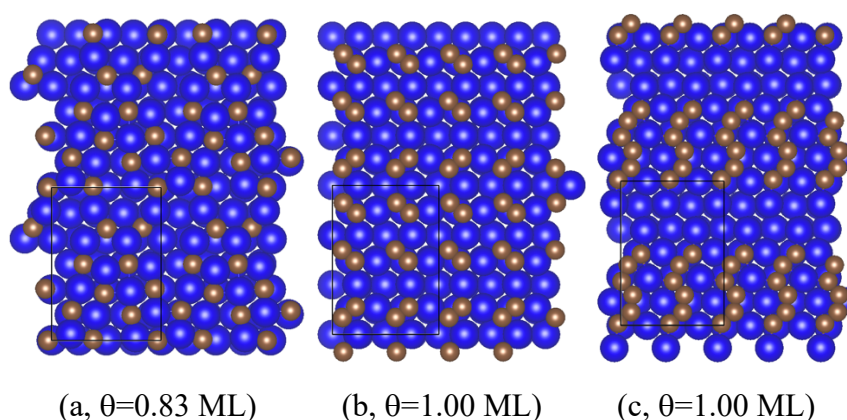**Figure 4.18:** Examples of C deposition at tB-offsite site (a), carbon dimer (b) and carbon rows (c).
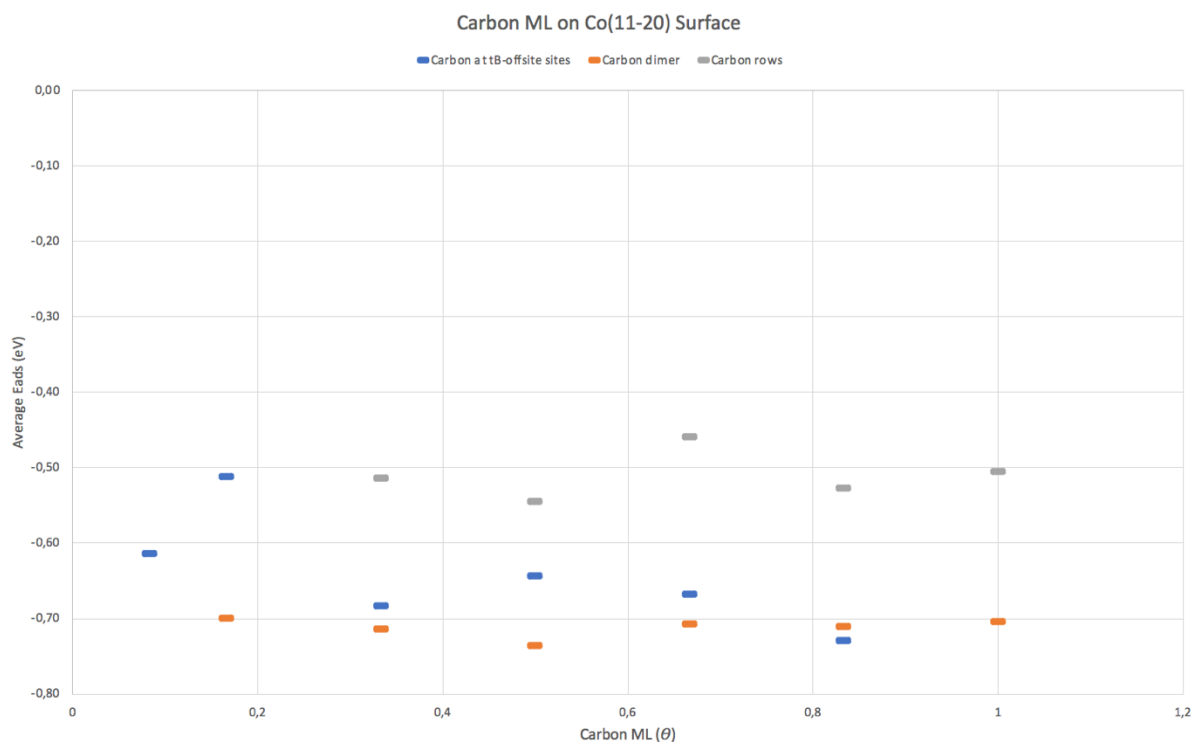
Figure 4.19: Average E_{ads} [eV] as a function of carbon ML with three different types of carbon deposition. Surface carbon at tB (offsite) sites (blue), carbon forming dimer (orange) and carbon rows (grey).

The results in Figure 4.19 indicates that all the three types of carbon deposition are very similar in E_{ads}. Carbon placed in rows have the highest average E_{ads}, which means that carbon was least stable at this deposition on the Co(11-20) surface. In general, the carbon likes to be in dimer on the Co(11-20) surface, except for carbon at 0.80 ML, where it prefers to be separately in a tB (offsite) site. However, there was just a slight difference in the E_{ads} at that coverage. By increasing the separate carbon to 1 ML, the carbon atoms was forming C-C bonds.

By comparing the carbon coverage on Co(0001) surface and Co(11-20) surface it was noted that the carbon has lower E_{ads} at 0.33, 0.66, 0.88 and 1.00 ML on Co(11-20) surface. This indicates that the carbon chemisorbs stronger on the corrugated hcp Co(11-20) surface than the closed-packed hcp Co(0001) surface.

Previous experiments showed that high acetylene coverage gives graphitic carbon, and low acetylene coverage gives atomic carbon on Co(0001) surface [57, 59]. This can be linked to the results found here. If acetylene undergoes a decomposition to carbon on Co(0001) surface (Fig. 4.14), the results illustrate that a higher coverage of carbon gives graphene fragments, while at low coverage carbon deposits in dimer (Fig. 4.17). In a study performed by Weststrate *et al.* [6] they mention that atomic carbon occur to the surface at low acetylene coverage. However, since

the CO and H_2 can still adsorb around 60 % to the surface this would not affect the catalytic activity of Co in FTS. Since hydrogen can still adsorbs to the surface, the hydrogen can access the carbon and hydrogenate it. They also discussed how graphene forming can occurs due to high coverage of acetylene or on a carbon precovered surface. If this happens, graphene can inhibit the adsorption of CO and H_2, which makes it a strong poisoning for the Co-catalyst in FTS. The key ingredient for graphene formation was found to be acetylene which is formed in the first step of the chain growth reaction in FTS. However, the carbon build-up process is slow on the Co catalyst, and are only a side reaction in FTS [6].

5. Conclusion & Further Work

5.1. Conclusion

The goal of this thesis was to characterize the carbon formation mechanism that can occur on Co catalyst in FTS. This was carried out by analyzing the acetylene decomposition mechanism on Co surfaces and carbon deposition. Where the first step was to identify the favorable site for acetylene and the relevant intermediates. Five different hcp Co facets was made in order to perform the investigation.

First principle spin polarized DFT calculation was implemented in VASP to get an approximated solution of the many-body Schrödinger equation. The adsorbates C, H, CH, C_2, C_2H and C_2H_2 were placed above high symmetry sites on Co(0001), Co(11-20), Co(10-10), Co(10-11) and Co(10-12). There was also performed a vibrational analysis on all the adsorbate to verify the stable sites on the facets, and to calculate the ZPE correction. The adsorption energy was calculated with both PBE functional and DFT-D3 functional to include the vdW interactions. There was a significant difference for the E_{ads} calculated with both functionals, which indicates that the vdW interaction plays a role in the adsorption. It is concluded that the vdW interaction may increase with increasing weight of the atom/molecule.

Some of the E_{ads} calculated on the surfaces were compared with other calculations. Although, there was a slight derivation, it is concluded that the results found here were in good agreement with other results. In general, the Co(10-11) surface binds the adsorbates 0.03-1.25 eV stronger than the other surfaces. This may be due to the presence of undercoordinated sites, and the fact that the surface is open with a high surface energy of 147 meV/Å^2. The closed-packed Co(0001) is concluded to be the most thermodynamical stable surface, because the surface free energy was the lowest (E_{surf}=125 meV/Å^2). Which may also be the reason why this surface binds the weakest with the adsorbates, except hydrogen and acetylene which binds the second strongest on this surface. The surfaces Co(11-20) and Co(10-12) have the highest computed surface free energy of 152 meV/Å^2, and is therefore noted as the least stable surfaces in this study.

The acetylene may decompose on the surfaces to form carbon that could deactivate the hcp Co catalyst. In this study, there were proposed three decomposition reaction mechanism. CI-NEB was used to calculate the activation energy and reaction energy for each C-C bond scission and C-H bond scission of acetylene and its intermediates on Co(0001) and Co(11-20) surfaces.

Since the barrier for the C-C bond breaking was higher than for the C-H bond breaking, it is concluded that dehydrogenation of acetylene is the preferred reaction. Since the C-C bond breaking of C_2 molecule was high on both surfaces (E_a=1.60 eV and E_a=2.02 eV), the acetylene decomposition may stop at the C_2 specie.

The dehydrogenation reaction of acetylene was investigated at 0 K, 298.15 K, 450 K and 600 K by calculating the Gibbs free energy. At 0 K the dehydrogenation reaction was strongly exothermic for both surfaces, but with increasing temperature, the dehydrogenation reaction became more thermodynamically neutral. FTS with hcp Co catalyst operates at low temperature below 500 K, and therefore the decomposition of acetylene at 450 K will give an insight into how the energy profile will be in the synthesis. The C_2H molecule was the most thermodynamical stable adsorbate on the Co(0001) surface, which indicates that the decomposition of the acetylene may stop after the first dehydrogenation. On the Co(11-20) surface the C_2 molecule was the most thermodynamical stable adsorbate at 450 K, which indicates that the acetylene dehydrogenate in two steps. Overall, the dehydrogenation of acetylene had lower energy profile over Co(11-20) surface, which indicates that the decomposition reaction is structure sensitive and favorable over this surface.

The carbon deposition on Co(0001) and Co(11-20) surfaces at different ML were also investigated. If the acetylene decompose to carbon it is interesting to gain an insight into the distribution and location of the carbon on the surfaces. For the Co(0001) surface, the carbon was placed separately, in carbon dimer and in graphene fragment on the surface. At low coverage, carbon deposited in carbon dimer, and at high coverage carbon deposits in graphene fragments on the surface. For the Co(11-20) surface, carbon was placed separately, in carbon dimer and in carbon rows. Overall, the carbon adsorbed stronger on this surface and likes to deposits in carbon dimer at this surface.

5.2. Further Work

In this thesis, five facets were made, but only on two of them was the acetylene decomposition examined. Therefore, further investigation of acetylene decomposition on the three remaining surfaces Co(10-10), Co(10-11) and Co(10-12) could have been done. It could been interesting to see how the barrier and reaction pathways would change with the different surfaces. The findings in this thesis showed that the adsorbate binds strongest to the Co(10-11) surface among the five facets. This could be engaging to look deeper into with analysis of change density and d band center. By performing this method one could get a better understanding of why the adsorbates bind strongest to this particularly surface.

In further work the scanning tunneling microscopy (STM) image could been simulated to compare with the theoretical results for the carbon overlayer found here. Also, the core level binding energies and the chemical shift could have been performed, to get an insight into carbon overlayer at different temperatures. This could be compared with other experimental results from X-ray photoelectron spectroscopy (XPS) to verify the accuracy of the method.

Bibliography

[1]   Chorkendorff, I. and Niemantsverdriet, J. W. Concepts of Modern Catalysis and Kinetics [Internet]. Weinheim: Wiley-VCH; 2017. [Retrieved: 17.02.21]. Available from: https://books.google.no/books?hl=no&lr=&id=OE0nDwAAQBAJ&oi=fnd&pg=PP2&dq=concepts+of+modern+catalysis+and+kinetics&ots=jQ3hbUdzYZ&sig=eBd0oDGVH1jDciE2nlABRIaTJug&redir_esc=y#v=onepage&q&f=true

[2]   Chen, C., Wang, Q., Zhang, R., Hou, B., Li, D., Jia, L. and Wang, B. High coverage CO adsorption and dissociation on the Co(0001) and Co(100) surfaces from DFT and thermodynamics. Applied Catalysis A: General. 2016;523:209-220.

[3]   National Energy Technology Laboratory. Fisher-Tropsch Synthesis [Internet]. U.S. Department of Energy [Retrieved: 29.04.21]. Available from: https://www.netl.doe.gov/research/coal/energy-systems/gasification/gasifipedia/ftsynthesis

[4]   Chen, Q., Svenum, I. H., Qi, Y., Gavrilovic, L., Chen, D., Holmen, A. and Blekkan, E. A. Potassium adsorption behavior on hcp cobalt as model systems for the Fischer–Tropsch synthesis: a density functional theory study. Physical Chemistry Chemical Physics. 2017;19:12246-12254.

[5]   Rytter, E. and Holmen, A. Deactivation and Regeneration of Commercial Type Fischer-Tropsch Co-Catalysts—A Mini-Review. Advanced in Catalyst Deactivation. 2015;5(2):478-499.

[6]   Weststrate, C. J., Kizilkaya, A. C., Rossen, E. T. R., Verhoeven, M. W. G. M., Ciobîca, I. M., Saib, A. M. and Niemantsverdriet, J. W. Atomic and Polymeric Carbon on Co(0001): Surface Reconstruction, Graphene Formation, and Catalyst Poisoning. The Journal of Physical Chemistry. 2012;116(21):11575-11583.

[7]   de la Peña O'Shea, V. A., de la Piscina, P. R., Homs, N., Aromí, G. and Fierro, J. L. G. Development of Hexagonal Closed-Packed Cobalt Nanoparticles Stable at High Temperature. Chemistry of Material Article. 2009;21(23):5637-5643.

[8]   Bartholomew, C. H. Carbon Deposition in Steam Reforming and Methanation. Catalyst Reviews Science and Engineering. 2007;24(1):67-112.

[9]   Weststrate, C. J., Ciobîca, I. M., Saib, A. M., Moodley, D. J. and Niemantsverdriet, J. W. Fundamental issue on practical Fischer-Tropsch catalysts: How surface science can help. 2014:228;106-122.

[10]   Nørskov, J. K., Stundt, F., Abild-Pedersen, F. and Bligaard, T. Fundamental Concept in Heterogeneous Catalysis. Somerset: John Wiley & Sons; 2014.

[11]   Rosei, F. and Rosei, R. Atomic description of elementary surface processes: diffusion and dynamics. Surface Science. 2002;500(1-3):395-413.

[12]   Chemistry Learner. Van der Waals Forces. [Retrieved: 18.01.21]. Available from: https://www.chemistrylearner.com/chemical-bonds/van-der-waals-forces

[13]   Khan Academy. Intramolecular and intermolecular forces [Internet]. [Retrieved: 02.03.21]. Available from: https://www.khanacademy.org/science/class-11-chemistry-india/xfbb6cb8fc2bd00c8:in-in-states-of-matter/xfbb6cb8fc2bd00c8:in-in-intermolecular-forces/a/intramolecular-and-intermolecular-forces

[14]   Zohar, A. R. and Levy, S. T. Attraction vs. repulsion – learning about forces and energy in chemical bonding with the ELI-Chem simulation. Chemistry Education Research and Practice. 2019;20(4):667-684.

[15]   Toulhoat, H. Heterogeneous Catalysis: Use of Density Functional Theory. Encyclopedia of Material: Science and Technology. 2010:1-7.

[16]   Marques, M. A. L., Oliveira, M. J. T. and Burnus, T. LIBXC: A library of exchange and correlation functionals for density functional theory. Computer Physics Communications. 2012;183(10):2272-2281.

[17]   Sholl, D. and Steckel, J. A. Density Functional Theory. New Jersey: John Wiley & Sons; 2009.

[18]   Hyper Physics. The Hamiltonian [Internet]. [Retrieved: 20.01.21]. Available from: http://hyperphysics.phy-astr.gsu.edu/hbase/quantum/hamil.html

[19]   Engel, E. and Dreizler, R. M. Density functional Theory: An Advanced Course [Internet]. Frankfurt: Springer; 2010. [Retrieved: 03.03.21]. Available from: https://link.springer.com/content/pdf/10.1007%2F978-3-642-14090-7.pdf

[20]   Coulomb's Law – the force of interaction between electric charges [Internet]. [Retrieved: 13.05.21]. Available from: https://x-engineer.org/undergraduate-engineering/physics/electricity-magnetism/coulombs-law-force-electric-charges/

[21]   Morin, J. and Pelletier, J. M. Density Functional Theory: Principle, Applications and Analysis. New York: Nova Science Publishers; 2013.

[22]   Nix, R. Relaxation and Reconstruction [Internet]. Queen Mary: University of London; 2021 [Retrieved: 19.05.21]. Available   from: https://chem.libretexts.org/Bookshelves/Physical_and_Theoretical_Chemistry_Textbook_Maps/Book%3A_Surface_Science_(Nix)/01%3A_Structure_of_Solid_Surfaces/1.07%3A_Relaxation_and_Reconstruction

[23]   Ning, Z. First Principles quantitative modeling of molecular devices [Thesis]. Waterloo: University of Waterloo; 2011.

[24]   Martin, R. M. Electronic Structure: Basic Theory and Practical Methods. Contemporary Physics. 2011;52(1):77.

[25]   Kubicki, J. D. and Watts, H. D. Quantum Mechanical Modeling of the Vibrational Spectra of Minerals with a Focus on Clays. Minerals. 2019;9(3):141-161.

[26]   Ptácek, P., Soukal, F. and Opravil, T. Introduction to the Transition State Theory. IntechOpen. 2018.

[27]   Nudged   Elastic   Band   [Internet].   [Retrieved: 10.03.21].   Available   from: https://theory.cm.utexas.edu/vtsttools/neb.html

[28]   SCM.   Nudged   Elastic   Band   (NEB)   [Internet].   [Retrieved: 05.06.21].   Available   from: https://www.scm.com/doc/AMS/Tasks/NEB.html

[29]   Transition States [Internet]. [Retrieved: 19.05.21]. Available from: http://scienide2.uwaterloo.ca/~nooijen/Chem-440-computational/Lab_Gaussian_transition_states.pdf

[30]   Harvey, D. Thermodynamics and Equilibrium Chemistry [Internet]. DePauw University; 2020 [Retrieved: 08.03.21]. Available   from: https://chem.libretexts.org/Bookshelves/Analytical_Chemistry/Book%3A_Analytical_Chemistry_2.1_(Harvey)/06%3A_Equilibrium_Chemistry/6.02%3A_Thermodynamics_and_Equilibrium_Chemistry

[31]   Atkins, P. W., De Paula, J. and Keeler, J. Atkins' Physical Chemistry. 11. edition. Oxford: Oxford University Press; 2018.

[32]   Jørgensen, M. and Grönbeck, H. Adsorbate Entropies with Complete Potential Energy Sampling in Microkinetic Modeling. The Journal of Physical Chemistry. 2017;121(13):7199-7207.

[33]   Simons, J. Harmonic Vibrational Motion [Internet]. University of Utah; 2020 [Retrieved: 27.04.21]. Available from: https://chem.libretexts.org/Bookshelves/Physical_and_Theoretical_Chemistry_Textbook_Maps/Book%3A_Quantum_Mechanics__in_Chemistry_(Simons_and_Nichols)/01%3A_The_Basic_Tools_of_Quantum_Mechanics/1.07%3A_Harmonic_Vibrational_Motion

[34]   About VASP [Internet]. [Retrieved: 18.01.21]. Available from: https://www.vasp.at/about/

[35]   The   VASP   manual   [Internet].   [Retrieved: 18.01.21].   Available   from: https://www.vasp.at/wiki/index.php/The_VASP_Manual

[36]   Liu, J. X., Su, H. Y., Sun, D. P., Zhang, B. Y. and Li, W. X. Crystallographic Dependence of CO Activation on Cobalt Catalysts: HCP versus FCC. ACS Publications. 2013;135(44):16284-16287.

[37]   Liu, L., Qin, C., Yu, M., Wang, Q., Wang, J., Hou, B., Jia, L. and Li, D. Morphology Evolution of Hcp Cobalt Nanoparticles Induced by Ru Promoter. ChemCatChem. 2020;12(7):2083-2090.

[38]   Fan, H. and El-Awady, J. A. Molecular Dynamics Simulations of Orientation Effects During Tensions, Compression, and Bending Deformations of Magnesium Nanocrystals. Journal of Applied Mechanics. 2015;82(10):101006-101017.

[39]   VESTA. 2021. [Retrieved: 10.04.21]. Available from: https://jp-minerals.org/vesta/en/

[40]   van Helden, P., van den Berg, J. A. and Weststrate, C. J. Hydrogen Adsorption on Co Surfaces: A Density Functional Theory and Temperature Programmed Desorption Study. ACS Catalysis. 2012;2(6):1097-1107.

[41]   Strømsheim, M. D., Svenum, I. H., Farstad, M. H., Weststrate, C. J., Borg, A. and Venvik, H. J. CO-Induced Surface Reconstruction of the Co(11−20) Surface-A Combined Theoretical and Experimental Investigation. The Journal of Physical Chemistry. 2020;124(52):28488-28499.

[42]   Lindroos, M. Barnes, C. J. Hu, P. and King, D. A. The termination and multilayer relaxation at the Co(10-10) surface. Chemical Physics Letters. 1990;173(1):92-96.

[43]   Liu, H., Zhang, R., Ling, L., Wang, Q., Wang, B. and Li, D. Insight into the preferred formation mechanism of long-chain hydrocarbons in Fischer–Tropsch synthesis on Hcp Co(10−11) surfaces from DFT and microkinetic modeling. Royal Society of Chemistry. 2017;7:3758-3776.

[44]   Weststrate, C. J., Mahmoodinia, M., Farstad, M. H., Svenum I. H., Strømsheim, M. D., Niemantsverdriet, J. W. and Venvik, H. J. Interaction of hydrogen with flat (0001) and corrugated (11–20) and (10–12) cobalt surfaces: Insights from experiment and theory. Catalysis Today. 2020;342:124-130.

[45]   Prior, K. A., Schwaha, K., Bridge, M. E. and Lambert, R. M. Surface structure of the non-unique planes hexagonal metals: A LEED study of Co(10-12). Chemical Physical Letters. 1979;65(3):472-475.

[46]   Blöchl, P. E. Projector augmented-wave method. Physical Review B. 1994;50(24):17953-17979.

[47]   Joos, L., Filot, I. A. W., Cottenier, S., Hensen, E. J. M., Waroquier, M., Speybroeck, V. V. and van Santen, R. A. Reactivity of CO on Carbon-Covered Cobalt Surfaces in Fischer–Tropsch Synthesis. ACS Publications. 2014;118(10):5317-5327.

[48]   DFT-D3 [internet]. [Retrieved: 10.02.21]. Available from: https://www.vasp.at/wiki/index.php/DFT-D3

[49]   Jansen, A. P. J., Agrawal, R. and Spanu, L. Thermodynamics and kinetics of carbon deposits on cobalt: a combined density functional theory and kinetic Monte Carlo study. Physical Chemistry Chemical Physics. 2016;18:28515-28523.

[50]   Zhang, M., Huang, H. and Yu, Y. Insight into the Mechanism of Ethylene Decomposition Over Co(0001) Surface: Formation of Carbon Species. Catalysis Letters. 2019;149:744-752.

[51]   Zhang, Z., Liu, S., Hou, X., Qi, L. and Li, W. Effect of potassium on carbon adsorption on the Co(0001) surface. Journal of Molecular Modeling. 2020;26:133-142.

[52]   Liu, J. X., Su, H. Y. and Li, W. X. Structure sensitivity of CO methanation on Co(0001), (10-12) and (11-20) surfaces: Density functional theory calculations. Catalysis Today. 2013;215:36-42.

[53]   Ferrin, P., Kandoi, S., Nilekar, A. U. and Mavrikakis, M. Hydrogen adsorption, absorption and diffusion on and in transition metal surfaces: A DFT study. Surface Science. 2012;606(7-8):679-689.

[54]   Qi, Y., Yang, J., Duan, X., Zhu, Y. A., Chen, D. and Holmen, A. Discrimination of the mechanism of CH4 formation in Fischer–Tropsch synthesis on Co catalysts: a combined approach of DFT, kinetic isotope effects and kinetic analysis. Catalysis Science & Technology. 2014;4:3534-3543.

[55]   Zhang, R., Li, K., Liu, H., He, L. and Wang, B. Insight into the C-C chain growth in Fisher-Tropsch synthesis on HCP Co(10-10) surface: The effect of crystal facets on the preferred mechanism. Computational Material Science. 2018;145:263-279.

[56]   Ernst, K. H., Schwarz, E. and Christmann, K. The interaction of hydrogen with cobalt(10-10) surface. The Journal of Chemical Physics. 1994;101(6):5388-5401.

[57]   Ramsvik, T., Borg, A., Venvik, H. J., Hnasteen, F., Kildemo, M. and Worren, T. Acetylene chemisorption and decomposition on the Co(11-20) single crystal surface. Surface Science. 2002;499:183-192.

[58]   Weststrate, C. J. and Niemantsverdriet, J. W. Understanding FTS selectivity: the crucial role of surface hydrogen. Faraday Discussion. 2017;197:101-116.

[59]   Vaari, J., Lahtinen, J. and Hautojärvi, P. The adsorption and decomposition of acetylene on clean and K-covered Co(0001). Catalysis Letters. 1997;44:43-49.

Appendices

APPENDIX A: Input-files

Example of input files (Fig. A.1), example of KPOINTS file (Fig. A.2) and example of POSCAR file (Fig. A.3).

```
General:
  SYSTEM  = Co_hcp
  PREC    = Accurate
  ENCUT   = 500
  ISMEAR  = 0
  SIGMA   = 0.1
  ISYM    = 2
  NELMDL  = -5
  NELM    = 200
  LREAL   = Auto
Memory handling:
  NCORE   = 32
  NSIM    = 4
  LPLANE  = .TRUE.
  LSCALU  = .FALSE.
Optimization:
  ISIF    = 2
  IBRION  = 2
  NSW     = 400
Convergency criterion:
  EDIFFG  = -0.01
  EDIFF   = 1.00e-5
Output options:
  LWAVE   = .TRUE.
  LCHARG  = .TRUE.
Dipole:
  IDIPOL  = 3
  LDIPOL  = .TRUE.
Spin:
  ISPIN   = 2
  MAGMOM  = 54*3.0 1*1.0
```

Figure A.1: INCAR file.

```
Max k-point distance:
0
Gamma
 5  5  1
 0  0  0
```

Figure A.2: KPOINTS file.

```
Co   C
 1.0000000000000000
      7.4760000000000000    0.0000000000000000    0.0000000000000000
      3.7380000000000000    6.4744059186924625    0.0000000000000000
      0.0000000000000000    0.0000000000000000   26.0625000000000000
    54    1
Selective dynamics
Cartesian
   7.4759999999999724   1.4387568708205420   0.0000000000000000    F    F    F
   2.4919999999999902   1.4387568708205420   0.0000000000000000    F    F    F
   4.9840000000000089   1.4387568708205420   0.0000000000000000    F    F    F
   8.7219999999999818   3.5968921770513784   0.0000000000000000    F    F    F
   3.7379999999999987   3.5968921770513784   0.0000000000000000    F    F    F
   6.2300000000000173   3.5968921770513784   0.0000000000000000    F    F    F
   9.9679999999999644   5.7550274832821682   0.0000000000000000    F    F    F
   4.9839999999999822   5.7550274832821682   0.0000000000000000    F    F    F
   7.4759999999999991   5.7550274832821682   0.0000000000000000    F    F    F
   0.0000000000000000   0.0000000000000000   2.0124999999999824    F    F    F
   2.4920000000000178   0.0000000000000000   2.0124999999999824    F    F    F
   4.9839999999999822   0.0000000000000000   2.0124999999999824    F    F    F
   1.2460000000000093   2.1581353062308368   2.0124999999999824    F    F    F
   3.7380000000000271   2.1581353062308368   2.0124999999999824    F    F    F
   6.2299999999999915   2.1581353062308368   2.0124999999999824    F    F    F
   2.4919999999999911   4.3162706124616266   2.0124999999999824    F    F    F
   4.9840000000000089   4.3162706124616266   2.0124999999999824    F    F    F
   7.4759999999999733   4.3162706124616266   2.0124999999999824    F    F    F
   7.4759999999999724   1.4387568708205420   4.0496314173144228    T    T    T
   2.4919999999999902   1.4387568708205420   4.0496314173144228    T    T    T
   4.9840000000000089   1.4387568708205420   4.0496314173144228    T    T    T
   8.7219999999999818   3.5968921770513784   4.0496314173144228    T    T    T
   3.7379999999999987   3.5968921770513784   4.0496314173144228    T    T    T
   6.2300000000000173   3.5968921770513784   4.0496314173144228    T    T    T
   9.9679999999999644   5.7550274832821682   4.0496314173144228    T    T    T
   4.9839999999999822   5.7550274832821682   4.0496314173144228    T    T    T
   7.4759999999999991   5.7550274832821682   4.0496314173144228    T    T    T
   0.0000000000000000   0.0000000000000000   6.0323875046663771    T    T    T
   2.4920000000000178   0.0000000000000000   6.0323875046663771    T    T    T
   4.9839999999999822   0.0000000000000000   6.0323875046663771    T    T    T
   1.2460000000000093   2.1581353062308368   6.0323875046663771    T    T    T
   3.7380000000000271   2.1581353062308368   6.0323875046663771    T    T    T
   6.2299999999999915   2.1581353062308368   6.0323875046663771    T    T    T
   2.4919999999999911   4.3162706124616266   6.0323875046663771    T    T    T
   4.9840000000000089   4.3162706124616266   6.0323875046663771    T    T    T
   7.4759999999999733   4.3162706124616266   6.0323875046663771    T    T    T
   7.4759999999999724   1.4387568708205420   8.0784548281222026    T    T    T
   2.4919999999999902   1.4387568708205420   8.0784548281222026    T    T    T
   4.9840000000000089   1.4387568708205420   8.0784548281222026    T    T    T
   8.7219999999999818   3.5968921770513784   8.0784548281222026    T    T    T
   3.7379999999999987   3.5968921770513784   8.0784548281222026    T    T    T
   6.2300000000000173   3.5968921770513784   8.0784548281222026    T    T    T
   9.9679999999999644   5.7550274832821682   8.0784548281222026    T    T    T
   4.9839999999999822   5.7550274832821682   8.0784548281222026    T    T    T
   7.4759999999999991   5.7550274832821682   8.0784548281222026    T    T    T
   0.0000000000000000   0.0000000000000000  10.0274522415123624    T    T    T
   2.4920000000000178   0.0000000000000000  10.0274522415123624    T    T    T
   4.9839999999999822   0.0000000000000000  10.0274522415123624    T    T    T
   1.2460000000000093   2.1581353062308368  10.0274522415123624    T    T    T
   3.7380000000000271   2.1581353062308368  10.0274522415123624    T    T    T
   6.2299999999999915   2.1581353062308368  10.0274522415123624    T    T    T
   2.4919999999999911   4.3162706124616266  10.0274522415123624    T    T    T
   4.9840000000000089   4.3162706124616266  10.0274522415123624    T    T    T
   7.4759999999999733   4.3162706124616266  10.0274522415123624    T    T    T
 _2.5379999999999985   1.2948811837384926  12.0274522415123606    T    T    T
```
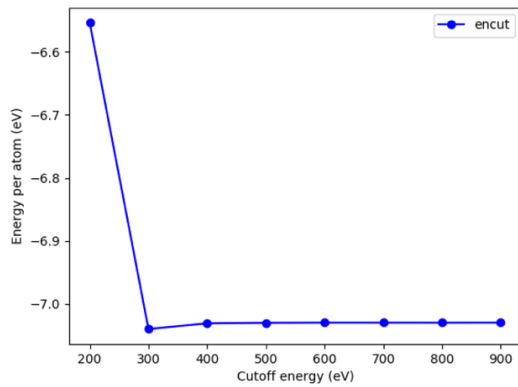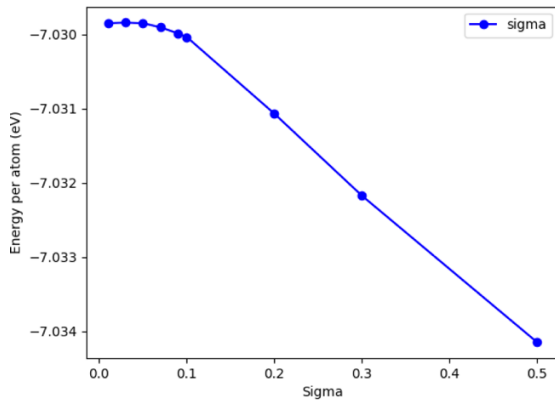
Figure A.3: POSCAR file.
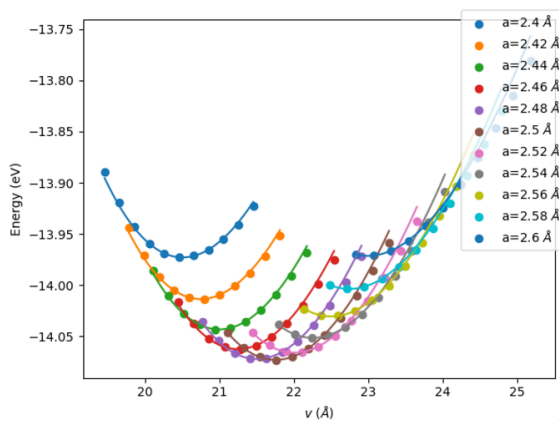
APPENDIX B: Convergence Test

Convergence test of energy cutoff (Fig. B.1), sigma value (Fig. B.2) and lattice constant (Fig. B.3) performed on Co bulk.

Figure B.1: Energy per atom of hcp Co [eV] as a function of the energy cutoff [eV].

Figure B.2: Energy per atom of hcp Co [eV] as a function of sigma.

Figure B.3: Energy [eV] as a function of atomic volume [Å] with different lattice constant (a).

APPENDIX C : Script of Surfaces

Script of the surfaces Co(0001) (Fig. C.1), Co(11-20) (Fig. C.2), Co(10-10) (Fig. C.3), Co(10-11) (Fig. C.4) and Co(10-12) (Fig. C.5)

```python
#!/usr/bin/env python
from ase.lattice.surface import hcp0001
from ase.io import write
from ase.constraints import FixAtoms
from ase.visualize import view

atoms=hcp0001('Co', size=(3,3,6), vacuum=8.0, a=2.492, c=4.025)

# Copy atoms in order to modify
at = atoms.copy()

# Translate atom in z-direction - placing atom with index0 at z=0
at.translate([[0., 0.,-at[0].z]])

# Wrap all atoms inside box
at.wrap()

# Constraints
constraint=FixAtoms(mask=at.positions[:, 2] < 3.2)
at.set_constraint(constraint)


# View atoms
view(at)

# write to POSCAR
at.write('POSCAR', sort=False, direct=True, vasp5=True)
```

Figure C.1: Script of Co(0001) surface.

```python
#!/usr/bin/env python
# -*- coding: utf-8 -*-

"""
"""

import logging

import numpy as np

import ase
import ase.io
from ase import Atom
from ase.visualize import view
#from vasptb.utils import view
from ase.spacegroup import crystal, Spacegroup
from ase.build import surface, fcc211, fcc100, sort
from ase.build.surface import _surface
from oase.ibuild.makesurf import SurfaceVectors

from ase.constraints import FixAtoms

from operator import itemgetter


np.set_printoptions(suppress=True)
#logging.basicConfig(level=logging.DEBUG)


def sort_z(atoms):
    """Sorts atoms - first according to position - z, x, y
       followed by chemical symbols
       Returns a sorted atoms instance
    """

    orders = [(atom.index, round(atom.x, 3), round(atom.y, 3),
               -round(atom.z, 3), atom.index) for atom in atoms]
    orders.sort(key=itemgetter(3, 1, 2))

    at = atoms.copy()

    for index, order in enumerate(orders):
        at[index].position = atoms[order[0]].position.copy()
        at[index].symbol = atoms[order[0]].symbol


    syms = at.get_chemical_symbols()
    orders2 = sorted([(sym, i) for i, sym in enumerate(syms)])

    indices = [i for sym, i in orders2]

    at2 = at[indices]
    return at2
# --------------- Co-hcp bulk --------------------

a = 2.492
c = 4.025
Co_hcp = crystal('Co',
                 [(1/3, 2/3, 3/4)],
                 spacegroup=194,
                 cellpar=[a, a, c, 90, 90, 120])
#view(Co_hcp)


# --------------- Make slabs --------------------
# OASE version
#planes = [(1, 1, 1)]

planes = [(0,0,1), (1,1,0)]

# skal ikke med: (3,2,1) = ???
#for hkl in planes:
#    print('=== %s ===' % (hkl, ))
#    surfs = SurfaceVectors(Cu_ccp, hkl=hkl, maxlen=15)
#    print(surfs)
#    #print()
#
#    slabs1 = surfs.get_slabs(0)
#    print(slabs1)
#    #print()
#
#    slab1 = slabs1.get_slab(0, vacuum=15)
#    #slab1 = slab1.repeat([int(np.ceil(10/slab1.cell[0][0])),
#    #                     int(np.ceil(10/slab1.cell[1][1])),1])
#    del slab1[[atom.index for atom in slab1 if atom.position[2] < 0.5]]
#    slab1.write('POSCAR.Cu' + str(hkl[0]) + str(hkl[1]) + str(hkl[2]) + '_oase', sort=True, direct=True, vasp5=True)
#    #view(slab1)
#    #print()
#
#    # ASE version
#    print('=== %s ===' % (hkl, ))
#    s = surface(Cu_ccp, hkl, layers = 6, periodic = True)
#    s.center(vacuum = 15, axis = 2)
#    s = s.repeat([int(np.ceil(15.5/s.cell[0][0])),
#                 int(np.ceil(15.5/s.cell[1][1])),1])
#
#    s.write('POSCAR.Cu' + str(hkl[0]) + str(hkl[1]) + str(hkl[2]) + '_test', sort = True, direct = True, vasp5 = True)
#    #view(s)
#
####

###
'''
hkl = (0,0,1)
s = surface(Co_hcp, hkl, layers = 10, periodic = True)
s.center(vacuum = 15, axis = 2)
s = s.repeat([1,1,1])

s.write('POSCAR.Co' + str(hkl[0]) + str(hkl[1]) + str(-hkl[0]-hkl[0])  + str(hkl[2]), sort = True, direct = True, vasp5 = True)
view(s)
'''

hkl = (1,1,0)
s = surface(Co_hcp, hkl, layers = 6, periodic = True)
s.center(vacuum = 8, axis = 2)
s = s.repeat([2,3,1])

s.translate(-s.positions[0])
s.wrap()

s_sorted=sort_z(s)

c = FixAtoms(mask=s_sorted.positions[:, 2] < 2.0)
s_sorted.set_constraint(c)



s_sorted.write('POSCAR.Co' + str(hkl[0]) + str(hkl[1]) + str(-hkl[0]-hkl[0]) +  str(hkl[2]), sort = False, direct = True, vasp5 = True)
view(s)
```

Figure C.2: Script of Co(11-20) surface.

```python
#!/usr/bin/env python
# -*- coding: utf-8 -*-

"""
"""

import logging

import numpy as np

import ase
import ase.io
from ase import Atom
from ase.visualize import view
#from vasptb.utils import view
from ase.spacegroup import crystal, Spacegroup
from ase.build import surface, fcc211, fcc100, sort
from ase.build.surface import _surface
#from oase.ibuild.makesurf import SurfaceVectors

from ase.constraints import FixAtoms

from operator import itemgetter


np.set_printoptions(suppress=True)
#logging.basicConfig(level=logging.DEBUG)


def sort_z(atoms):
    """Sorts atoms - first according to position - z, x, y
       followed by chemical symbols
       Returns a sorted atoms instance
    """

    orders = [(atom.index, round(atom.x, 3), round(atom.y, 3),
               -round(atom.z, 3), atom.index) for atom in atoms]
    orders.sort(key=itemgetter(3, 1, 2))

    at = atoms.copy()

    for index, order in enumerate(orders):
        at[index].position = atoms[order[0]].position.copy()
        at[index].symbol = atoms[order[0]].symbol


    syms = at.get_chemical_symbols()
    orders2 = sorted([(sym, i) for i, sym in enumerate(syms)])

    indices = [i for sym, i in orders2]

    at2 = at[indices]
    return at2

# --------------- Co-hcp bulk ---------------------

a = 2.492
c = 4.025
Co_hcp = crystal('Co',
                 [(1/3, 2/3, 3/4)],
                 spacegroup=194,
                 cellpar=[a, a, c, 90, 90, 120])
#view(Co_hcp)


# make Co(10-10)
hkl = (1,0,0)
s = surface(Co_hcp, hkl, layers = 6, periodic = True)
s.center(vacuum = 8, axis = 2)
s = s.repeat([3,2,1])

s.translate(-s.positions[0])
s.wrap()

s_sorted=sort_z(s)

c = FixAtoms(mask=s_sorted.positions[:,2]<3.0)
s_sorted.set_constraint(c)



s_sorted.write('POSCAR.Co' + str(hkl[0]) + str(hkl[1]) + str(-hkl[0]-hkl[1]) +  str(hkl[2]), sort = False, direct = True, vasp5 = True)
view(s)
```
Figure C.3: Script of Co(10-10) surface.

```python
#!/usr/bin/env python
# -*- coding: utf-8 -*-

"""
"""

import logging

import numpy as np

import ase
import ase.io
from ase import import Atom
from ase.visualize import view
#from vasptb.utils import view
from ase.spacegroup import import crystal, Spacegroup
from ase.build import import surface, fcc211, fcc100, sort
from ase.build.surface import _surface
#from oase.ibuild.makesurf import SurfaceVectors

from ase.constraints import FixAtoms

from operator import itemgetter


np.set_printoptions(suppress=True)
#logging.basicConfig(level=logging.DEBUG)


def sort_z(atoms):
    """Sorts atoms - first according to position - z, x, y
       followed by chemical symbols
       Returns a sorted atoms instance
    """

    orders = [(atom.index, round(atom.x, 3), round(atom.y, 3),
              -round(atom.z, 3), atom.index) for atom in atoms]
    orders.sort(key=itemgetter(3, 1, 2))

    at = atoms.copy()

    for index, order in enumerate(orders):
        at[index].position = atoms[order[0]].position.copy()
        at[index].symbol = atoms[order[0]].symbol

    syms = at.get_chemical_symbols()
    orders2 = sorted([(sym, i) for i, sym in enumerate(syms)])

    indices = [i for sym, i in orders2]

    at2 = at[indices]
    return at2
# ---------------- Co-hcp bulk ---------------------

a = 2.492
c = 4.025
Co_hcp = crystal('Co',
                 [(1/3, 2/3, 3/4)],
                 spacegroup=194,
                 cellpar=[a, a, c, 90, 90, 120])
#view(Co_hcp)


# make Co(10-11)
hkl = (1,0,1)
s = surface(Co_hcp, hkl, layers = 8, periodic = True)
print(s)

# Delete atoms

# Top row
at1 = s[[atom.index for atom in s if atom.position[2] < 14.0]]
print(at1)

# Bottom 3 rows
at = at1[[atom.index for atom in at1 if atom.position[2] > 3.0]]
print(at)


at.write('POSCAR.Co' + str(hkl[0]) + str(hkl[1]) + str(-hkl[0]-hkl[1]) + str(hkl[2]) +'_1x1', sort = False, direct = True, vasp5 = True)
#view(s_sorted)


at = at.repeat([2,3,1])
at.center(vacuum = 8, axis = 2)


#Flytt atomene til z=0
#at.translate([0., 0., -at[0].position[2]])
at.translate(-at[0].position)

#sorter i z
at=sort_z(at)
at.wrap()


#Fix bottom atoms
c = FixAtoms(mask=at.positions[:, 2] < 2.5)
at.set_constraint(c)

at.write('POSCAR.Co' + str(hkl[0]) + str(hkl[1]) + str(-hkl[0]-hkl[1]) + str(hkl[2])+'_2x3', sort = False, direct = True, vasp5 = True)
```

Figure C.4: Script of Co(10-11) surface.

```python
# -*- coding: utf-8 -*-
"""
"""
from __future__ import division
from __future__ import print_function

import logging

import numpy as np

import ase
import ase.io
from ase import Atom
from ase.visualize import view
#from vasptb.utils import view
from ase.spacegroup import crystal, Spacegroup

from oase.ibuild.makesurf import SurfaceVectors

from ase.constraints import FixAtoms

np.set_printoptions(suppress=True)
#logging.basicConfig(level=logging.DEBUG)



# --------------- Co-hcp bulk --------------------
a=2.492
c=4.025


Co_hcp = crystal('Co',
                 [(1/3, 2/3, 3/4)],
                 spacegroup=194,
                 cellpar=[a, a, c, 90, 90, 120])
'''
# --------------- Make slab Co(0001) --------------------
hkl = (0, 0, 1)
print('=== %s ===' % (hkl, ))
surfs = SurfaceVectors(Co_hcp, hkl=hkl, maxlen=10)
print(surfs)
print()

slabs = surfs.get_slabs(0)
print(slabs)
print()

slab = slabs.get_slab(0, rep=(1, 1, 2), vacuum=10)
slab.write('POSCAR.Co_0001', sort=True, direct=True, vasp5=True)
view(slab)
print()


# --------------- Make slab Co(11-20) --------------------
hkl = (1, 1, 0)
print('=== %s ===' % (hkl, ))
surfs = SurfaceVectors(Co_hcp, hkl=hkl, maxlen=10)
print(surfs)
print()

slabs = surfs.get_slabs(0)
print(slabs)
print()

slab = slabs.get_slab(0, rep=(1, 1, 2), vacuum=10)
slab.write('POSCAR.Co_11-20', sort=True, direct=True, vasp5=True)
view(slab)
print()
'''
# --------------- Make slab Co(10-12) --------------------
hkl = (1, 0, 2)
print('=== %s ===' % (hkl, ))
surfs = SurfaceVectors(Co_hcp, hkl=hkl, maxlen=10)
print(surfs)
print()

slabs1 = surfs.get_slabs(0)
print(slabs1)
print()

slab1 = slabs1.get_slab(0, rep=(4, 1, 2), vacuum=16)
slab1.write('POSCAR.Co' + str(hkl[0]) + str(hkl[1]) + str(-hkl[0]-hkl[1]) +  str(hkl[2]) + 'old_cart', sort = False, direct = False, vasp5 = True)
#slab1.write('POSCAR.Co_10-12_A', sort=True, direct=True, vasp5=True)
#view(slab1)
print()


atoms = slab1.copy()
print('atoms:', atoms)

for atom in atoms:
    print(atom.index, atom.position[2])
at = atoms[[atom.index for atom in atoms if atom.position[2] < 11.0]]
at.write('POSCAR.Co' + str(hkl[0]) + str(hkl[1]) + str(-hkl[0]-hkl[1]) +  str(hkl[2]) + 'old_cart_del_top', sort = False, direct = False, vasp5 = True)



print('at:', at)

uc = at.get_cell()
new_uc = at.get_cell()
new_uc[2] = [0., 0., uc[2][2]]
at.set_cell(new_uc)
at.wrap()
c = FixAtoms(mask=at.positions[:, 2] < 4.2)
at.set_constraint(c)


at.write('POSCAR.Co' + str(hkl[0]) + str(hkl[1]) + str(-hkl[0]-hkl[1]) +  str(hkl[2]) + '_4x1', sort = False, direct = False, vasp5 = True)
```
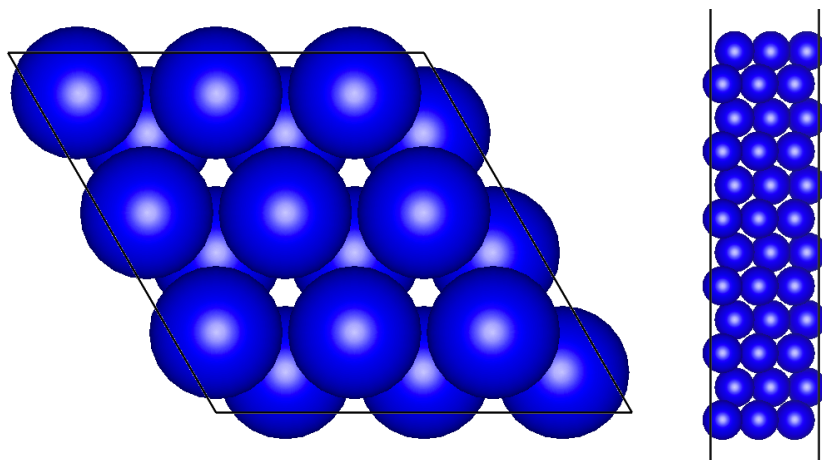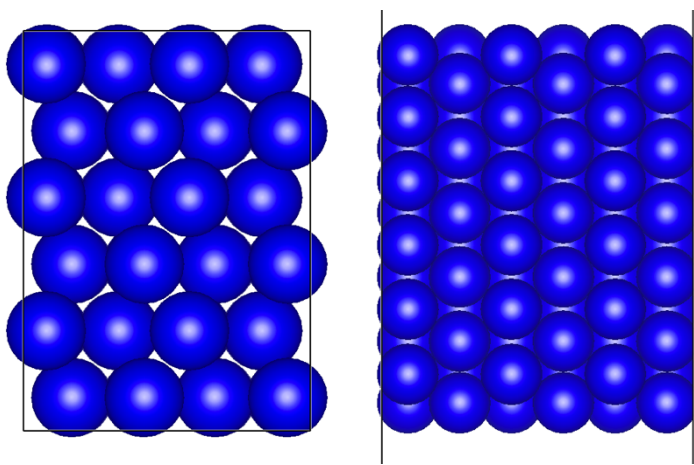
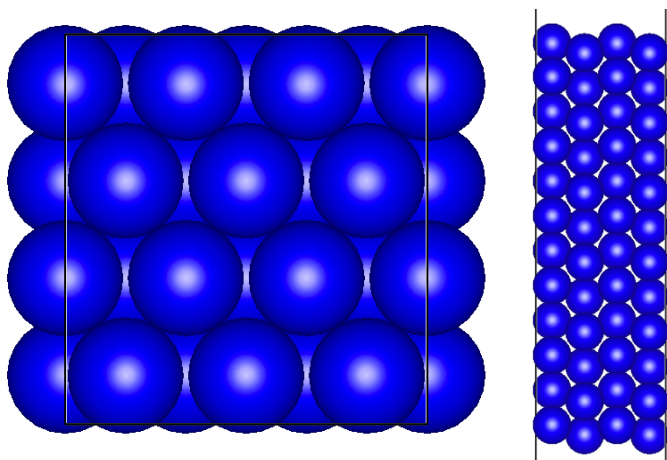**Figure C.5:** Script of Co(10-12) surface.

The slabs used in calculation of the surface free energy can be seen in Figure D.1, D.2, D.3, D.4 and D.5.
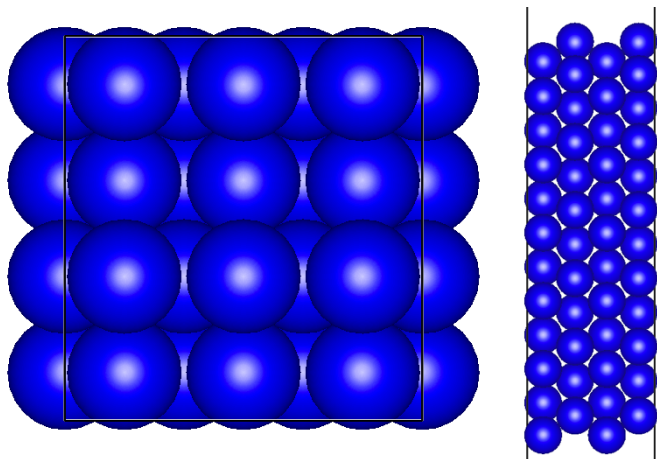

Figure D.1: The slab model of Co(0001) repeated with two in front (left) and side views (right).
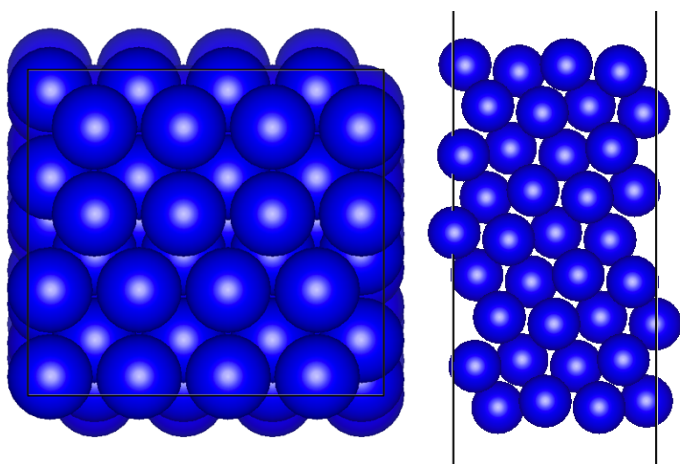

Figure D.2: The slab model of Co(11-20) repeated with two in front (left) and side views (right).
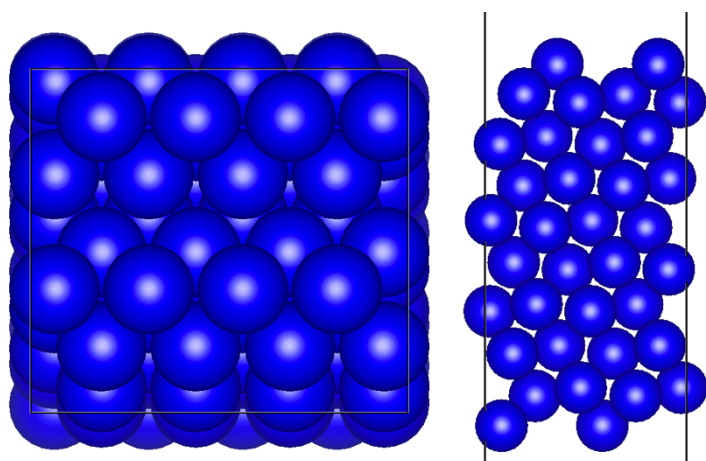

Figure D.3: The slab model of Co(10-10)A repeated with two in front (left) and side views (right).
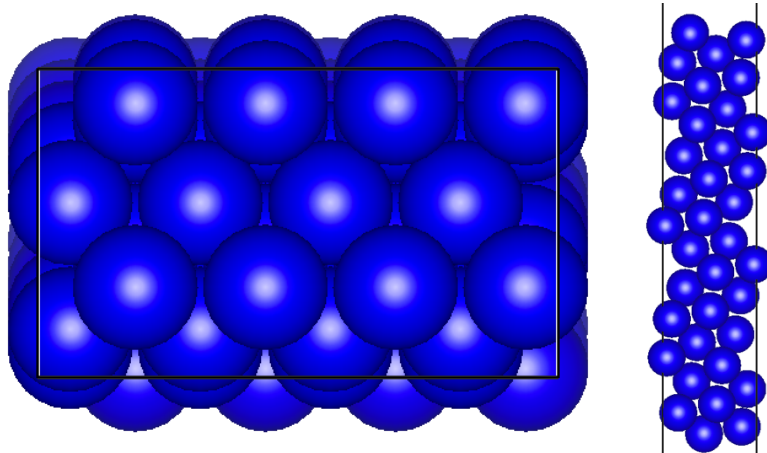
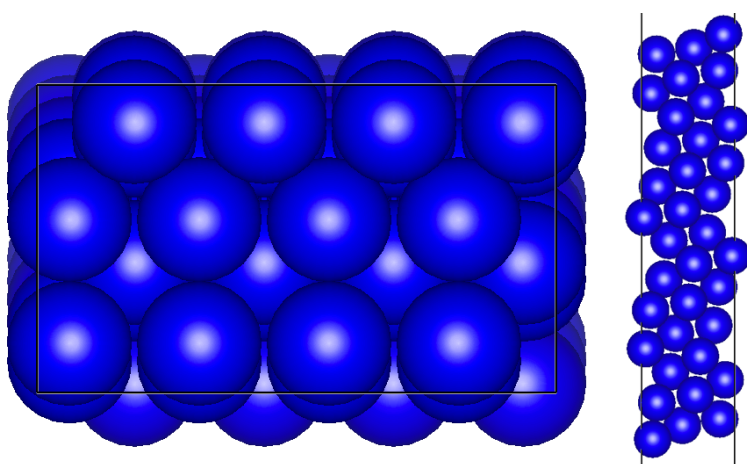**Figure D.4:** The slab model of Co(10-10)B repeated with two in front (left) and side views (right).

Figure D.5: The slab model of Co(10-11)A repeated with two in front (left) and side views (right)

Figure D.6: The slab model of Co(10-11)B repeated with two in front (left) and side views (right).

Figure D.7: The slab model of Co(10-12)A repeated with two in front (left) and side views (right).

Figure D.8: The slab model of Co(10-12)B repeated with two in front (left) and side views (right).

APPENDIX E: Submission Script

Figure E.1 shows the submission script used in VASP

```bash
#!/bin/bash
#SBATCH --job-name=Co
#SBATCH --account=nn9355k

#SBATCH --nodes=4
#SBATCH --ntasks-per-node=32
#SBATCH --time=32:00:00


# JOB-SPECIFIC VARIABLES
export POSCARNAME=POSCAR
export RESULTSDIR=results

echo $RESULTSDIR

set -o errexit # Make bash exit on any error


# load modules
module purge
module load StdEnvNew
#module load VASP/5.4.4-intel-2018b
module load VASP/5.4.4-intel-2018a

# VASP executable
export MPIEXEC_LOCAL=srun
export VASPLOC=vasp_std

vaspcommand="$MPIEXEC_LOCAL $VASPLOC"


## Source utility functions
#source ~svenum/vasp/vasptb/scripts/runvasp.sh


## Variables for job queue
jobid=$SLURM_JOB_ID
WORKDIR=/cluster/work/users/$USER/$SLURM_JOB_ID     #$SLURM_SUBMIT_DIR
SUBMITDIR=$SLURM_SUBMIT_DIR


## Set up work directory
mkdir -p $WORKDIR
chmod +s $WORKDIR

# Go to submitdir and make softling
cd $SUBMITDIR
ln -s $WORKDIR scratch_$SLURM_JOB_ID

## Copy files to WORKDIR
cp IN* $WORKDIR
cp KPOINTS* $WORKDIR
cp POTCAR $WORKDIR
cp $POSCARNAME $WORKDIR/POSCAR

## Run vasp in workdir
cd $WORKDIR


echo "Starting calculations..."
echo ""

date > a

n=1
echo "Running calculation ... loop $n"
cp IN$n INCAR
cp KPOINTS$n KPOINTS
$vaspcommand
cp POSCAR POSCAR$n
cp CONTCAR POSCAR
mv CONTCAR CONTCAR$n
cp OUTCAR OUTCAR$n

n=2
echo "Running calculation ... loop $n"
cp IN$n INCAR
cp KPOINTS$n KPOINTS
$vaspcommand
cp POSCAR POSCAR$n
cp CONTCAR POSCAR
mv CONTCAR CONTCAR$n
cp OUTCAR OUTCAR$n

n=3
echo "Running calculation ... loop $n"
cp IN$n INCAR
$vaspcommand
cp POSCAR POSCAR$n
cp CONTCAR POSCAR
mv CONTCAR CONTCAR$n
cp OUTCAR OUTCAR$n

date > b


## Clean up
rm -r WAVECAR

mkdir  $SUBMITDIR/$RESULTSDIR
cp -upr $WORKDIR/* $SUBMITDIR/$RESULTSDIR/.

cd $SUBMITDIR
rm -rf $WORKDIR scratch_*
```

Figure E.1: Submission script.

APPENDIX F: Gibbs Free Energy Scripts

The Gibbs free energy was calculated with the script shown in Figure F.1 for the gas phases H_2 and C_2H_2, and the script shown in Figure F.2 for the adsorbed species on the surfaces.

```python
#!/usr/bin/env python

from ase.build import molecule
from ase.calculators.emt import EMT
from ase.optimize import QuasiNewton
from ase.vibrations import Vibrations
from ase.thermochemistry import IdealGasThermo
from ase.io import read


import os
cwd = os.getcwd()

atoms = read(os.path.join(cwd, 'results', 'CONTCAR'))
natoms = len(atoms)

from ase.calculators.vasp import Vasp

# Get potential energy from OUTCAR using Vasp calculator
path_e = os.path.join(cwd, 'results')
os.chdir(path_e)
# Must be in the acutal folder where the corresponding OUTCAR is
calc_e = Vasp(restart=True)
atoms.set_calculator(calc_e)
#using ase to get the potential energy
potentialenergy=atoms.get_potential_energy()
print('potential energy:', potentialenergy)

# Get potential energy from OUTCAR using Vasp calculator
path_vib = os.path.join(cwd, 'results', 'vib')
os.chdir(path_vib)
# Must be in the acutal folder where the corresponding OUTCAR is
calc_vib = Vasp(restart=True)
atoms.set_calculator(calc_vib)

# using ase to read the vibrational energies in meV
real_vib, im_vib = calc_vib.read_vib_freq()
vib_energies_meV = real_vib + im_vib

print(real_vib, im_vib)
print('vib energies in meV:', vib_energies_meV)

# revese list of vib_energies and give in eV
vib_energies = []
for vib in reversed(vib_energies_meV):
    vib_energies.append(vib/1000.)

print('vib energies in eV:', vib_energies)

# eller skriv inn manuelt for acetylene
# Acetylene
geometry = 'linear'
symmetrynumber = 2
spin = 0




thermo = IdealGasThermo(vib_energies=vib_energies,
                        potentialenergy=potentialenergy,
                        atoms=atoms,
                        geometry=geometry,
                        symmetrynumber=symmetrynumber,
                        spin=spin)


G = thermo.get_gibbs_energy(temperature=600, pressure=101325.)
```
Figure F.1: The Gibbs free energy script for the gas phases.

```python
#!/usr/bin/env python

from numpy import array
from ase.thermochemistry import HarmonicThermo


vibs = array([3026.980632, 3007.72359, 1210.992319, 1048.475449, 834.960363, 809.395347, 706.162986, 457.989354, 428.965127, 301.992443, 294.526947, 275.221161])

vib_energies = vibs / 8065.54429   # convert to eV from cm^-1
potentialenergy = -392.6395215

thermo = HarmonicThermo(vib_energies=vib_energies,
                        potentialenergy=potentialenergy)

F = thermo.get_helmholtz_energy(temperature=600)
```
Figure F.2: The Gibbs free energy script for the adsorbed species.

APPENDIX G: Vibrational Frequencies on Gas Phases

Table G.1 shows the frequencies for each gas phase obtained from the vibrational analysis and the calculated ZPE value. The gas phase C and H has no frequencies because it is a single atom. The calculated energy performed with VASP together with the ZPE value, can also be seen in the table.

Table G.1: Frequencies, ZPE value and calculated energy [eV] for the gas species.

Gas phase	ν_i [cm^{-1}]	ZPE [eV]	Energy [eV]
C	-	-	-1.39
H	-	-	-1.12
CH	3035	0.1881	-5.36
C_2	1642	0.1018	-9.55
H_2	4331	0.2685	-6.50
C_2H	3384, 2033, 10, 10	0.3370	-15.52
C_2H_2	3449, 3352, 2011, 738, 738, 607, 610	0.7133	-22.24

APPENDIX H: Vibrational Frequencies on Adsorbed Species

Frequencies values and calculated ZPE value for Co(0001) (Table H.1), Co(11-20) (Table H.2), Co(10-10) (Table H.3), Co(10-11) (Table H.4) and Co(10-12) (Table H.5)

Table H.1: Frequencies and calculated ZPE values on Co(0001) surface.

Adsorbate	Site	v_i [cm^{-1}]	ZPE [eV]
C	hcp	573, 491, 484	0.0960
	fcc	583, 442, 433	0.0904
	top	884, 164i, 172i	-
H	hcp	1127, 832, 830	0.1729
	fcc	1136, 894, 882	0.1805
	top	1804, 371i, 373i	-
CH	hcp	3006, 642, 638, 584, 405, 395	0.3514
	fcc	3022, 640, 634, 608, 359, 355	0.3483
	top	3079, 839, 638, 634, 181i, 185i	-
C$_2$	fcc-hcp	1379, 495, 424, 375, 346, 344	0.2084
	top	1631, 454, 95i, 99i, 176i, 195i	-
C$_2$H	fcc-hcp	3072, 1328, 867, 715, 485, 425, 377, 284, 270	0.4850
	hcp	3368, 1778, 574, 570, 318, 211, 201, 83, 51i	-
	fcc	3370, 1791, 572, 569, 324, 211, 198, 23i, 47i	-
	top	3383, 1908, 582, 582, 416, 234, 232, 45, 25	0.4592
C$_2$H$_2$	fcc-hcp	3027, 3008, 1211, 1048, 835, 809, 706, 458, 429, 302, 295, 275	0.7689

Table H 2: Frequencies and calculated ZPE values on Co(11-20) surface.

Adsorbate	Site	ν_i [cm^{-1}]	ZPE [eV]
C	tB (offsite)	534, 412, 382	0.0824
	bB	654, 60, 329	0.0912
H	tB (offsite)	1172, 817, 326i	-
	bB	991, 872, 658	0.1562
	bA	1334, 1083, 317	0.1695
	bAB$_2$	1367, 582, 334	0.1415
CH	tB (offsite)	2947, 680, 588, 561, 383, 303	0.3386
	bB	2912, 690, 539, 508, 490, 296	0.3370
C$_2$	tB-tB (offsite)	1502, 551, 375, 334. 329, 143	0.2004
	tB-tB (offsite)2	1492, 510, 398, 325, 162, 53	0.1823
	tB-bB	1253, 515, 453, 382, 303, 256	0.1960
	bA-tB	1365, 490, 440, 375, 340, 200	0.1991
C$_2$H	tB-tB (offsite)	3037, 1324, 918, 703, 457, 390, 362, 239, 188	0.477
	tB-tB (offsite)2	3056, 1347, 884, 603, 420, 263, 278, 272, 91	0.4534
	tB-bB	3053, 1251, 861, 567, 425, 395, 312, 270, 226	0.4562
	tB-bB2	2985, 1152, 894, 644, 489, 432, 402, 272, 195	0.4628
	bA-tB	3113, 1337, 853, 629, 435, 422, 321, 261, 205	0.4696
C$_2$H$_2$	tB-tB (offsite)	3006, 2389, 1277, 1245, 999, 790, 592, 492, 398, 276, 194, 175	0.7335
	tB-tB (offsite)2	2993, 2970, 1097, 1038, 940, 792, 709, 498, 420, 343, 315, 144	0.7580
	hAAB-hAAB	2961, 2934, 1318, 1082, 891, 793, 615, 422, 393, 284, 179, 164	0.7462

Table H.3: Frequencies and calculated ZPE values on Co(10-10) surface.

Adsorbate	Site	ν_i [cm^{-1}]	ZPE [eV]
C	$3f_1$	600, 463, 437	0.0930
	b_2	553, 498, 399	0.0898
H	$3f_1$	1152, 945, 756	0.1769
	b_2	1118, 879, 580	0.1598
CH	$3f_1$	3016, 659, 638, 612, 399, 344	0.3513
	b_2	2984, 704, 633, 570, 407, 268	0.3451
C_2	b_1-$3f_1$	1485, 483, 387, 267, 254, 239	0.1930
	b_2-$3f_1$	1306, 502, 449, 384, 351, 203	0.1981
	$3f_1$-$3f_1$	1230, 536, 458, 379, 241, 235	0.1909
	$3f_2$-$3f_2$	1509, 580, 421, 317, 276, 214	0.2056
C_2H	b_1-$3f_1$	3200, 1516, 773, 611, 460, 390, 291, 225, 200	0.4752
	b_2-$3f_1$	3042, 1222, 886, 678, 490, 431, 325, 288, 227	0.4704
	b_2-$3f_1$2	3041, 1262, 887, 696, 489, 414, 390, 297, 226	0.4775
	b_1	4482, 1105, 629, 342, 265, 367i, 374i, 1460i, 1473i	-
	b_1-t_1	3232, 1617, 762, 616, 469, 410, 277, 220, 71	0.4757
C_2H_2	b_2-$3f_1$	2995, 2981, 1133, 1068, 857, 802, 689, 471, 426, 304, 263, 236	0.7579
	t_1	6403, 3407, 671, 484, 480, 176i, 202i, 402i, 680i, 682i, 2933i, 2995i	-
	t_2	7348, 3398, 496, 420, 402, 280i, 341i, 459i, 697i, 721i, 3254i, 3419i	-
	b_1-t_1	3176, 2916, 1476, 931, 742, 713, 531, 477, 390, 164, 133, 79	0.7271
	$3f_1$-$3f_1$	3092, 3078, 1177, 1005, 818, 797, 710, 527, 389, 353, 319, 122	0.7679

Table H.4: Frequencies and calculated ZPE values on Co(10-11) surface.

Adsorbate	Site	ν_i [cm^{-1}]	ZPE [eV]
C	4fh	624, 594, 378	0.0990
	fcc	562, 459, 432	0.0900
	hcp	564, 484, 417	0.0909
H	4fh	728, 641, 618	0.1232
	fcc	1121, 863, 861	0.1764
	hcp	1128, 839, 806	0.1719
CH	4fh	2878, 643, 619, 461, 444, 425	0.3393
	fcc	3009, 628, 627, 602, 376, 360	0.3472
	hcp	3004, 648, 644, 614, 397, 339	0.3500
C$_2$	4fh-fcc	1049, 587, 468, 450, 328, 270	0.1954
	4fh-hcp	1242, 483, 415, 371, 352, 337	0.1983
	bridge	2922, 557, 33i, 89i, 1209i, 1229i	-
	fcc-hcp	1406, 488, 420, 391, 361, 352	0.2120
	4fh-4fh	1494, 564, 425, 292, 273, 228	0.2031
C$_2$H	4fh-fcc	3048, 1122, 862, 739, 519, 479, 385, 308, 137	0.4711
	4fh-bridge	3146, 1306, 805, 611, 457, 391, 338, 301, 265	0.4724
	4fh-bridge2	3158, 1346, 805, 612, 441, 387, 348, 272, 238	0.416
	fcc-bridge	3197, 1476, 780, 633, 459, 390, 324, 217, 207	0.4763
	4fh-hcp	2971, 1165, 865, 659, 476, 446, 371, 262, 233	0.4618
	fcc-hcp	3055, 1314, 867, 695, 464, 422, 398, 312, 274	0.4837
	top	4089, 735, 457, 437, 194i, 229i, 534i, 1176i, 1179i	-
C$_2$H$_2$	4fh-fcc	3047, 2974, 1031, 999, 823, 800, 702, 481, 426, 350, 315, 160	0.7506
	4fh-hcp	3003, 2904, 1048, 1038, 809, 778, 645, 469, 358, 347, 284, 232	0.7387
	4fh-4fh	3010, 2974, 1274, 1101, 903, 844, 714, 483, 436, 275, 207, 200	0.7700
	fcc-hcp	3011, 2991, 1197, 1056, 838, 814, 698, 460, 431, 299, 282, 269	0.7654

Table H.5: Frequencies and calculated ZPE values on Co(10-12) surface.

Adsorbate	Site	v_i [cm^{-1}]	ZPE [eV]
C	tC	551, 400, 325	0.0791
	bC	681, 469, 301	0.0899
	4fh	584, 580, 372	0.0952
H	tC	1105, 894, 644	0.1639
	bA	1292, 1140, 286	0.1685
	bC	957, 936, 628	0.1563
	3hBBC	1104, 891, 769	0.1713
	4fh	790, 600, 546	0.1201
	bAB	1306, 1042, 124	0.1532
CH	tC	2935, 636, 563, 541, 336, 334	0.3314
	bC	2906, 676, 583, 492, 457, 268	0.3336
	3hBBC	2967, 646, 565, 557, 378, 302	0.3326
	4fh	2898, 633, 631, 447, 441, 409	0.3385
C$_2$	tA-bAB	1523, 482, 442, 294, 146, 140i	-
	tC-tC	1343, 531, 411, 382, 322, 286	0.2030
	bA-4fh	1376, 433, 387, 349, 277, 253	0.1906
	4f-4fh	1523, 546, 420, 292, 246, 213	0.2009
	3hBBC-4fh	1172, 543, 435, 412, 294, 273	0.1940
C$_2$H	tA	4086, 613, 490, 489, 100i, 151i, 591i, 591i, 1147i, 1157i	-
	tC-bC	3047, 1084, 921, 698, 472, 410, 362, 234, 193	0.4600
	tC-tC	3054, 1249, 902, 589, 441, 403, 300, 256, 158	0.4557
	bA-4fh	3146, 1379, 777, 601, 446, 366, 378, 285, 261	0.4706
	bB	4022, 1175, 634, 277, 236, 340i, 451i, 1155i, 1191i	-
	bB-4fh	3146, 1379, 777, 601, 446, 366, 328, 285, 261	0.4664
	4fh-4fh	3100, 1433, 866, 690, 474, 420, 320, 243, 89	0.4733
	bAB-4fh	408, 3130, 1191, 732, 445, 398, 329, 270, 27115i	-
C$_2$H$_2$	tB	6309, 4097, 845, 467, 456, 239i, 297i, 333i, 1174i, 1180i, 2689i, 2906i	-
	tA-bA	3165, 2924, 1485, 930, 737, 719, 535, 460, 362, 133, 111, 59	0.7203
	tC-bA	3108, 2896, 1207, 1015, 805, 767, 652, 484, 384, 359, 212, 140	0.7457
		3002, 2987, 1084, 1052, 922, 817, 741, 491, 431, 376, 342, 189	0.7709
	tC-bC	2997, 2403, 1231, 1129, 945, 655, 523, 443, 306, 237, 202, 131	0.6945
	tC-3hBBC	2996, 2403, 1231, 1129, 945, 655, 523, 443, 306, 237, 202, 131	0.6945
	4fh-4fh	2996, 2970, 1280, 1105, 906, 843, 697, 483, 443, 276, 207, 184	0.7681

APPENDIX I: ZPE Calculation

Example of a ZPE calculation:

C_2H_2 adsorbed on fcc-hcp site on Co(0001). After the vibrational analysis, the vibrational frequencies (v_i) become:

[3026.98063, 3007.72359, 1210.99232, 1048.47545, 834.960363, 809.395347, 706.162986, 457.989354, 428.965127, 301.992443, 294.526947, 275.221161] cm^{-1}

The frequencies were converted into m^{-1} by multiplying with 100. The speed of light (c=299792458 m/s) were used to convert the frequencies from m^{-1} to s^{-1} with the formula:

$$v = c * v_i$$

Planck´s constant (h=4.1357E-15 eV*s) were used to calculate the ZPE value for each frequency with equation:

$$ZPE = \frac{h*v}{2}$$

The ZPE were calculated for each mode with the equation:

$$ZPE = \sum_i hv_i$$

APPENDIX J: CI-NEB Graph Co(0001) Surface

Graph for CI-NEB calculations on Co(0001) surface Figure J.1, J.2 and J.3 shows the C-H scission graphs and Figure J4, J.5 and J.6 shows the C-C scission graphs.
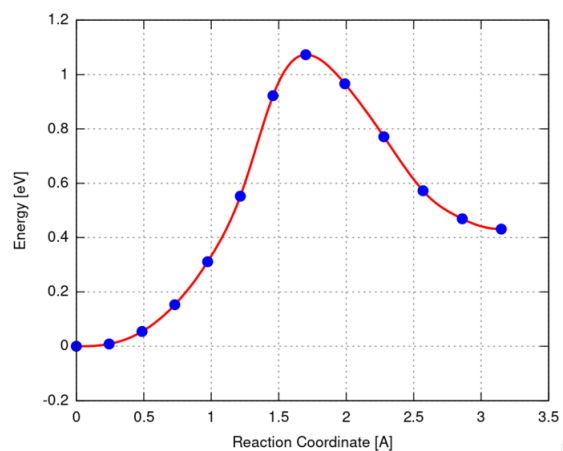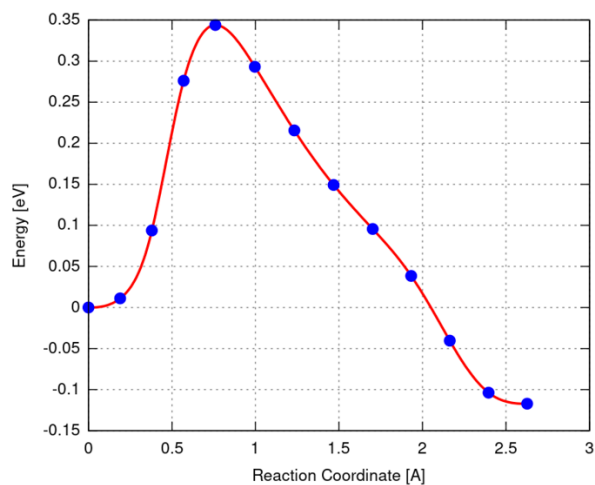
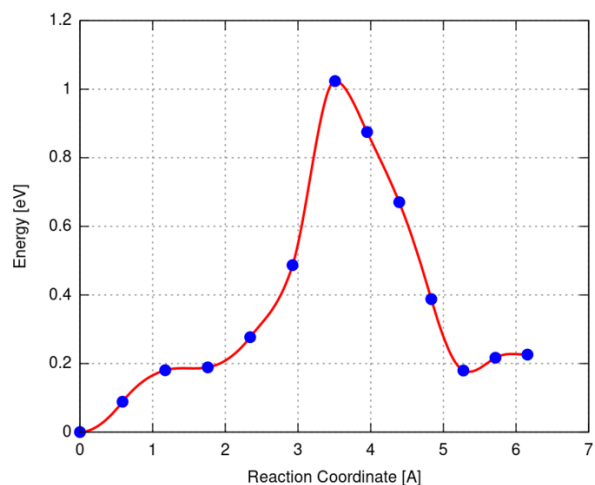**Figure J.1:** CI-NEB graph for reaction $C_2H_2 \rightarrow C_2H + H$ on Co(0001) surface.
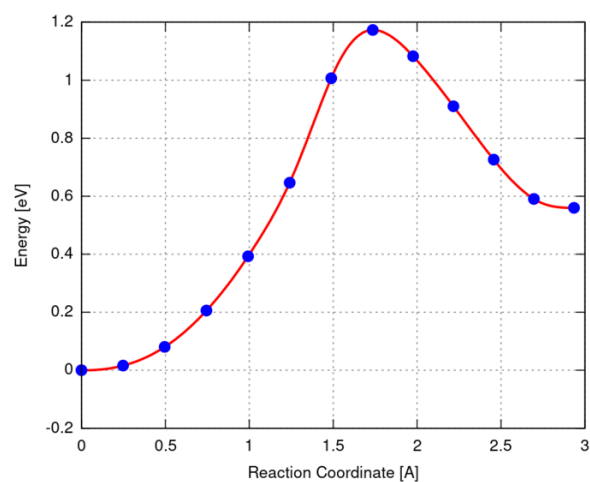
Figure J.2: CI-NEB graph for reaction $C_2H \rightarrow C_2 + H$ on Co(0001) surface.
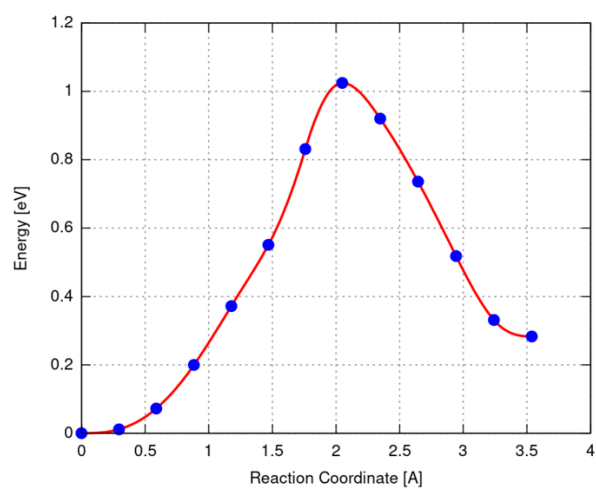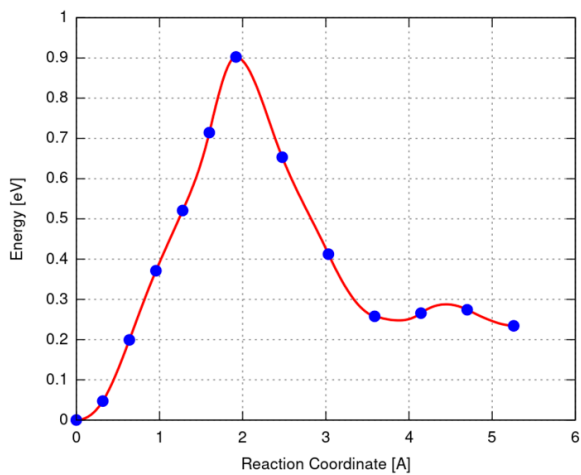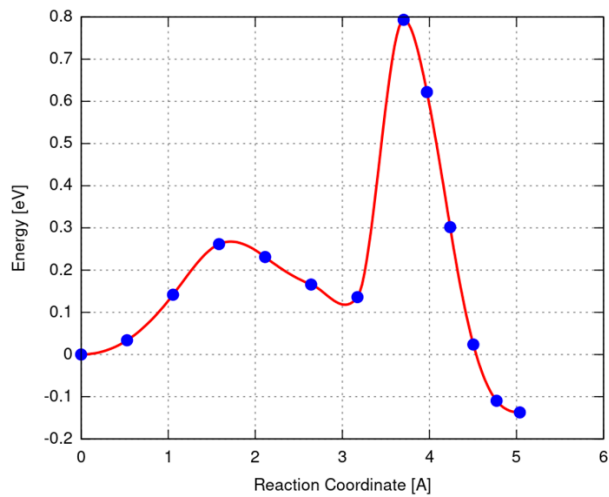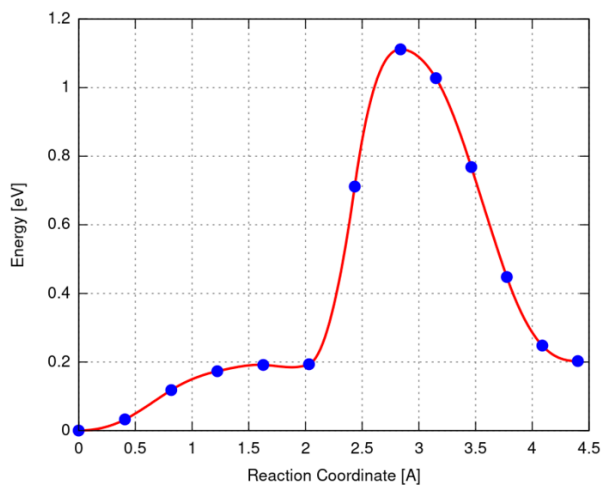
Figure J.3: CI-NEB graph for reaction $CH \rightarrow C + H$ on Co(0001) surface.
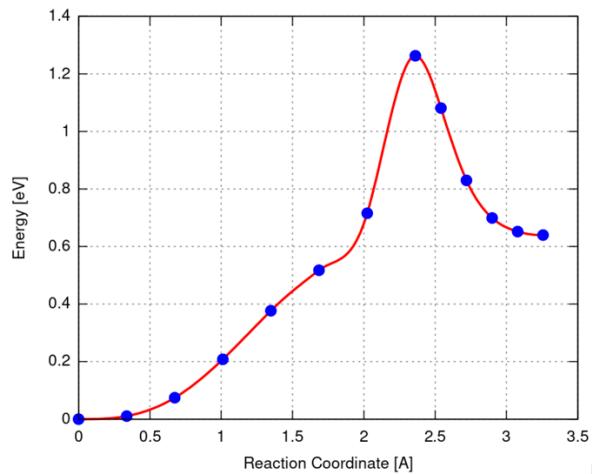
Figure J.4: CI-NEB graph for reaction $C_2H_2 \rightarrow CH + CH$ on Co(0001) surface.
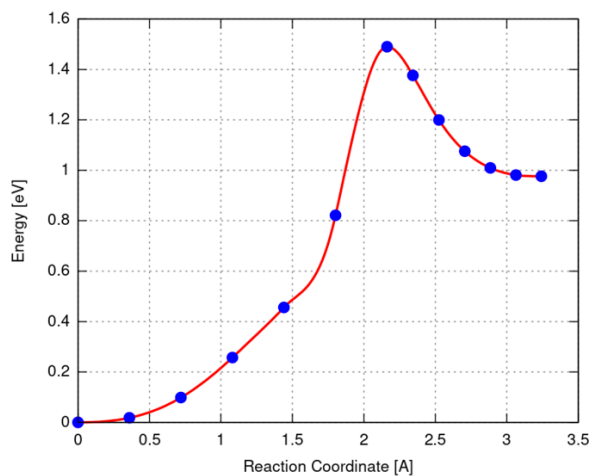
Figure J.5: CI-NEB graph for reaction $C_2H \rightarrow C + CH$ on Co(0001) surface.
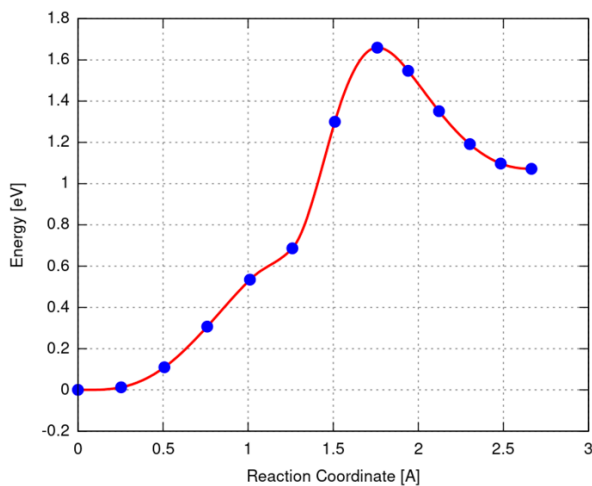
Figure J.6: CI-NEB graph for reaction $C_2 \rightarrow C + C$ on Co(0001) surface.

XXIII

APPENDIX K: CI-NEB Graph Co(11-20) Surface

Graph for CI-NEB calculations on Co(11-20) surface Figure K.1, K.2 and K.3 shows the C-H scission graphs and Figure K.4, K.5 and K.6 shows the C-C scission graphs.

Figure K.1: CI-NEB graph for reaction $C_2H_2 \rightarrow C_2H + H$ on Co(11-20) surface.

Figure K.2: CI-NEB graph for reaction $C_2H \rightarrow CH + H$ on Co(11-20) surface.
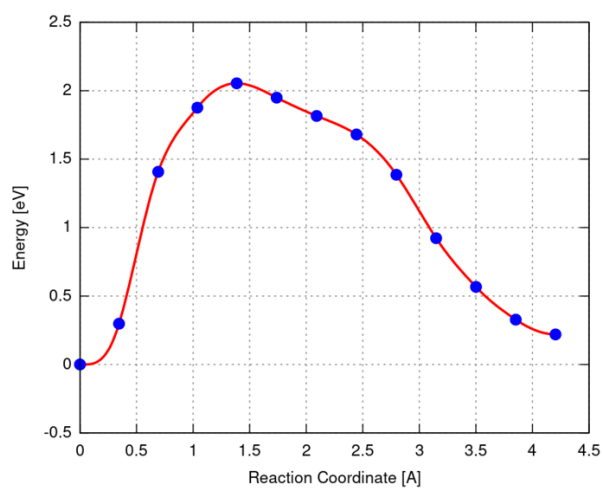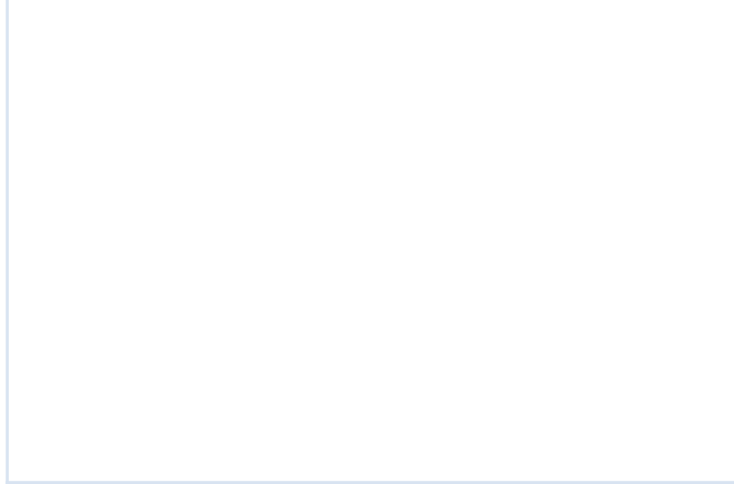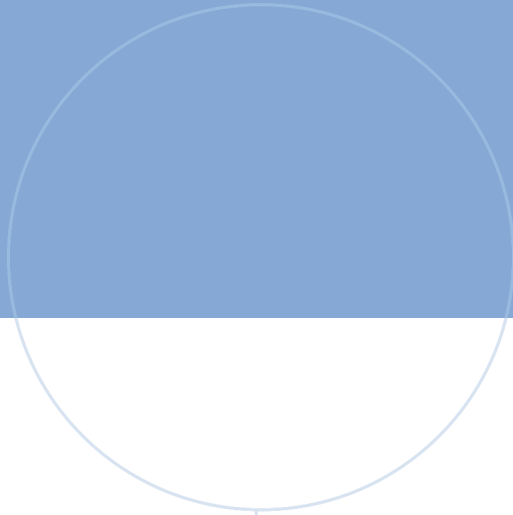

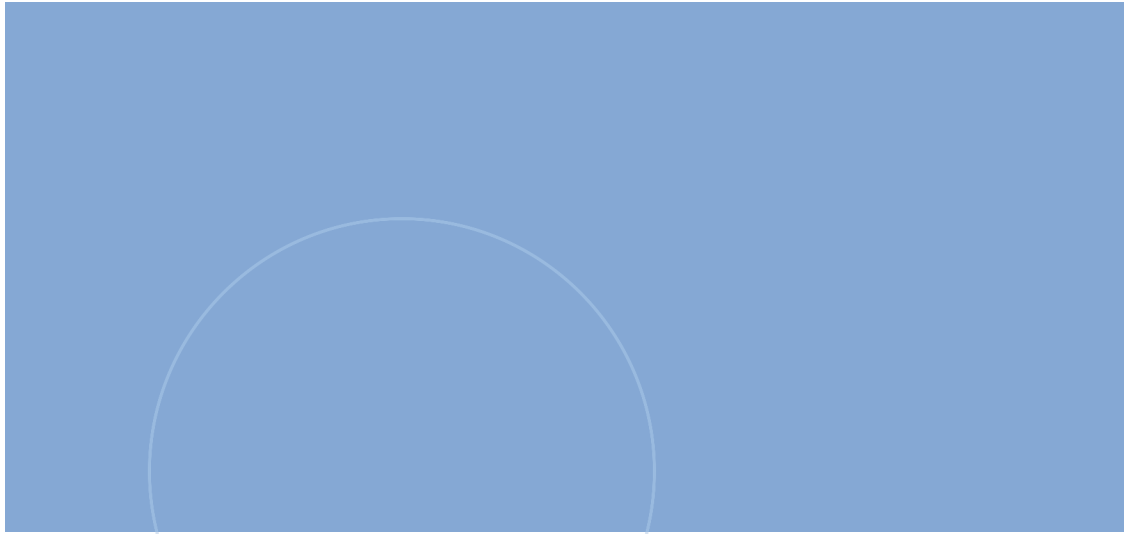**Figure K.3:** CI-NEB graph for reaction $CH \rightarrow C + H$ on Co(11-20) surface.

Figure K 4: CI-NEB graph for reaction $C_2H_2 \rightarrow CH + CH$ on Co(11-20) surface.

Figure K.5: CI-NEB graph for reaction $C_2H \rightarrow C + CH$ on Co(11-20) surface.

Figure K.6: CI-NEB graph for reaction $C_2 \rightarrow C + C$ on Co(11-20) surface.

XXV